Fall 2016

Unconventional phase transitions in random systems

Hatem Nuri Barghathi

Department: Physics

UNCONVENTIONAL PHASE TRANSITIONS IN RANDOM SYSTEMS

by

HATEM NURI BARGHATHI

A DISSERTATION

Presented to the Graduate Faculty of the

MISSOURI UNIVERSITY OF SCIENCE AND TECHNOLOGY

In Partial Fulfillment of the Requirements for the Degree

DOCTOR OF PHILOSOPHY

in

PHYSICS

2016

Approved by

Dr. Thomas Vojta, Advisor
Dr. Gerald Wilemski
Dr. Julia Medvedeva
Dr. Paul E. Parris
Dr. Uwe C. Täuber

DEDICATION

To my beloved family:

my mother Zakiya, my late father Nuri,

my wife Salwa, my Sons Nuri and Loai,

my brother Anis, and my sister Maha.

PUBLICATION DISSERTATION OPTION

This dissertation has been prepared in the form of seven papers:

Paper I, Pages 18–31, has been published as *Phase Transitions on Random Lattices: How Random is Topological Disorder?*, published in Physical Review Letters **113**, 120602 (2014) with Thomas Vojta.

Paper II, Pages 32–44, has been published as *Random Fields at a Nonequilibrium Phase Transition*, published in Physical Review Letters **109**, 170603 (2012) with Thomas Vojta.

Paper III, Pages 45–86, has been published as *Random Field disorder at an absorbing state transition in one and two dimensions*, published in Physical Review E **93**, 022120 (2016) with Thomas Vojta.

Paper IV, Pages 87–117, has been published as *Enhanced rare-region effects in the contact process with long-range correlated disorder*, published in Physical Review E **90**, 042132 (2014) with Ahmed K. Ibrahim and Thomas Vojta.

Paper V, Pages 118–150, has been published as *Contact process on generalized Fibonacci chains: Infinite-modulation criticality and double-log periodic oscillations*, published in Physical Review E **89**, 012112 (2014) with David Nozadze and Thomas Vojta.

Paper VI, Pages 151–171, has been published as *Infinite-randomness criticality in a randomly layered Heisenberg magnet*, published in Physical Review B **84**, 184202 (2011) with Fawaz Hrahsheh and Thomas Vojta.

Paper VII, Pages 172–196, has been published as *Strong-randomness phenomena in quantum Ashkin-Teller model*, published in Physica Scripta **T165**, 014040 (2015) with Fawaz Hrahsheh, José A. Hoyos, Rajesh Narayanan, and Thomas Vojta.

In addition, the dissertation contains an introductory section (Sec. 1) and a brief summary (Sec. 2).

ABSTRACT

In this thesis we study the effects of different types of disorder and quasiperiodic modulations on quantum, classical and nonequilibrium phase transitions. After a brief introduction, we examine the effect of topological disorder on phase transitions and explain a host of violations of the Harris and Imry-Ma criteria that predict the fate of disordered phase transitions. We identify a class of random and quasiperiodic lattices in which a topological constraint introduces strong anticorrelations, leading to modifications of the Harris and Imry-Ma criteria for such lattices. We then investigate whether or not the Imry-Ma criterion, that predicts that random-field disorder destroys phase transitions in equilibrium systems in sufficiently low dimensions, also holds for nonequilibrium phase transitions. We find that the Imry-Ma criterion does not apply to a prototypical absorbing state nonequilibrium transition.

In addition, we study the effect of disorder with long-range spatial correlations on the absorbing state phase transition in the contact process. Most importantly, we find that long-range correlations enhance the Griffiths singularities and change the universality class of the transition. We also investigate the absorbing state phase transition of the contact process with quasiperiodic transition rates using a real-space renormalization group which yields a complete theory of the resulting exotic infinite-modulation critical point.

Moreover, we study the effect of quenched disorder on a randomly layered Heisenberg magnet by means of a large-scale Monte-Carlo simulations. We find that the transition follows the infinite-randomness critical point scenario. Finally, we investigate the effect of quenched disorder on the first-order phase transition in the N-color quantum Ashkin-Teller model by means of strong-disorder renormalization group theory. We find that disorder rounds the first-order quantum phase transition in agreement with the quantum version of the Imry-Ma criterion.

ACKNOWLEDGMENTS

I am deeply grateful to my adviser Dr. Thomas Vojta for his generous support and encouragement. This thesis would not have been possible without his inspiration and patient guidance. Thanks again to you, Dr. Vojta, I am so proud to be your student; I will be forever in your debt.

I would like to thank all my committee members, Dr. Gerald Wilemski, Dr. Paul Parris, Dr. Julia Medvedeva, and Dr. Uwe C. Täuber for their valuable discussions and accessibility. To Dr. Wilemski, you are truly an outstanding person and an able educator and, I thank you very much. To Dr. Täuber, I am very fortunate to have you as one of my committee members.

I would like to thank our chairman, Dr. George D. Waddill and our graduate coordinator, Dr. Jerry Peacher. Also, the staff in the Physics Department: Pamela J. Crabtree, Janice Gargus, Ellen Marie Kindle, Russell L. Summers, Ronald Woody, Andy Stubbs and Charles A. Mcwhorter for their help.

Also, I would like especially to give my thanks to my friends Dr. Rabi Khanal and Ahmed K. Ibrahim. Thank you for your help and support.

To my friend Mohamed Saleh Ibrahim, I don't know where I would be now if it weren't for your huge help and support. I thank you from the bottom of my heart. I would like to thank my father-in-law Salem Ali Elshwehdi for his support and encouragement. Your words always inspire me.

I would like to express my gratitude to my wife, Salwa. Thank you, my love, for all your aid and support.

Finally, my love and thanks go to my mother Zakiya for her endless love and support. Her pure love is what made me who I am.

TABLE OF CONTENTS

Page

PAPER

LIST OF ILLUSTRATIONS

PAPER II

PAPER III

LIST OF TABLES

SECTION

1. INTRODUCTION

1.1. EQUILIBRIUM AND NONEQUILIBRIUM PHASE TRANSITIONS

What is a phase transition? A phase transition is an abrupt change in the macroscopic properties of an interacting many-body system in response to tuning a control parameter such as temperature, magnetic field or pressure. An everyday example of a phase transition is the melting of ice cubes in a glass of water. The phase (solid, liquid or gas) in which water exists depends on the value of the control parameters as shown in Fig. 1.1. The transition between two different phases starts to happen at the boundary between the phases, where they coexist. Phase coexistence is the most important characteristic of a *discontinuous* (*first-order*) phase transition. A discontinuous phase transition usually involves *latent heat* which is the amount of energy that is required to be released or absorbed to complete the transition from one phase to the other. The boundary between the gas and

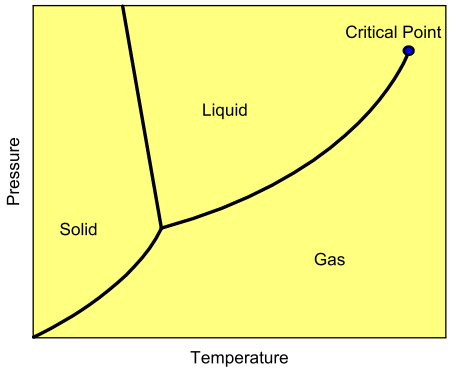

Fig. 1.1. Schematic phase diagram of water.

liquid phases of water vanishes at higher pressure and higher temperature, where the gas and the liquid phases merge in one fluid phase. The point at which the two phases merge is the *critical point* of a *continuous* (*second-order*) phase transition. At a continuous phase transition, the system is always in one distinct phase, i.e., there is no phase coexistence [1].

1.1.1. Landau Theory. One of the first approaches to understanding phase transitions in many-body systems is the mean-field theory (MFT). In the MFT approximation, the effects on one body by the rest of the system through interactions are treated as an external force (field) that depends on the average state of the other bodies. Hence, the problem is simplified to a one-body problem. Early examples of MFT are the Weiss theory of ferromagnetism [2] and the van der Waals theory of the liquid gas transition [3]. Landau [4, 5, 6, 7] generalized the MFT, first by proposing the concept of the order parameter which is a thermodynamic observable that has a finite value in the ordered phase and vanishes in the disordered phase. For example, in the case of the liquid-gas critical point of water (Fig.1.1), the order parameter is the difference between the densities of water in the two phases. Analogously, at the ferromagnetic critical point, the order parameter is the magnetization m. Landau also postulated that the free energy F_L is an analytical function of the order parameter m. Accordingly, the free energy can be expanded as a power series of the order parameter m

$$F_L = F_L(0) - hm + rm^2 + vm^3 + um^4 + O(m^5)\,, \tag{1.1}$$

where h is the external field conjugate to the order parameter and r, v and u are system parameters that are independent of the order-parameter. In the vicinity of the critical point ($|m| \ll 1$), higher order terms can be ignored. In the absence of an external field and if the system exhibits a symmetry with respect to the sign of the scalar order parameter, the free energy F_L must be an even function of m, i.e., $v = 0$. In this case, for $r \geq 0$ the free energy has only one minimum at $m = 0$ that represents the thermodynamical state of the system

in the disordered phase. If r is decreased below zero, the system undergoes a continuous phase transition where the single minimum will split continuously into two symmetrical minima of F_L at

$$m = \pm\sqrt{\frac{-r}{2u}}, \tag{1.2}$$

representing the ordered phase ($m \neq 0$). Accordingly, r is a measure of the distance from the critical point at $r = 0$. Eq. (1.2) shows a power-law dependence of m on r,

$$m \sim (-r)^{\beta}, \tag{1.3}$$

where $\beta = 1/2$ is the order parameter exponent. Landau theory can also describe a discontinuous phase transition. For instance, for $r < 0$ in the previous example and in the presence of an external field $h < 0$, the system will be in a phase with $m < 0$. If the field is raised to $h > 0$ the phase of the system will discontinuously change to a phase with $m > 0$. The transition point, in this case, is at $h = 0$ where the system could be in either of the two phases (phase coexistence). Moreover, for $v \neq 0$ and $h = 0$, a discontinuous phase transition could occur by tuning r.

1.1.2. Fluctuations and Landau-Ginzburg-Wilson Theory. The fluctuations of the order parameter about its mean value are ignored in Landau theory. In fact, the strength of the order parameter fluctuations increases with decreasing the system's dimensionality d such that for $d \leq d_c^-$, where d_c^- is the lower critical dimension, the fluctuations are strong enough to destroy the phase transition by preventing the ordered phase. On the other hand, for $d \geq d_c^+$, where d_c^+ is the upper critical dimension, the fluctuations can be neglected, ensuring the validity of Landau theory. For d in the range $d_c^+ > d > d_c^-$, the effects of the fluctuations are limited to changing the critical behavior of the phase from the predictions of Landau theory.

In order to extend the validity of Landau theory below d_c^+, one must consider the spatial fluctuations of the order parameter by using a spatially varying order parameter field $\phi(\vec{x})$ and its gradient $\nabla\phi(\vec{x})$ and generalize the Landau free energy Eq. (1.1) to the Landau-Ginzburg-Wilson functional

$$S[(\phi(\vec{x})] = \int d^d\vec{x}\{-h\phi(\vec{x}) + r\phi^2(\vec{x}) + v\phi^3(\vec{x}) + u\phi^4(\vec{x}) + [\nabla\phi(\vec{x})]^2\}\,. \tag{1.4}$$

In contrast to the Landau free energy (1.1), this cannot be solved in closed form. However, it forms the basis for a number of sophisticated analytical techniques.

1.1.3. Scaling Hypothesis. Close to the critical point, observables show a power-law dependence on the external control parameters such as r and h. This observation applies also to the correlation length ξ which diverges at the critical point ($r = 0$) as

$$\xi \sim r^{-\nu}\,. \tag{1.5}$$

Here, ν is the correlation length critical exponent. This implies that close to the critical point, the only relevant length is the correlation length. Therefore, the scaling hypothesis states that in the vicinity of the critical point, rescaling all length scales by an arbitrary factor b^{-1} is equivalent to rescaling the external control parameters r and h by factors of b^{y_r} and b^{y_h} respectively. In other words, replacing r and h by $b^{y_r}r$ and $b^{y_h}h$, respectively, changes the correlation length by a factor of b^{-1} and the free energy f by a factor of b^d leading to the scaling forms [8, 9]

$$\xi(r,h) = b\xi(b^{y_r}r, b^{y_h}h)\,, \tag{1.6}$$

$$f(r,h) = b^{-d}f(b^{y_r}r, b^{y_h}h)\,. \tag{1.7}$$

Choosing the arbitrary factor $b = r^{-1/y_r}$ in Eq. (1.6) leads to

$$\xi(r, h) = r^{-1/y_r} \xi_S(r^{-y_h/y_r} h) , \tag{1.8}$$

where ξ_S is a unary function with $r^{-y_h/y_r} h$ as its argument. Thus, in the absence of a field ($h = 0$), one retrieves Eq. (1.5) with $\nu = 1/y_r$.

Moreover, other observables such as the order parameter $m = -(\partial f/\partial h)$, susceptibility $\chi = (\partial m/\partial h)$ and specific heat $C = -T(\partial^2 f/\partial^2 r)$ have similar scaling forms which can be found by taking the appropriate derivatives of the free energy using Eq. (1.7):

$$m(r, h) = b^{y_h - d} m(b^{1/\nu} r, b^{y_h} h) , \tag{1.9}$$

$$\chi(r, h) = b^{2y_h - d} \chi(b^{1/\nu} r, b^{y_h} h) , \tag{1.10}$$

$$C(r, h) = b^{2/\nu - d} C(b^{1/\nu} r, b^{y_h} h) . \tag{1.11}$$

Setting $b = r^{-\nu}$ and $h = 0$ in Eqs. (1.9, 1.10, 1.11) gives

$$m \sim r^{(d - y_h)\nu} = r^{\beta} , \tag{1.12}$$

$$\chi \sim r^{(d - 2y_h)\nu} = r^{-\gamma} , \tag{1.13}$$

$$C \sim r^{d\nu - 2} = r^{-\alpha} , \tag{1.14}$$

where γ and α are the susceptibility and specific heat critical exponents, respectively. Also, setting $b = h^{-1/y_h}$ and $r = 0$ in Eq. (1.9) gives

$$m \sim h^{d/y_h - 1} = h^{1/\delta}, \tag{1.15}$$

where δ is the critical isotherm exponent. Accordingly, the critical exponents are not all independent. Instead we get the scaling relations.

$$\alpha = 2 - d\nu, \tag{1.16}$$

$$2\beta + \gamma + \alpha = 2, \tag{1.17}$$

$$\beta(\delta - 1) = \gamma, \tag{1.18}$$

which are known as Josephson's, Rushbrooke's, and Widom's scaling relations, respectively [8, 10, 11].

1.1.4. Nonequilibrium Phase Transitions. In the previous sections, we only discussed phase transitions in equilibrium systems. Nonetheless, studies of nonequilibrium systems have shown that continuous and discontinuous transitions also occur away from equilibrium [12, 13, 14, 15] and many of the concepts introduced above carry over to nonequilibrium transitions, for example scaling and critical behavior. One example is the *contact process* which was introduced by Harris [16] (see also Refs. [17, 18, 19]) as a prototypical model that undergoes a nonequilibrium continuous phase transition. This model is defined on a hypercubic lattice in d dimensions. The sites of the lattice can be in one of two states, either active A or inactive I. The system then evolves as a Markov process in continuous time according to two processes. The first process is the spontaneous decay of

active sites which become inactive with a decay rate μ. The other process is the activation process in which an inactive site is activated by its nearest neighbor with activation rate λ.

The fate of the system is determined by the ratio λ/μ. For $\lambda/\mu \gg 1$, the activation overcomes the decay in the system resulting in a non-zero average of the density of active sites $\rho(t)$ at all times. Eventually, $\rho(t)$ converges to a steady state density $\rho_s > 0$ defining the active phase of the system. In contrast, if $\lambda/\mu \ll 1$, the decay overwhelms the activation in the system. Therefore the system is destined to be trapped in the absorbing state in which all sites are inactive. Thus $\rho_s = 0$ represents the absorbing phase.

Starting from the active phase ($\lambda/\mu \gg 1$), as we decrease the ratio λ/μ (control parameter), the system undergoes a continuous transition to the absorbing phase at the critical ratio $(\lambda/\mu)_c$. Near the critical point, ρ_s shows a power-law dependence on the distance from criticality $r \sim |\lambda/\mu - (\lambda/\mu)_c|$,

$$\rho_s \sim r^{\beta}, \tag{1.19}$$

where β is the order parameter critical exponent. Similarly, the correlation length ξ (which is the characteristic size of a cluster of active sites) behaves as

$$\xi \sim r^{\nu}, \tag{1.20}$$

where ν is the correlation length critical exponent. Moreover, the correlation time ξ_t fulfills

$$\xi_t \sim \xi^z, \tag{1.21}$$

as in the equilibrium case. The exponents β, ν and z define the universality class of the transition which is known as the directed percolation universality class [20, 21].

1.2. QUENCHED DISORDER

In reality, the existence of pure systems is rather the exception than the rule because different types of defects and impurities introduce disorder into the system. Therefore, studying the effect of disorder on phase transitions has attracted a great deal of attention [12, 22, 23]. In general, disorder is classified based on its time dependence into quenched (time-independent) and annealed (time-dependent) disorder. In this work, we only consider quenched disorder. Moreover, it is important to distinguish between random-field and random-mass disorder.

Random-mass (or random T_c) disorder does not break any of the order parameter symmetries. Instead, it locally changes the preference for one phase or the other. In the Landau-Ginzburg-Wilson functional (Eq. (1.4)), random-mass disorder can be introduced by making the distance r from criticality a random function of position,

$$r = r_0 + \delta r(\vec{x}) \,. \tag{1.22}$$

In contrast, random-field disorder breaks the order parameter symmetry. In the Landau-Ginzburg-Wilson functional (Eq. (1.4)), random-field disorder arises when the field conjugate to the order parameter is random,

$$h = h_0 + \delta h(\vec{x}) \,. \tag{1.23}$$

1.2.1. Imry-Ma Criterion. Do first-order phase transitions survive random-mass disorder? Imry and Wortis [24] provided an answer to this question through a heuristic argument in which they test whether or not macroscopic phase coexistence is possible in the presence of random-mass disorder. In their argument, they consider a single d-dimensional domain of one phase and of linear size L embedded in a much larger domain of the second

phase (see Fig. 1.2). If σ is the surface tension, then the corresponding increase in the free energy due to the surface formation is

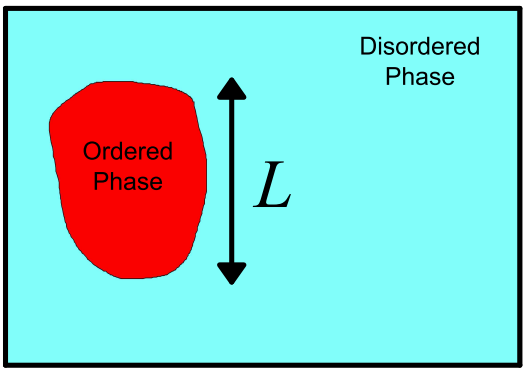

Fig. 1.2. Derivation of the Imry-Ma Criterion criterion.

$$f_{surf} \sim \sigma L^{d-1} \,. \tag{1.24}$$

The typical fluctuation of the random-mass term over a volume L^d can be estimated from central limit theorem to be of the order of $\sigma_{dis} L^{d/2}$, where σ_{dis} is the standard deviation of the random-mass disorder. If the domain is in a favorable location within the system, this will decrease the free energy by

$$f_{dis} \sim \sigma_{dis} L^{d/2} \,. \tag{1.25}$$

The survival of the first-order phase transition means that the two phases can still coexist at a macroscopic scale, i.e., the size L of such domains must be limited. This is true if $f_{surf} > f_{dis}$. From Eqs. (1.24,1.25), this is possible only if $d > 2$. In other words, random-mass disorder prevents a first-order phase transition if

$$d \leq 2 \,. \tag{1.26}$$

Based on a similar argument, Imry and Ma [25] derived the same inequality (1.26) for the stability of a continuous phase transition against random-field disorder. It is therefore called the Imry-Ma criterion. These results were later proven rigorously by Aizenman and Wehr [26].

1.2.2. Harris Criterion. Based on a heuristic argument, Harris [27] developed a criterion that tests the stability of a clean critical point (continuous phase transition) against random-mass disorder. Here, we derive the Harris criterion. Consider a system that undergoes a continuous phase transition in the presence of random-mass disorder at the critical temperature T_c, with the assumption that the clean critical behaivior of the system is stable against random-mass disorder. Starting with the system in one of the two phases at temperature T away from T_c, we divide the system into blocks of a linear size that is equal to the correlation length ξ(see Fig.1.3). The local critical temperature T_c^i of a block i will

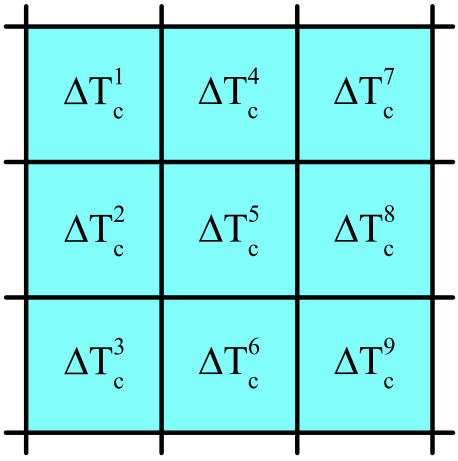

Fig. 1.3. Schematic representation of a system with random-mass. Each block of linear size ξ has different local critical temperature.

vary, as it depends on the values of the disordered local microscopic parameters. Let ΔT_c be the variation of this local critical temperature. If the temperature T approaches T_c then, as long as T is outside of the range $T_c \pm \Delta T_c$, all the blocks are in the same phase and the

transition can be uniform. Otherwise, some of the blocks will be in one phase while the rest are in the other phase, and the transition cannot be uniform. In other words, the necessary condition for the stability of the clean critical point is that, as the critical temperature is approached, the condition $\Delta T_c \ll |T - T_c|$ always holds.

The fluctuations of the local critical temperature of the blocks can be estimated from the central limit theorem as

$$\Delta T_c \sim \xi^{-d/2}, \tag{1.27}$$

where ξ depends on the distance from the critical point as

$$\xi \sim |T - T_c|^{-\nu}. \tag{1.28}$$

This leads to

$$\frac{\Delta T_c}{|T - T_c|} \sim |T - T_c|^{d\nu/2-1}. \tag{1.29}$$

This means that the necessary condition for the stability of the clean critical point is

$$d\nu > 2. \tag{1.30}$$

This is the famous Harris criterion.

1.3. STRONG-DISORDER RENORMALIZATION GROUP THEORY

The renormalization group theory (RG) [1, 28, 29] is a powerful technique to analyze the changes of the physical properties of systems that undergo phase transitions. The basic idea is to coarse grain the system (by eliminating short-distance degrees of freedom and rescaling all lengths) and to map the coarse-grained system onto the original system with

different parameter values. If a system is undergoing a continuous phase transition then the correlation length ξ is the only relevant length scale close to the critical point, and it diverges at criticality. This means that the critical point must be a fixed point of the RG transformation at which the system maps onto itself.

Consider, for example, a lattice spin system. In this case, the RG transformation consists of dividing the system into blocks of linear size ba (where a is the lattice constant), replacing each block by a single coarse-grained spin using some mapping relations, and finally rescaling the length scale by a factor of b. This recovers the original system, but with rescaled parameters. After each step, the free energy of the system will have the same dependence on the rescaled system parameters as the initial ones. Thereby, the RG can be used to prove the scaling hypothesis discussed in Sec.1.1.3.

The strong-disorder renormalization group (SDRG) method [30], introduced by Ma, Dasgupta, and Hu [31, 32], is a powerful RG method developed to deal with disordered systems. As we will use the SDRG in Papers V and VII, let us illustrate the SDRG method by considering Fisher's [33, 34] solution of the random transverse-field Ising chain (TFIC).

1.3.1. Random Transverse-Field Ising Chain Model. The TFIC model is defined by the Hamiltonian

$$H = -\sum_i J_i \sigma_i^z \sigma_{i+1}^z - \sum_i h_i \sigma_i^x \,, \tag{1.31}$$

where σ_i^x and σ_i^z are the x and z components of the spin operator at site i. $J_i > 0$ and $h_i > 0$ are the nearest-neighbor interaction and transverse field strengths at site i, respectively. Both J_i and h_i are drawn from independent random distributions $P(J_i)$ and $R(h_i)$ with typical values of J_{typ} and h_{typ} respectively.

The TFIC model undergoes a quantum (zero temperature) phase transition between a ferromagnetic ground state phase at $J_{typ} \gg h_{typ}$ where the spins are aligned in the $\pm z$-direction and a paramagnetic phase at $J_{typ} \ll h_{typ}$ in which the spins point in the transverse

field direction (x-direction). Such a transition is called a quantum phase transition because it is driven by the quantum fluctuations that arise from the uncertainty of the quantum variables (σ^x and σ^z do not commute). The TFIC model was solved by Fisher [33] using the SDRG method which we now discuss.

1.3.2. Recursion Relations. First, we identify the largest energy scale Ω in the system which could correspond to either a coupling between two spins or a field at one site. If the largest energy scale turns out to be the field $h_i \gg J_{i-1}, J_i$ at site i then the direction of the spin σ_i is almost fixed in the field direction (x-direction) with no contribution to the magnetization in the z-direction which is the order parameter of the transition. Despite the pinning of the spin σ_i, virtual excitations still provide a weak coupling between its nearest neighbors.To find this effective coupling consider the local Hamiltonian

$$H_h = -h_i\sigma_i^x - J_{i-1}\sigma_{i-1}^z\sigma_i^z - J_i\sigma_i^z\sigma_{i+1}^z, \tag{1.32}$$

which can be written as $H = H_0 + H_1$ with $H_1 = -J_{i-1}\sigma_{i-1}^z\sigma_i^z - J_i\sigma_i^z\sigma_{i+1}^z$ being a perturbation to the strong field term $H_0 = -h_i\sigma_i^x$. Using second order perturbation theory in H_1 we get the effective local Hamiltonian

$$H_{h,eff} = -\tilde{J}\sigma_{i-1}^z\sigma_{i+1}^z, \tag{1.33}$$

where $\tilde{J}$ is defined by the recursion relations

$$\tilde{J} = \frac{J_{i-1}J_i}{h_i} < J_{i-1}, J_i\,. \tag{1.34}$$

This renormalization group step is schematically explained in Fig. 1.4. Note that this approximation gets better and better with increasing disorder. The contribution of H_h to the total Hamiltonian H is then replaced by $H_{h,eff}$ and a constant term that can be dropped.

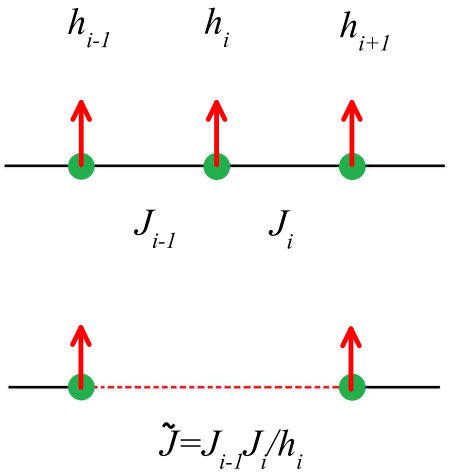

Fig. 1.4. A schematic representation of a Strong-disorder renormalization group site decimation step.

Analogously, if the largest energy scale is the coupling $J_i \gg h_i, h_{i+1}$ between the spins at site i an $i+1$ then the two spins σ_i and σ_{i+1} strongly prefer to be parallel to each other along the z-direction. Accordingly, they can be considered as a large single spin $\tilde{\sigma}$ with an effective magnetic moment

$$\tilde{\mu} = \mu_i + \mu_{i+1}\,, \tag{1.35}$$

where μ_i and μ_{i+1} are the moments of the original sites. Similarly, by treating the local Hamiltonian

$$H_J = H_0 + H_1 = -J_i\sigma_i^z\sigma_{i+1}^z - h_i\sigma_i^x - h_{i+1}\sigma_{i+1}^x\,, \tag{1.36}$$

using second order perturbation theory, where $H_0 = -J_i\sigma_i^z\sigma_{i+1}^z$ and $H_1 = -h_i\sigma_i^x - h_{i+1}\sigma_{i+1}^x$, we get the effective local Hamiltonian

$$H_{J,eff} = -\tilde{h}\tilde{\sigma}^z\,, \tag{1.37}$$

where recursion relations for $\tilde{h}$ is

$$\tilde{h} = \frac{h_i h_{i+1}}{J_i} < h_i, h_{i+1} \, . \tag{1.38}$$

This renormalization group step is schematically explained in Fig. 1.5. The contribution

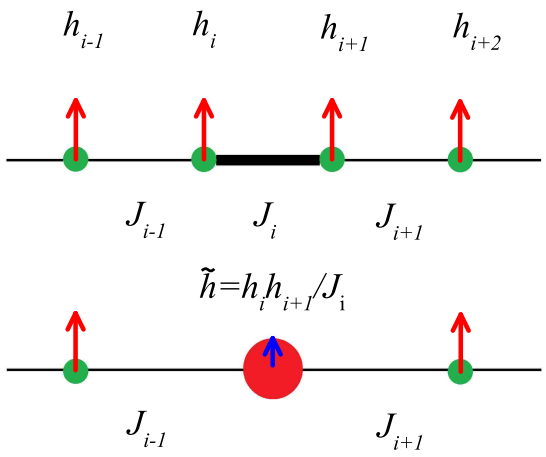

Fig. 1.5. A schematic representation of a Strong-disorder renormalization group coupling decimation step.

of H_J to H is then replaced by $H_{J,eff}$ and a constant term that can be dropped.

1.3.3. Flow Equations and Results. By iterating the SDRG steps outlined above the system's largest energy scale Ω gets smaller and smaller and the number of degrees of freedom gets reduced, but the structure of the Hamiltonian does not change. At any stage of the SDRG flow, h and J are independent random variables with probability distributions $P(J, \Omega)$ and $R(h, \Omega)$ which evolve as $\Omega \to 0$. Therefore, it's important to study the evolution of $P(J, \Omega)$ and $R(h, \Omega)$. The SDRG flow equations of these distribution were found by Fisher [33] to be

$$-\frac{\partial P(J,\Omega)}{\partial \Omega} = [P(\Omega,\Omega) - R(\Omega,\Omega)]P(J,\Omega) + R(\Omega,\Omega)\int dJ_1 dJ_2 \;\; P(J_1,\Omega)P(J_2,\Omega)\;\delta(J - J_1 J_2/\Omega)\,, \quad (1.39)$$

$$-\frac{\partial R(h,\Omega)}{\partial \Omega} = [R(\Omega,\Omega) - P(\Omega,\Omega)]R(h,\Omega) + P(\Omega,\Omega)\int dh_1 dh_2 \; R(h_1,\Omega)R(h_2,\Omega)\;\delta(h - h_1 h_2/\Omega)\,. \quad (1.40)$$

The critical point of the Hamiltonian (Eq. (1.31)) is located at $< \ln h_i >=< \ln J_i >$ as also follows from self-duality [35]. Fisher found that the solution of the flow equations at the critical point is

$$P(J;\Omega) = \frac{1}{\Gamma J}\left(\frac{J}{\Omega}\right)^{1/\Gamma}\,, \quad (1.41)$$

$$R(h;\Omega) = \frac{1}{\Gamma h}\left(\frac{h}{\Omega}\right)^{1/\Gamma}\,. \quad (1.42)$$

with $\Gamma = \ln(\Omega_0/\Omega)$ where Ω_0 is the initial largest energy scale in the system. Under the SDRG flow, as $\Omega \to 0$, the width of the distributions (1.41,1.42)) diverges which means that the disorder gets stronger and stronger suggesting that the results of the SDRG are asymptotically exact. Moreover, the diverging width of the distributions is what gives such a critical point the name infinite-randomness critical point.

To understand the characteristics of the critical behaver, let us consider the behavior of some quantities of the system. First, from the evolution of the number of surviving clusters, the evolution of the typical distance l that separates two surviving clusters is found to be

$$l \sim [\ln(\Omega_0/\Omega)]^{1/\psi}\,, \quad (1.43)$$

where $\psi = 1/2$ is the tunneling exponent. The logarithmic dependence of the length scale on the energy scale (instead of a power-law dependence as in the case of a clean system) is

called the activated dynamical scaling. Moreover, the flow of the typical magnetic moment μ that is governed by recursion relation (Eq. (1.35)) is found to be

$$\mu \sim [\ln(\Omega_0/\Omega)]^{\phi} \ , \tag{1.44}$$

where the exponent ϕ is equal to the golden ratio $(\sqrt{5}+1)/2$. Furthermore, the correlation length ξ shows a power-law dependence on r, as in the clean case,

$$\xi \sim |r|^{-\nu} \, , \tag{1.45}$$

but with different exponent value $\nu = 2$ that saturates the Harris inequality $d\nu \geq 2$. The universality class of the transition can be defined via the exponents ψ, ϕ and ν, and all other exponents can be found from scaling relations.

PAPER

I. PHASE TRANSITIONS ON RANDOM LATTICES: HOW RANDOM IS TOPOLOGICAL DISORDER?

Hatem Barghathi and Thomas Vojta

Department of Physics, Missouri University of Science and Technology, Rolla, MO 65409, USA

ABSTRACT[*]

We study the effects of topological (connectivity) disorder on phase transitions. We identify a broad class of random lattices whose disorder fluctuations decay much faster with increasing length scale than those of generic random systems, yielding a wandering exponent of $\omega = (d-1)/(2d)$ in d dimensions. The stability of clean critical points is thus governed by the criterion $(d+1)\nu > 2$ rather than the usual Harris criterion $d\nu > 2$, making topological disorder less relevant than generic randomness. The Imry-Ma criterion is also modified, allowing first-order transitions to survive in all dimensions $d > 1$. These results explain a host of puzzling violations of the original criteria for equilibrium and nonequilibrium phase transitions on random lattices. We discuss applications, and we illustrate our theory by computer simulations of random Voronoi and other lattices.

[*]Published in Physical Review Letters **113**, 120602 (2014).

Two of the central results on phase transitions in disordered systems are the Harris and Imry-Ma criteria. The Harris criterion [1] governs the stability of critical points against disorder. If the correlation length exponent ν of a d-dimensional clean system fulfills the inequality $d\nu > 2$, weak disorder is irrelevant and does not change the critical behavior. If $d\nu < 2$, disorder is relevant, and the character of the transition must change [2]. The Imry-Ma criterion [3] governs the stability of macroscopic phase coexistence: Disorder destroys phase coexistence by domain formation in dimensions $d \leq 2$ [4]. As a consequence, disorder rounds first-order phase transitions in $d \leq 2$. The predictions of these criteria and their generalizations to long-range correlated disorder [5, 6] agree with the vast majority of explicit results on classical, quantum, and nonequilibrium systems in which the disorder stems from random coupling strengths or spatial dilution.

Puzzling results have been reported, however, on phase transitions in *topologically disordered* systems, i.e., systems on lattices with random connectivity. For example, the Ising magnet on a three-dimensional (3D) random Voronoi lattice displays the same critical behavior as the Ising model on a cubic lattice [7, 8] even though Harris' inequality is violated. An analogous violation was found for the 3-state Potts model on a 2D random Voronoi lattice [9]. The regular 2D 8-state Potts model features a first-order phase transition. In contrast to the prediction of the Imry-Ma criterion, the transition remains of first order on a random Voronoi lattice [10].

The nonequilibrium transition of the contact process features an even more striking discrepancy. This system violates Harris' inequality [11]. Disorder introduced via dilution or random transition rates results in an infinite-randomness critical point and strong Griffiths singularities [12, 13]. In contrast, the contact process on a 2D random Voronoi lattice shows clean critical behavior and no trace of the exotic strong-randomness physics [14].

To explain the unexpected failures of the Harris and Imry-Ma criteria, several authors suggested that, perhaps, the existing results are not in the asymptotic regime. Thus, much larger systems would be necessary to observe the true asymptotic behavior which,

presumably, agrees with the Harris and Imry-Ma criteria. However, given the large systems employed in some of the cited work, this would imply enormous crossover lengths which do not appear likely because the coordination number fluctuations of the Voronoi lattice are not particularly small [15]. What, then, causes the failure of the Harris and Imry-Ma criteria on random Voronoi lattices?

In this Letter, we show that 2D random Voronoi lattices belong to a broad class of random lattices whose disorder fluctuations feature strong anticorrelations and thus decay qualitatively faster with increasing length scale than those of generic random systems. This class comprises lattices whose total coordination (total number of bonds) does not fluctuate. Such lattices are particularly prevalent in 2D because the Euler equation of a 2D graph imposes a topological constraint on the coordination numbers. However, higher-dimensional realizations exist as well. The suppressed disorder fluctuations lead to an important modification of the Harris criterion: The random connectivity is irrelevant at clean critical points if $(d+1)\nu > 2$. Topological disorder is thus less relevant than generic randomness. The Imry-Ma criterion is modified as well, allowing first-order transitions to survive in all dimensions $d > 1$. This explains the puzzling literature results on 2D random Voronoi lattices mentioned above. In the rest of this Letter, we sketch the derivation of these results and illustrate them by simulations.

Random lattice or cell structures occur in many areas of physics, chemistry, and biology such as amorphous solids, foams, and biological tissue. Consider a many-particle system on such a random lattice, e.g., a classical or quantum spin system, lattice bosons, or a nonequilibrium problem such as the contact process. In all these examples, the disorder of the many-particle system stems from the random connectivity of the underlying lattice. In the following, we therefore analyze the fluctuations of the coordination number q_i (the number of nearest neighbors of site i) for different random lattices, starting with the 2D random Voronoi lattice (Fig. 1). The Voronoi-Delaunay construction is an algorithm for

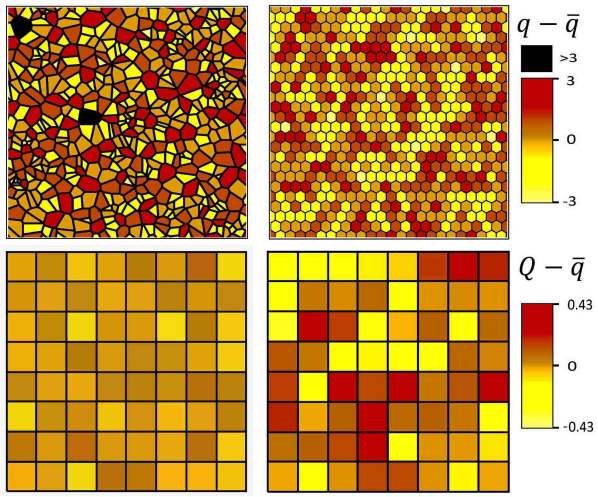

Fig. 1. Top row: coordination numbers q_i of individual sites in a random Voronoi lattice (left) and a diluted hexagonal lattice (right). Bottom row: average coordination number Q_μ of blocks with $L_b = 8$. The strong suppression of the fluctuations in the Voronoi lattice is clearly visible. (The same color (gray) scale is used left and right).

building a cell network from a set of lattice sites [16]. The Voronoi cell of a site consists of all points in the plane that are closer to this site than to any other. Sites whose Voronoi cells share an edge are considered neighbors. The graph of all bonds connecting pairs of neighbors defines a triangulation of the plane called the Delaunay triangulation. Our simulations start by performing the Voronoi-Delaunay construction [17] for N points placed at independent random positions within a square of side $L = N^{1/2}$ (density fixed at unity). To study the coordination number fluctuations, we divide the system into square blocks of side L_b and calculate the block-averaged coordination number

$$Q_\mu = N_{b,\mu}^{-1} \sum_{i \in \mu} q_i \tag{1}$$

for each block. $N_{b,\mu}$ is the number of sites in block μ, and the sum runs over all these sites. The relevant quantity is the standard deviation σ_Q of the block-averaged coordination

numbers defined by

$$\sigma_Q^2(L_b) = \left[(Q_\mu - \bar{q})^2\right]_\mu \tag{2}$$

where $[\ldots]_\mu$ denotes the average over all blocks μ, and $\bar{q}$ is the global average coordination number of the lattice.

Figure 2 compares the fluctuations in a random Voronoi lattice and a bond-diluted square lattice (both with periodic boundary conditions). In the diluted lattice, the fluc-

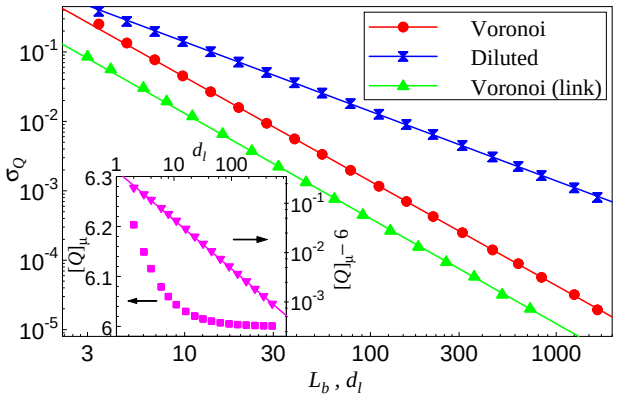

Fig. 2. Standard deviation σ_Q of the average coordination number $[Q]_\mu$ of blocks of size L_b for a random Voronoi lattice and a square lattice with 50% bond dilution (100 lattices with 5000^2 sites each). The lines are fits to $\sigma_Q \sim L_b^{-a}$ giving exponents $a = 1.001(2)$ (diluted) and 1.501(3) (Voronoi). Also shown is σ_Q for clusters defined via the link distance d_l (100 lattices with 2000^2 sites) giving $a = 1.52(2)$. Inset: $[Q]_\mu$ and $[Q]_\mu - \bar{q}$ of the link-distance clusters vs. d_l. The line is a fit to $([Q]_\mu - \bar{q}) \sim d_l^{-b}$ yielding $b = 0.99(1)$.

tuations accurately follow $\sigma_Q \sim L_b^{-d/2} = L_b^{-1}$, as expected for uncorrelated disorder. In contrast, the fluctuations in the Voronoi lattice decay faster and follow $\sigma_Q \sim L_b^{-3/2}$. An illustration of the suppressed fluctuations in the Voronoi lattice is shown in Fig. 1.

In addition to real-space blocks, we also study clusters based on the link distance, the smallest number of bonds (links) that separate two sites. To construct such clusters, we start from a random seed site and add its neighbors, neighbors of neighbors and so on until we reach a maximum link distance d_l. This construction introduces a bias towards

large q_i (as sites with more neighbors are more likely to be added to the cluster). Thus, the cluster average $[Q]_\mu$ is larger than the global average $\bar{q} = 6$, see inset of Fig. 2. The excess decays only slowly with cluster size, $([Q]_\mu - 6) \sim d_l^{-1}$. For the link-distance clusters we therefore use $\sigma_Q^2(d_l) = \left[(Q_\mu - [Q]_\mu)^2\right]_\mu$ rather than eq. (2). The resulting data, also shown in Fig. 2, demonstrate that the fluctuations of the link-distance clusters decay with the same power, $\sigma_Q \sim d_l^{-3/2}$, as those of the real-space blocks. Had we not corrected for the size-dependence of $[Q]_\mu$, we would have obtained a spurious decay exponent of (-1) [18].

How can we understand the rapidly decaying disorder fluctuations? The Euler equation of a 2D graph consisting of N sites, E edges (nearest-neighbor bonds), and F facets reads $N - E + F = \chi$. Here, χ is the Euler characteristic, a topological invariant of the underlying surface. Periodic boundary conditions are equivalent to a torus topology, yielding $\chi = 0$ [19]. Every facet of a Delaunay triangulation is a triangle. As each triangle has three edges, and each edge is shared by two triangles, $3F = 2E$. This implies $E = 3N$, i.e., the total coordination does not fluctuate, and the average coordination number is $\bar{q} = 2E/N = 6$ for any disorder realization. (This also follows from the angle sum in any triangle being π: As each site has a total angle of 2π, 6 triangles meet at a site on average.) Now consider a block of size L_b as introduced above. The relation $3F = 2E$ holds for all triangles and edges completely inside the block. Any deviation of the block-averaged coordination number Q_μ from $\bar{q} = 6$ must thus stem from the block surface. The number of facets crossing the surface scales linearly with L_b. Assuming that each of these facets makes an independent random contribution to Q_μ leads to the estimate $\sigma_Q(L_b) \sim L_b^{1/2}/L_b^2 = L_b^{-3/2}$ in perfect agreement with the numerical data.

To substantiate these arguments, we study the coordination number correlation function

$$C(\mathbf{r}) = \frac{1}{N} \sum_{ij} (q_i - \bar{q})(q_j - \bar{q}) \delta(\mathbf{r} - \mathbf{r}_{ij}) \tag{3}$$

where $\mathbf{r}_{ij}$ is the vector from site i to j. Its integral over a block of radius r yields the bulk contribution to the fluctuations of the average coordination number

$$\sigma^2_{Q,\mathrm{bulk}}(r) = D(r) = \frac{2\pi}{N_r}\int_0^r dr'\, r'\, C(r') \tag{4}$$

where N_r is the number of sites in the block. The data presented in Fig. 3

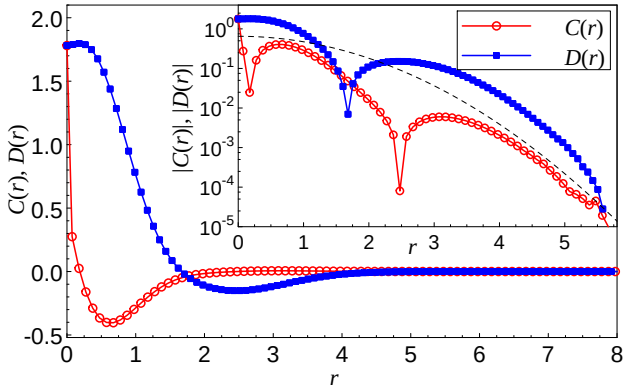

Fig. 3. Coordination number correlation function $C(r)$ and its integral $D(r)$ vs. distance r averaged over 10^7 lattices of 24^2 sites. Inset: Semi-log plot of $|C(r)|$ and $|D(r)|$. The envelope of $C(r)$ follows a Gaussian with a characteristic length $x_0 \approx 1.25$ (dashed line).

show that $|C(r)|$ decays faster than exponential with distance r. Its integral $D(r)$ also decays rapidly to zero, confirming that the total coordination is not fluctuating. The topological constraint imposed by the Euler equation thus leads to strong coordination number anticorrelations that are fully established within 5 or 6 typical nearest-neighbor distances.

How general are these results? Are they restricted to 2D random Voronoi lattices or do they apply to other lattices as well? The fixed total coordination is a direct consequence of the Euler equation $N - E + F = \chi$ and the triangle condition $3F = 2E$. It thus applies to any tiling of the plane with triangles. Analogously, if we tile the plane with arbitrary quadrilaterals, $4F = 2E$. This yields a fixed average coordination number of

precisely $\bar{q} = 2E/N = 4$. We have thus identified a broad class of 2D lattices in which the coordination fluctuations are suppressed because the total coordination is constrained. In addition to random Voronoi lattices it includes, e.g., regular lattices with bond-exchange defects which are related to the topological models of Le Caër [20]. It also includes deterministic quasiperiodic lattices such as the Penrose and Ammann-Beenker tilings [21] (using rhombic tiles) as well as random tilings [22] whose tiles are either all triangles or all quadrilaterals.

What about higher dimensions? The Euler equation for a 3D tessellation, $N - E + F - C = \chi$, contains one extra degree of freedom, viz., the number C of 3D cells. The total coordination of a random tetrahedralization is therefore *not* fixed by a topological constraint, in agreement with the fact that the solid-angle sum in a tetrahedron is *not* a constant. Consequently, 3D random Voronoi lattices do *not* belong to our class of lattices with a constrained total coordination. However, 3D members of our class do exist. They include, e.g., lattices built exclusively from rhombohedra such as the icosahedral tiling and its random variants [23] (the solid angle sum of a rhombohedron is fixed at 4π) as well as generalizations of the bond-exchange lattices to 3D.

We now generalize to arbitrary dimension our estimate of the fluctuations of the block-averaged coordination number. As the bulk contribution is suppressed by the anticorrelations, the main contribution stems from the surface. The number of cells or facets close to the surface scales as L_b^{d-1} with block-size L_b. In the generic case, i.e., in the absence of further constraints or long-range correlations, these surface cells make independent random contributions to Q_μ. This leads to

$$\sigma_Q(L_b) \sim L_b^{(d-1)/2}/L_b^d = L_b^{-(d+1)/2}. \tag{5}$$

Casting this result in terms of the wandering exponent ω defined via $\sigma_Q \sim L_b^{-d(1-\omega)}$ [24], we obtain $\omega = (d-1)/(2d)$. This needs to be compared to uncorrelated randomness for which $\sigma_Q \sim L_b^{-d/2}$ and $\omega = 1/2$.

We have verified the prediction (5) for several lattices in addition to the 2D Voronoi lattice. The first is a random lattice produced from a triangular lattice by performing random bond exchanges. A bond exchange (left inset of Fig. 4) consists in randomly choosing a rhombus made up of two adjacent triangles and replacing the short diagonal (dotted) with the long one (solid). The second example is the deterministic quasiperiodic Ammann-Beenker

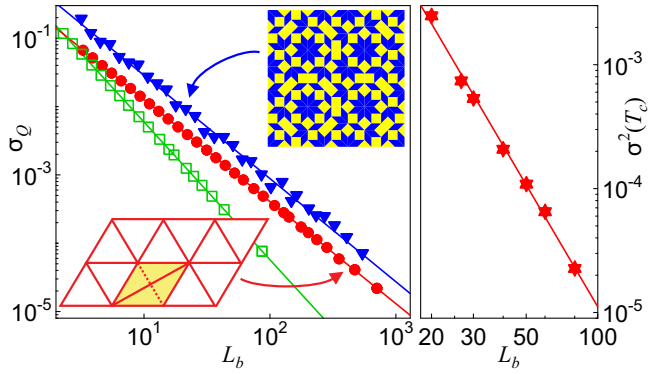

Fig. 4. Left: σ_Q vs. L_b for the Ammann-Beenker tiling (8th generation, 6430084 sites, triangles), a triangular lattice with 50% bond-exchange defects (100 lattices with 2000^2 sites, circles), and a rhombohedral lattice with 50% bond-exchange defects (100 lattices with 300^3 sites, open squares). The lines are power-law fits giving exponents of 1.51(3), 1.498(2), and 2.01(1), respectively. Right: $\sigma^2(T_c)$ vs. L_b for an Ising model on a random Voronoi lattice (100 lattices of 100^2 sites, 10^5 Monte Carlo sweeps each). The line is a fit to $\sigma(T_c) \sim L_b^{-c}$ giving $c = 1.56(7)$.

tiling. For both lattices, the numerical data (Fig. 4) follow $\sigma_Q(L_b) \sim L_b^{-3/2}$ in agreement with (5) [25] Finally, we have studied a 3D rhombohedral lattice with bond-exchange defects. The numerical data are in excellent agreement with the prediction $\sigma_Q(L_b) \sim L_b^{-2}$.

We now use these results to derive the analog of the Harris criterion for many-particle systems on random lattices in our class. Following Harris and Luck [1, 24], we

compare the fluctuations of the local distance from criticality between correlation volumes with the global distance from criticality. If the interactions between the sites are restricted to nearest neighbors and of equal strength, the disorder fluctuations are governed by (5) and decay as $\xi^{-(d+1)/2}$ with correlation length ξ. The global distance from criticality scales as $\xi^{-1/\nu}$. A clean critical point is thus stable if $\xi^{-(d+1)/2} < \xi^{-1/\nu}$ for $\xi \to \infty$. This yields the stability (Harris-Luck) criterion $(d+1)\nu > 2$. The topological disorder is thus less relevant than generic uncorrelated randomness for which the Harris criterion reads $d\nu > 2$.

The Imry-Ma criterion compares the free energy gain due to forming a domain that takes advantage of a disorder fluctuation with the energy cost of the domain wall. In our class of lattices, the gain scales as $L_b^{d\omega} = L_b^{(d-1)/2}$ while the cost of a domain wall scales as L_b^{d-1}. Forming large domains is thus unfavorable in all dimensions $d > 1$ implying that first-order transitions can survive.

The coordination number fluctuations determine the bare (in the renormalization group sense) disorder of the many-particle system. To study an example of disorder renormalizations, we calculate the local critical temperatures T_c of the Ising model, $H = -J \sum_{\langle ij \rangle} S_i S_j$, on a random Voronoi lattice by Monte-Carlo simulations. The right panel of Fig. 4 shows the variance of the block T_c (defined as the maximum of the susceptibility) as a function of block size. The data follow $\sigma(T_c) \sim L_b^{-3/2}$ in agreement with the coordination number. In general, disorder renormalizations can be expected to generate weak uncorrelated disorder even if the bare disorder is anticorrelated [26]. Our results suggest that this uncorrelated disorder, if any, is very weak (as it is invisible on length scales below $L_b \approx 100$) and thus unobservable in most experiments and simulations.

In summary, we have studied the effects of topological disorder on phase transitions. We have identified a broad class of random lattices characterized by strong disorder anticorrelations. Such lattices are ubiquitous in 2D because the Euler equation imposes a topological constraint on the coordination numbers. However, we have also found higher-dimensional realizations. The anticorrelations lead to modifications of the Harris and

Imry-Ma criteria. This explains most of the puzzling apparent failures of the usual criteria discussed in the introduction. Note that another type of anticorrelations was recently found to protect a clean critical point in a quantum spin chain [27]. Moreover, local disorder correlations that change the degree of frustration in a spin glass can qualitatively change its phase diagram [28].

Interestingly, the 3D random Voronoi lattice does not belong to our class of lattices with constraint total coordination. Preliminary numerical results suggest that its coordination number fluctuations decay more slowly than (5) but still faster than the uncorrelated randomness result $L_b^{-d/2}$, at least for blocks with $L_b < 400$. Further work will be necessary to understand the fate of phase transitions on 3D Voronoi lattices.

So far, we have considered systems in which all pairs of neighbors interact equally strongly. If this is not so, e.g., because the interactions depend on the distance between neighboring sites, the disorder anticorrelations are destroyed. The critical behavior is thus expected to cross over to that of uncorrelated disorder. We have explicitly observed this crossover in the contact process [29].

It will be interesting to study transitions that violate even the modified stability criterion $(d+1)\nu > 2$. A prime example is the quantum phase transition of the transverse-field Ising magnet on a 2D random Voronoi lattice. Its clean critical behavior is in the (2+1)D Ising universality class with $\nu \approx 0.630$ and thus violates $(d+1)\nu > 2$. As the anticorrelations strongly suppress the rare region probability [29], we also expect significant modifications of the quantum Griffiths singularities.

This work was supported by the NSF under Grant Nos. DMR-1205803 and PHYS-1066293. We acknowledge the hospitality of the Aspen Center for Physics.

BIBLIOGRAPHY

[1] A. B. Harris. Effect of random defects on the critical behaviour of Ising models. *J. Phys. C*, 7:1671, 1974.

[2] T. Vojta. Rare region effects at classical, quantum, and non-equilibrium phase transitions. *J. Phys. A*, 39:R143, 2006; Quantum Griffiths effects and smeared phase transitions in metals: theory and experiment. *J. Low Temp. Phys.*, 161:299, 2010.

[3] Yoseph Imry and Shang-keng Ma. Random-field instability of the ordered state of continuous symmetry. *Phys. Rev. Lett.*, 35:1399–1401, Nov 1975; Yoseph Imry and Michael Wortis. Influence of quenched impurities on first-order phase transitions. *Phys. Rev. B*, 19:3580–3585, Apr 1979; Kenneth Hui and A. Nihat Berker. Random-field mechanism in random-bond multicritical systems. *Phys. Rev. Lett.*, 62:2507–2510, May 1989; Michael Aizenman and Jan Wehr. Rounding of first-order phase transitions in systems with quenched disorder. *Phys. Rev. Lett.*, 62:2503–2506, May 1989.

[4] If the randomness breaks a continuous symmetry, the marginal dimension is $d = 4$.

[5] Abel Weinrib and B. I. Halperin. Critical phenomena in systems with long-range-correlated quenched disorder. *Phys. Rev. B*, 27:413–427, Jan 1983.

[6] T. Nattermann. Instabilities in ising systems with short- and long-range-correlated quenched random fields. *J. Phys. C*, 16(33):6407, 1983.

[7] Wolfhard Janke and Ramon Villanova. Ising model on three-dimensional random lattices: A Monte Carlo study. *Phys. Rev. B*, 66:134208, Oct 2002.

[8] F.W.S. Lima, U.M.S. Costa, and R.N. Costa Filho. Critical behavior of the 3d Ising model on a poissonian random lattice. *Physica A*, 387(7):1545 – 1550, 2008.

[9] F.W.S. Lima, U.M.S. Costa, M.P. Almeida, and J.S. Andrade Jr. Critical behavior of a three-state Potts model on a Voronoi lattice. *Eur. J. Phys. B*, 17(1):111–114, 2000.

[10] Wolfhard Janke and Ramon Villanova. Two-dimensional eight-state Potts model on random lattices: A Monte Carlo study. *Phys. Lett. A*, 209(3 - 4):179 – 183, 1995.

[11] H. Hinrichsen. Nonequilibrium critical phenomena and phase transitions into absorbing states. *Adv. Phys.*, 49:815, 2000; G. Odor. Universality classes in nonequilibrium lattice systems. *Rev. Mod. Phys.*, 76:663, 2004.

[12] J. Hooyberghs, F. Iglói, and C. Vanderzande. Strong-disorder fixed point in absorbing-state phase transitions. *Phys. Rev. Lett.*, 90:100601, 2003; Absorbing state phase transitions with quenched disorder. *Phys. Rev. E*, 69:066140, 2004.

[13] T. Vojta and M. Dickison. Critical behavior and Griffiths effects in the disordered contact process. *Phys. Rev. E*, 72:036126, 2005; T. Vojta, A. Farquhar, and J. Mast. Infinite-randomness critical point in the two-dimensional disordered contact process. *Phys. Rev. E*, 79:011111, 2009; Thomas Vojta. Monte carlo simulations of the clean and disordered contact process in three dimensions. *Phys. Rev. E*, 86:051137, Nov 2012.

[14] Marcelo M. de Oliveira, S. G. Alves, S. C. Ferreira, and Ronald Dickman. Contact process on a Voronoi triangulation. *Phys. Rev. E*, 78:031133, Sep 2008.

[15] The standard deviation of the coordination number is about 20% of its average in both 2D and 3D.

[16] A. Okabe, B. Boots, K. Sugihara, and S.N. Chiu. *Spatial Tessellations: Concepts and Applications of Voronoi Diagrams*. Wiley, Chichester, 2000.

[17] We use an efficient algorithm inspired by M. Tanemura, T. Ogawa, and N. Ogita. *J. Comp. Phys.*, 51(2):191 – 207, 1983.

[18] This may explain why an earlier study of the random Voronoi lattice, W. Janke and M. Weigel, *Phys. Rev. B*, 69:144208, Apr 2004, reported the uncorrelated randomness result $\sigma_Q \sim d_l^{-1}$.

[19] Other boundary conditions with different values of χ will just produce subleading corrections to our results.

[20] G Le Caer. Topological models of cellular structures. *J. Phys. A*, 24(6):1307, 1991; Topological models of 2d cellular structure. ii. z=5. *J. Phys. A*, 24(19):4655, 1991.

[21] B. Grünbaum and G. C. Shephard. *Tilings and Patterns*. Freeman, New York, 1986.

[22] C. L. Henley. Random tiling models. In P. J. Steinhardt and D. P. Divincenzo, editors, *Quasicrystals: The State of the Art*, pages 459–560. World Scientific, Singapore, 1999.

[23] Laurence J. Shaw, Veit Elser, and Christopher L. Henley. Long-range order in a three-dimensional random-tiling quasicrystal. *Phys. Rev. B*, 43:3423–3433, Feb 1991.

[24] J. M. Luck. A classification of critical phenomena on quasi-crystals and other aperiodic structures. *EPL (Europhysics Letters)*, 24(5):359, 1993.

[25] The results for the Ammann-Beenker tiling were obtained using generic random orientations of the blocks. If square blocks are oriented parallel to the symmetry axes of the tiling, the surface terms in this *nonrandom* lattice add constructively leading to $\sigma_Q(L_b) \sim L_b^{-1}$.

[26] Moshe Schwartz, Jacques Villain, Yonathan Shapir, and Thomas Nattermann. Binary fluids in vycor: Anticorrelated random fields. *Phys. Rev. B*, 48:3095–3099, Aug 1993.

[27] J. A. Hoyos, N. Laflorencie, A. P. Vieira, and T. Vojta. Protecting clean critical points by local disorder correlations. *EPL (Europhysics Letters)*, 93(3):30004, 2011.

[28] E. Ilker and A.N. Berker. Overfrustrated and underfrustrated spin glasses in $d = 3$ and 2: Evolution of phase diagram and chaos including spin glass order in $d = 2$. *Phys. Rev. E*, 89:042139, 2014.

[29] H. Barghathi and T. Vojta. unpublished.

II. RANDOM FIELDS AT A NONEQUILIBRIUM PHASE TRANSITION

Hatem Barghathi and Thomas Vojta

Department of Physics, Missouri University of Science and Technology, Rolla, MO 65409, USA

ABSTRACT [*]

We study nonequilibrium phase transitions in the presence of disorder that locally breaks the symmetry between two equivalent macroscopic states. In low-dimensional equilibrium systems, such "random-field" disorder is known to have dramatic effects: It prevents spontaneous symmetry breaking and completely destroys the phase transition. In contrast, we show that the phase transition of the one-dimensional generalized contact process persists in the presence of random field disorder. The ultraslow dynamics in the symmetry-broken phase is described by a Sinai walk of the domain walls between two different absorbing states. We discuss the generality and limitations of our theory, and we illustrate our results by large-scale Monte-Carlo simulations.

[*]Published in Physical Review Letters **109**, 170603 (2012).

Impurities, defects, and other types of quenched disorder can have drastic effects on the long-time and large-distance behavior of many-particle systems. For example, disorder can modify the universality class of a critical point [1, 2], change a phase transition from first order to continuous [3, 4, 5], or smear a sharp transition over an interval of the tuning parameter [6]. Particularly strong effects arise from disorder that *locally* breaks the symmetry between two equivalent macroscopic states while preserving the symmetry globally (in the statistical sense). As this type of disorder corresponds to a random external field in a magnetic system, it is usually called random-field disorder. Recently, a beautiful example of a random-field magnet was discovered in $LiHo_xY_{1-x}F_4$ [7, 8, 9]. Random-field disorder naturally occurs when the order parameter breaks a *real-space* symmetry such in as nematic liquid crystals in porous media [10] and stripe states in high-temperature superconductors [11].

Imry and Ma [12] discussed random-field effects at equilibrium phase transitions based on an appealing heuristic argument. Consider a uniform domain of linear size L in d space dimensions. The free energy gain due to aligning this domain with the (average) local random field behaves as $L^{d/2}$ while the domain wall energy is of the order of L^{d-1} [13]. For $d < 2$, the system thus gains free energy by forming finite-size domains that align with the random field. In contrast, for $d > 2$, the uniform state is preferred. Building on this work, Aizenman and Wehr [5] proved rigorously that random-field disorder prevents spontaneous symmetry breaking in all dimensions $d \leq 2$ for Ising symmetry and $d \leq 4$ for continuous symmetry. Thus, random fields destroy an equilibrium phase transition in sufficiently low dimensions.

In nature, thermal equilibrium is rather the exception than the rule. Although equilibrium is an excellent approximation for some systems, many others are far from equilibrium and show qualitatively different behaviors. In recent years, phase transitions between different nonequilibrium states have attracted considerable attention. Examples can be found in population dynamics, chemical reactions, growing surfaces, granular flow

as well as traffic jams [14, 15, 16, 17, 18]. It is therefore important to study random-field effects at such nonequilibrium phase transitions. Are these transitions destroyed by random fields just like equilibrium transitions?

In this Letter, we address this question for a prominent class of nonequilibrium phase transitions, *viz.*, absorbing state transitions separating active, fluctuating states from inactive, absorbing states where fluctuations cease entirely. We develop a heuristic argument showing that random-field disorder which locally favors one of two equivalent absorbing states over the other does *not* prevent global spontaneous symmetry breaking in any dimension. The random fields thus do *not* destroy the nonequilibrium transition. In the symmetry-broken phase, the relevant degrees of freedom are domain walls between different absorbing states. Their long-time dynamics is given by a Sinai walk [19] leading to an ultraslow approach to the absorbing state during which the density of domain walls decays as $\ln^{-2}(t)$ with time t (see Fig. 1). We also study the behavior right at the critical point where we find even slower dynamics.

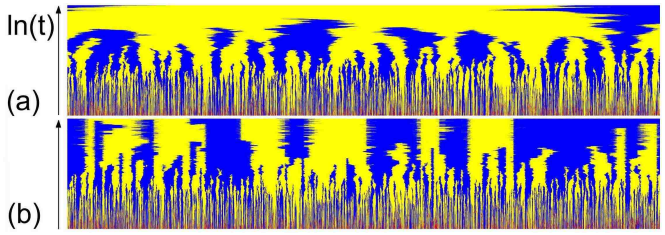

Fig. 1. Time evolution of the generalized contact process in the inactive phase: (a) without ($\mu = 5/6$) and (b) with random-field disorder ($\mu_h = 1, \mu_l = 2/3$). I_1 and I_2 are shown in yellow and blue (light and dark grey). Active sites between the domains are marked in red (middle grey). The difference between the diffusive domain wall motion (a) and the much slower Sinai walk (b) is clearly visible (part of a system of 10^5 sites for times up to 10^8).

In the remainder of the Letter, we sketch the derivation of the results; and we support them by Monte-Carlo simulations. For definiteness, we first consider the generalized contact

process with two absorbing states [20] in one dimension. We later argue that our heuristic argument applies to an entire class of absorbing state transitions.

The (simple) contact process [21] is a prototypical model featuring an absorbing state transition. Each site of a d-dimensional hypercubic lattice is either in the active (infected) state A or in the inactive (healthy) state I. The time evolution is a continuous-time Markov process with infected sites healing at a rate μ while healthy sites become infected at a rate $\lambda m/(2d)$ where m is the number of infected nearest neighbors. The long-time behavior is governed by the ratio of λ and μ. If $\mu \gg \lambda$, healing dominates over infection, and all sites will eventually be healthy. The absorbing state without any infected sites is thus the only steady state. For $\lambda \gg \mu$, the infection never dies out, leading to an active steady state with nonzero density of infected sites. The absorbing and active steady states are separated by a nonequilibrium transition in the directed percolation (DP) [22] universality class.

Following Hinrichsen [20], we generalize the contact process by allowing each site to be in one of $n + 1$ states, the active state A or one of n inactive states I_k ($k = 1 \ldots n$). The time evolution of the generalized contact process (GCP) is conveniently defined [20] via the transition rates for pairs of nearest-neighbor sites,

$$w(AA \to AI_k) = w(AA \to I_k A) = \bar{\mu}_k/n\,, \tag{1}$$

$$w(AI_k \to I_k I_k) = w(I_k A \to I_k I_k) = \mu_k\,, \tag{2}$$

$$w(AI_k \to AA) = w(I_k A \to AA) = \lambda\,, \tag{3}$$

$$w(I_k I_l \to I_k A) = w(I_k I_l \to A I_l) = \sigma\,, \tag{4}$$

with $k, l = 1 \ldots n$ and $k \neq l$. All other rates vanish. The GCP defined by (1) to (4) reduces to the simple contact process if we set $n = 1$ and $\bar{\mu}_k = \mu_k = \mu$ (up to rescaling all rates by the same constant factor [23]). The transition (4) permits competition between different inactive states as it prevents different domains from sticking together. Instead, they can

separate, and the domain walls can move. We now set $\bar{\mu}_k = \mu_k$ and $\lambda = \sigma = 1$ to keep the parameter space manageable [24]. This also fixes the time unit. Moreover, we focus on $d = 1$ and $n = 2$.

The long-time behavior again follows from comparing the infection rate λ with the healing rates μ_1 and μ_2. Consider two equivalent inactive states, $\mu_1 = \mu_2 = \mu$. For small μ, the system is in the active phase with nonzero density of infected sites. In this fluctuating phase, the symmetry between the two inactive states I_1 and I_2 is not broken, i.e., their occupancies are identical. If μ is increased beyond $\mu_c^0 \approx 0.628$ [20, 25], the system undergoes a nonequilibrium phase transition to one of the two absorbing steady states (either all sites in state I_1 or all in state I_2). At this transition, the symmetry between I_1 and I_2 is *spontaneously* broken. Its critical behavior is therefore not in the DP universality class but in the so-called DP2 class which, in $d = 1$, coincides with the parity conserving (PC) class [26]. If $\mu_1 \neq \mu_2$, one of the two inactive states dominates for long times, and the critical behavior reverts back to DP.

We introduce quenched (time-independent) disorder by making the healing rates $\mu_k(\mathbf{r})$ at site $\mathbf{r}$ independent random variables governed by a probability distribution $W(\mu_1, \mu_2)$. As we are interested in random-field disorder which locally breaks the symmetry between I_1 and I_2, we choose $\mu_1(\mathbf{r}) \neq \mu_2(\mathbf{r})$. Globally, the symmetry is preserved in the statistical sense implying $W(\mu_1, \mu_2) = W(\mu_2, \mu_1)$. An example is the correlated binary distribution

$$W(\mu_1, \mu_2) = \frac{1}{2}\delta(\mu_1 - \mu_h)\delta(\mu_2 - \mu_l) + \frac{1}{2}\delta(\mu_1 - \mu_l)\delta(\mu_2 - \mu_h) \tag{5}$$

with possible local healing rate values μ_h or μ_l [27].

To address our main question, namely whether the random-field disorder prevents the spontaneous breaking of the global symmetry between the two inactive states and thus destroys the nonequilibrium transition, we analyze the large-μ regime where all healing rates are larger than the clean critical value μ_c^0. In this regime, almost all sites quickly decay

into one of the two inactive states I_1 or I_2. The relevant long-time degrees of freedom are domain walls between I_1 and I_2 domains. They move via a combination of process (4) which creates an active site at the domain wall and process (2) which allows this active site to decay into either I_1 or I_2. Because of the disorder, the resulting domain wall hopping rates depend on the site $\mathbf{r}$. Importantly, the rates for hopping right and left are different because the underlying healing rates $\mu_1(\mathbf{r})$ and $\mu_2(\mathbf{r})$ are not identical.

The long-time dynamics in the large-μ regime is thus governed by a random walk of the domain walls. Due to the local left-right asymmetry, this random walk is not a conventional (diffusive) walk but a Sinai walk [29]. The typical displacement of a Sinai walker grows as $\ln^2(t/t_0)$ with time t [19] (t_0 is a microscopic time scale), more slowly than the well-known $t^{1/2}$ law for a conventional walk (see Fig. 1). When two neighboring domain walls meet, they annihilate, replacing three domains by a single one. Domain walls surviving at time t thus have a typical distance proportional to $\ln^2(t/t_0)$. The domains grow without limit, and their density decays as $\ln^{-2}(t/t_0)$. In the long-time limit, the system reaches a single-domain state, i.e., either all sites are in state I_1 or all in I_2. This implies that the symmetry between I_1 and I_2 is spontaneously broken (which of the two absorbing states the system ends up in depends on details of the initial conditions and of the stochastic time evolution). The nonequilibrium transition consequently persists in the presence of random-field disorder.

It is important to contrast the domain wall dynamics in our system with that of a corresponding equilibrium problem such as the random-field Ising chain (whose low-temperature state consists of domains of up and down spins [30]. The crucial difference is that the inactive states I_1 and I_2 in our system are absorbing: Active sites and new domain walls never arise in the interior of a domain. In contrast, inside a uniform domain of the random-field Ising chain, a spin flip (which creates two new domain walls) can occur anywhere due to a thermal fluctuation. This mechanism limits the growth of the typical

domain size to its equilibrium value dictated by the Imry-Ma argument [12], and thus prevents spontaneous symmetry breaking.

To verify these heuristic arguments and to illustrate the results, we perform Monte-Carlo simulations [25] of the one-dimensional GCP with random-field disorder. We use system sizes up to $L = 10^5$ and times up to $t = 2 \times 10^8$. The random-field disorder is implemented via the distribution (5) with $1.5\mu_l = \mu_h \equiv \mu$. Our simulations start from a fully active lattice (all sites in state A), and we monitor the density ρ of active sites as well as the densities ρ_1 and ρ_2 of sites in the inactive states I_1 and I_2, respectively. Figure 2 presents an overview of the time evolution of the density ρ.

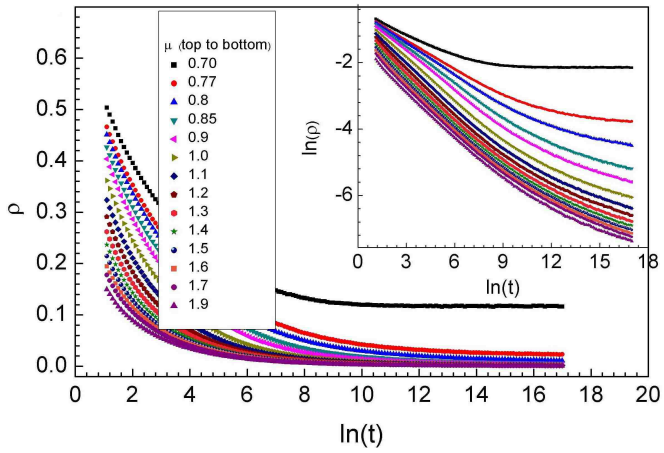

Fig. 2. Density ρ vs. time t for several values of the healing rate μ. The data are averages over 60 to 200 disorder configurations. Inset: The log-log plot shows that the density decay is slower than a power law for all μ.

We now focus on the curves with healing rates $\mu \gtrsim 1.0$ for which both $\mu_h = \mu$ and $\mu_l = 2\mu/3$ are larger than the clean critical value μ_c^0. The inset of Fig. 2 shows that the density continues to decay to the longest times studied for all these curves. However, the decay is clearly slower than a power law. To compare with our theoretical arguments, we note that active sites only exist near domain walls in the large-μ regime. We thus expect the density of active sites to be proportional to the domain wall density, yielding $\rho \sim \ln^{-2}(t/t_0)$.

To test this prediction we plot $\rho^{-1/2}$ vs. $\ln(t)$ in Fig. 3; in such a graph the expected behavior corresponds to a straight line. The figure shows that all curves with $\mu > 1$ indeed follow

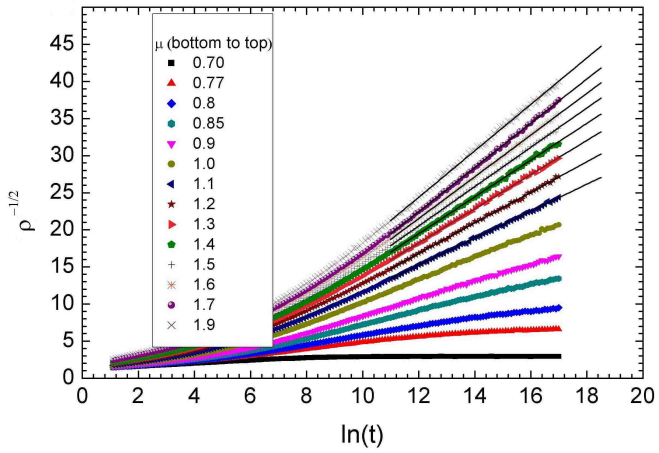

Fig. 3. $\rho^{-1/2}$ vs. $\ln(t)$ for several values of the healing rate μ. The solid straight lines are fits to the predicted behavior $\rho \sim \ln^{-2}(t/t_0)$.

the prediction over several orders of magnitude in time.

In addition to the inactive phase, we also study the critical point. To identify the critical healing rate μ_c, we extrapolate to zero both the stationary density $\rho_{st} = \lim_{t\to\infty} \rho(t)$ in the active phase and the inverse prefactor of the $\ln^{-2}(t/t_0)$ decay in the inactive phase. This yields $\mu_c \approx 0.80$ (see inset of Fig. 4). At this healing rate, the density decay is clearly slower than the $\ln^{-2}(t/t_0)$ law governing the inactive phase. This extremely slow decay and the uncertainty in μ_c prevent us from determining the functional form of the critical $\rho(t)$ curve unambiguously. If we assume a time dependence of the type $\rho(t) \sim \ln^{-x}(t/t_0)$ we find a value of $x \approx 0.5$. Moreover, from the dependence of the stationary density on the healing rate, $\rho_{st} \sim (\mu_c - \mu)^{\beta}$, we obtain $\beta \approx 1.5$. The values of x and β should be considered rough estimates. An accurate determination of the critical behavior of the GCP with random-field disorder requires a significantly larger numerical effort and remains a task for the future.

In summary, we have shown that the nonequilibrium phase transition of the one-dimensional GCP survives in the presence of random-field disorder, in contrast to one-dimensional equilibrium transitions that are destroyed by random fields. In the concluding paragraphs, we discuss the generality and limitations of our results.

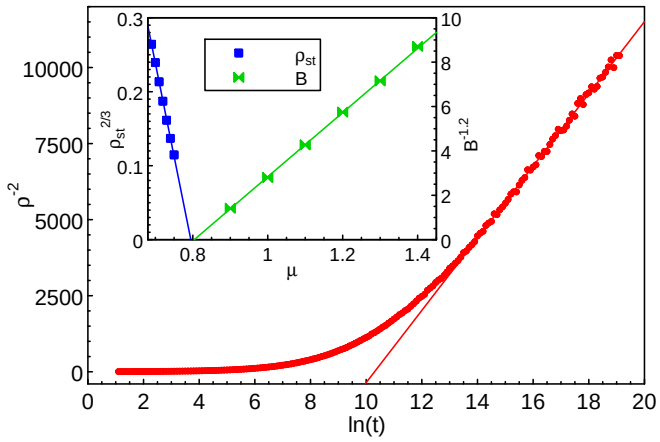

Fig. 4. Density vs. time at the critical healing rate $\mu_c = 0.8$, plotted as $\rho^{-1/x}$ vs. $\ln(t)$ with $x = 0.5$. The solid line is a fit to $\rho(t) \sim \ln^{-x}(t/t_0)$. Inset: Identifying μ_c from the stationary density ρ_{st} in the active phase and the prefactor of the $\rho = B \ln^{-2}(t/t_0)$ decay in the inactive phase.

The crucial difference between random-field effects in equilibrium systems such as the random-field Ising chain and in the GCP is the absorbing character of the inactive states I_1 and I_2 in the latter. The interior of an I_1 or I_2 domain is "dead" as no active sites and no new domain walls can ever arise there. In contrast, in an equilibrium system, pairs of new domain walls can appear in the interior of a uniform domain via a thermal fluctuation. This limits the growth of the typical domain size to the Imry-Ma equilibrium size and thus destroys the equilibrium transition (in sufficiently low dimensions). We expect our results to hold for all nonequilibrium phase transition at which the random-field disorder locally breaks the symmetry between two *absorbing* states. Other nonequilibrium transitions may

behave differently. For example, our theory does *not* apply if the random fields break the symmetry between two active states.

In the symmetry-broken inactive phase, the dynamics of the GCP with random-field disorder is ultraslow. It is governed by the Sinai random walk of domain walls between the two inactive states. This leads to a logarithmic time decay of the densities of both domain walls and active sites. Note that the Sinai coarsening dynamics has been studied in detail in the equilibrium random-field Ising chain [31] where it applies to a transient time regime before the domains reach the Imry-Ma equilibrium size.

Although our explicit results are for one dimension, we expect our main conclusion to hold in higher dimensions, too. In the interior of a uniform domain of an absorbing state, new active site (and new domain walls) cannot arise in any dimension. Moreover, the Imry-Ma mechanism by which the random fields destroy an equilibrium transition becomes less effective in higher dimensions. Indeed, Pigolotti and Cencini [32] report spontaneous symmetry breaking in a model of two species competing in a two-dimensional landscape with local habitat preferences. To further study this question, we plan to introduce random fields into our simulations of the two-dimensional GCP [33].

Finally, we turn to experiments. Although clear-cut realizations of absorbing state transitions were lacking for a long time [34], beautiful examples were recently found in turbulent liquid crystals [35], driven suspensions [36, 37], and superconducting vortices [38]. As they are far from equilibrium, biological systems are promising candidates for observing nonequilibrium transitions. A transition in the DP2 universality class (as studied here) occurs in a model of competing bacteria strains [39] which accurately describes experiments in colony biofilms [40]. Random-field disorder could be realized in such experiments by environments that locally favor one strain over the other.

We thank M. Muñoz and G. Odor for helpful discussions. This work has been supported by the NSF under Grant Nos. DMR-0906566 and DMR-1205803.

BIBLIOGRAPHY

[1] A. B. Harris and T. C. Lubensky. *Phys. Rev. Lett.*, 33:1540, 1974.

[2] G. Grinstein and A. Luther. *Phys. Rev. B*, 13:1329, 1976.

[3] Yoseph Imry and Michael Wortis. Influence of quenched impurities on first-order phase transitions. *Phys. Rev. B*, 19:3580–3585, Apr 1979.

[4] Kenneth Hui and A. Nihat Berker. Random-field mechanism in random-bond multicritical systems. *Phys. Rev. Lett.*, 62:2507–2510, May 1989.

[5] Michael Aizenman and Jan Wehr. Rounding of first-order phase transitions in systems with quenched disorder. *Phys. Rev. Lett.*, 62:2503–2506, May 1989.

[6] T. Vojta. Disorder-induced rounding of certain quantum phase transitions. *Phys. Rev. Lett.*, 90:107202, 2003; Smearing of the phase transition in Ising systems with planar defects. *J. Phys. A*, 36:10921, 2003; Broadening of a nonequilibrium phase transition by extended structural defects. *Phys. Rev. E*, 70:026108, 2004.

[7] S. M. A. Tabei, M. J. P. Gingras, Y.-J. Kao, P. Stasiak, and J.-Y. Fortin. Induced random fields in the $LiHo_xY_{1-x}F_4$ quantum ising magnet in a transverse magnetic field. *Phys. Rev. Lett.*, 97(23):237203, 2006.

[8] D. M. Silevitch, D. Bitko, J. Brooke, S. Ghosh, G. Aeppli, and T. F. Rosenbaum. A ferromagnet in a continuously tunable random field. *Nature*, 448:567, 2007.

[9] Moshe Schechter. $Liho_xy_{1-x}f_4$ as a random-field ising ferromagnet. *Phys. Rev. B*, 77(2):020401, 2008.

[10] Amos Maritan, Marek Cieplak, Tommaso Bellini, and Jayanth R. Banavar. Nematic-isotropic transition in porous media. *Phys. Rev. Lett.*, 72:4113–4116, Jun 1994.

[11] E. W. Carlson, K. A. Dahmen, E. Fradkin, and S. A. Kivelson. Hysteresis and noise from electronic nematicity in high-temperature superconductors. *Phys. Rev. Lett.*, 96:097003, Mar 2006.

[12] Yoseph Imry and Shang-keng Ma. Random-field instability of the ordered state of continuous symmetry. *Phys. Rev. Lett.*, 35:1399–1401, Nov 1975.

[13] This holds for discrete symmetry. For continuous symmetry the surface energy behaves as L^{d-2} resulting in a marginal dimension of 4.

[14] B. Schmittmann and R. K. P. Zia. Statistical mechanics of driven diffusive systems. In C. Domb and J. L. Lebowitz, editors, *Phase Transitions and Critical Phenomena*, volume 17, page 1. Academic, New York, 1995.

[15] J. Marro and R. Dickman. *Nonequilibrium Phase Transitions in Lattice Models*. Cambridge University Press, Cambridge, 1999.

[16] H. Hinrichsen. Nonequilibrium critical phenomena and phase transitions into absorbing states. *Adv. Phys.*, 49:815, 2000.

[17] G. Odor. Universality classes in nonequilibrium lattice systems. *Rev. Mod. Phys.*, 76:663, 2004.

[18] U. C. Täuber, M. Howard, and B. P. Vollmayr-Lee. Applications of field-theoretic renormalization group methods to reaction-diffusion problems. *J. Phys. A*, 38:R79, 2005.

[19] F. Solomon. Random walks in random environment. *Ann. Prob.*, 3:1, 1975; H. Kesten, M. Kozlov, and F. Spitzer. A limit law for random walk in a random environment. *Compositio Math.*, 30:145, 1975; Y. G. Sinai. Limit behaviour of one-dimensional random walks in random environments. *Theor. Probab. Appl.*, 27:256, 1982.

[20] H. Hinrichsen. Stochastic lattice models with several absorbing states. *Phys. Rev. E*, 55:219, 1997.

[21] T. E. Harris. Contact interactions on a lattice. *Ann. Prob.*, 2:969, 1974.

[22] P. Grassberger and A. de la Torre. *Ann. Phys. (NY)*, 122:373, 1979.

[23] The rescaling factor is the number of nearest-neighbor pairs a site belongs to; for a hypercubic lattice it is $2d$.

[24] According to Ref. [25], the qualitative behavior for $\bar{\mu}_k \neq \mu_k$ is identical to that for $\bar{\mu}_k = \mu_k$. Moreover, the precise value of σ is not important as long as it is nonzero.

[25] M. Y. Lee and T. Vojta. Phase transitions of the generalized contact process with two absorbing states. *Phys. Rev. E*, 81:061128, 2010.

[26] P. Grassberger, F. Krause, and T. von der Twer. A new type of kinetic critical phenomenon. *J. Phys. A*, 17:L105, 1984.

[27] Other disorder types can lead to different behaviors [28].

[28] G. Odor and N. Menyhard. Critical behavior of an even-offspringed branching and annihilating random-walk cellular automaton with spatial disorder. *Phys. Rev. E*, 73:036130, 2006, Nóra Menyhárd and Géza Ódor. One-dimensional spin-anisotropic kinetic ising model subject to quenched disorder. *Phys. Rev. E*, 76:021103, Aug 2007.

[29] Because our model preserves the global symmetry between I_1 and I_2, the Sinai walk is unbiased.

[30] In this analogy, we relate the ordered spin-up and spin-down states of the random-field Ising chain to the two absorbing states of the GCP.

[31] D. S. Fisher, P. Le Doussal, and C. Monthus. Random walks, reaction-diffusion, and nonequilibrium dynamics of spin chains in one-dimensional random environments. *Phys. Rev. Lett*, 80:3539, 1998; *Phys. Rev. E*, 64:066107, 2001.

[32] S. Pigolotti and M. Cencini. Coexistence and invasibility in a two-species competition model with habitat-preference. *J. Theor. Biology*, 265:609, 2010.

[33] Man Young Lee and Thomas Vojta. Generalized contact process with two symmetric absorbing states in two dimensions. *Phys. Rev. E*, 83:011114, Jan 2011.

[34] H. Hinrichsen. On possible experimental realizations of directed percolation. *Braz. J. Phys.*, 30:69, 2000.

[35] K. A. Takeuchi, M. Kuroda, H. Chate, and M. Sano. Directed percolation criticality in turbulent liquid crystals. *Phys. Rev. Lett.*, 99:234503, 2007.

[36] L. Corte, P. M. Chaikin, J. P. Gollub, and D. J. Pine. Random organization in periodically driven systems. *Nature Physics*, 4:420, 2008.

[37] Alexandre Franceschini, Emmanouela Filippidi, Elisabeth Guazzelli, and David J. Pine. Transverse alignment of fibers in a periodically sheared suspension: An absorbing phase transition with a slowly varying control parameter. *Phys. Rev. Lett.*, 107:250603, Dec 2011.

[38] S. Okuma, Y. Tsugawa, and A. Motohashi. Transition from reversible to irreversible flow: Absorbing and depinning transitions in a sheared-vortex system. *Phys. Rev. B*, 83:012503, Jan 2011.

[39] K. S. Korolev and David R. Nelson. Competition and cooperation in one-dimensional stepping-stone models. *Phys. Rev. Lett.*, 107:088103, Aug 2011.

[40] K. S. Korolev, Joao B. Xavier, David R. Nelson, and Kevin R. Foster. A quantitative test of population genetics using spatiogenetic patterns in bacterial colonies. *The American Naturalist*, 178:538, 2011.

III. RANDOM FIELD DISORDER AT AN ABSORBING STATE TRANSITION IN ONE AND TWO DIMENSIONS

Hatem Barghathi and Thomas Vojta

Department of Physics, Missouri University of Science and Technology, Rolla, MO 65409, USA

ABSTRACT[*]

We investigate the behavior of nonequilibrium phase transitions under the influence of disorder that locally breaks the symmetry between two symmetrical macroscopic absorbing states. In equilibrium systems such "random-field" disorder destroys the phase transition in low dimensions by preventing spontaneous symmetry breaking. In contrast, we show here that random-field disorder fails to destroy the nonequilibrium phase transition of the one- and two-dimensional generalized contact process. Instead, it modifies the dynamics in the symmetry-broken phase. Specifically, the dynamics in the one-dimensional case is described by a Sinai walk of the domain walls between two different absorbing states. In the two-dimensional case, we map the dynamics onto that of the well studied low-temperature random-field Ising model. We also study the critical behavior of the nonequilibrium phase transition and characterize its universality class in one dimension. We support our results by large-scale Monte Carlo simulations, and we discuss the applicability of our theory to other systems.

[*]Published in Physical Review E **93**, 022120 (2016).

I. INTRODUCTION

The effects of quenched disorder on phase transitions can be drastic. For example, disorder can change the universality class of a continuous phase transition [1, 2], destroy it by smearing [3], or round a first-order phase transition [4, 5, 6]. In particular, disorder that *locally* breaks the symmetry between two equivalent macroscopic states while preserving the symmetry globally (in the statistical sense) has strong effects on phase transitions. This type of disorder is usually called random-field disorder as it corresponds to a random external field in a magnetic system. An experimental realization of a random-field magnet was recently found in $LiHo_xY_{1-x}F_4$ [7, 8, 9]; in this system, random fields arise from the interplay of dilution, dipolar interactions, and a transverse magnetic field. Moreover, impurities and vacancies generically generate random-field disorder if the order parameter of the phase transition breaks a *real-space* symmetry. Such behavior occurs, e.g., in nematic liquid crystals in porous media [10] and stripe states in high-temperature superconductors [11].

Random-field disorder at equilibrium phase transitions was discussed by Imry and Ma [12]. Their argument can be summarized as follows. Consider a domain of one state embedded in a larger domain of the competing state. The formation of the domain requires a domain wall with a free energy cost of the order of the domain wall area, i.e., L^{d-1} [13], where L is the linear size of the embedded domain and d is the space dimension. In contrast, the average free energy gain due to aligning the embedded domain with the prevailing local random-field is of the order of $L^{d/2}$ as follows from the central limit theorem. Consequently, in $d > 2$ the system gains free energy by increasing the size of the domain without limit. On the other hand, for $d < 2$, the system prefers forming domains of a limited size. Based on this heuristic argument, Aizenman and Wehr [6] provided a rigorous proof that in all dimensions $d \leq 2$ ($d \leq 4$), random-field disorder prevents spontaneous symmetry breaking

for discrete (continuous) symmetry. Thus, equilibrium phase transitions in sufficiently low dimensions are destroyed by random-field disorder.

Recently, nonequilibrium phase transition between different steady states have attracted lots of attention. Analogous to equilibrium phase transitions, these transitions are characterized by large-scale fluctuations and collective behavior over large distance and long times. Examples include surface growth, granular flow, chemical reactions, spreading of epidemics, population dynamics and traffic jams [14, 15, 16, 17, 18]. The effects of so-called random-mass disorder, i.e., disorder that spatially modifies the tendency toward one phase or the other without breaking any symmetries, on nonequilibrium phase transitions have been studied in some detail. They turn out to be similar to the effects on classical and quantum equilibrium phase transitions, and include infinite-randomness criticality, Griffiths singularities, and smearing (see, e.g., Ref. [19] and references therein). This similarity remains true even in the case of long-range correlated random-mass disorder [20] and for topological disorder with long-range correlations [21]. Accordingly, it is important to investigate the effects of random fields on nonequilibrium phase transitions. Does an analog of the Aizenman-Wehr theorem also hold for nonequilibrium phase transitions?

To address this question, we study in this paper the generalized contact process (GCP) with two symmetric inactive states in one and two space dimensions. In the GCP, the nonequilibrium phase transition occurs between an active fluctuating phase and an inactive absorbing phase in which the system ends up in one of the inactive states, and all fluctuations cease entirely. Random-field disorder is introduced via transition rates that locally prefer one of the two competing absorbing states over the other. By studying the dynamics of the relevant degrees of freedom in the absorbing phase, which are domain walls between the two inactive states, we show that the competition between the two types of domains still ends with the system reaching one of the two absorbing states. This means that random field disorder does not destroy the absorbing state phase transition.

The dynamics of the system in the inactive phase can be mapped onto that of a low-temperature random-field Ising system. In one space dimension, the long-time dynamics of the domain walls is given by a Sinai walk resulting in an ultraslow decay toward the absorbing state where the density of domain walls decays as $\ln^{-2}(t)$ (see Fig. 1). In $d \geq 2$, the domain size asymptotically increases logarithmically with time. This leads to a slower decay of the domain walls density, $\ln^{-1}(t)$, than in the one-dimensional case. We also investigate the critical behavior of the phase transition between the active and inactive phases in one space dimension. At the critical point, the dynamics is even slower than in the inactive phase. We support our theoretical findings by performing large-scale Monte Carlo simulations of this model in one and two space dimensions.

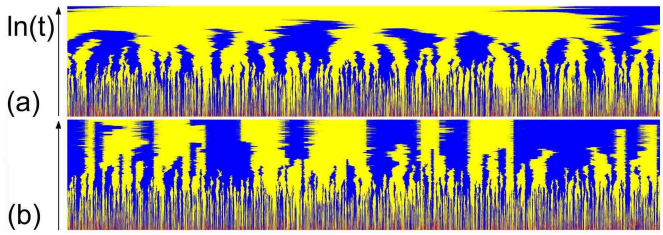

Fig. 1. Time evolution of the GCP in the inactive phase: (a) without ($\mu = 5/6$) and (b) with random-field disorder ($\mu_h = 1, \mu_l = 2/3$). I_1 and I_2 are shown in yellow and blue (light and dark gray). Active sites between the domains are marked in red (midtone gray). The difference between the diffusive domain wall motion (a) and the much slower Sinai walk (b) is clearly visible (part of a system of 10^5 sites for times up to 10^8).

This paper is organized as follows. We introduce the GCP with several absorbing states and random-field disorder in Sec. II. In Secs. III and IV we present our theory and Monte Carlo simulation results, respectively. We conclude in Sec. V. A short account of part of this work was already published in Ref. [22].

II. GENERALIZED CONTACT PROCESS AND RANDOM-FIELD DISORDER

First, we define the simple contact process [23], which is a prototypical model of a nonequilibrium phase transition. Every site $\mathbf{r}$ of a d-dimensional hypercubic lattice can either be in the active state A or in the inactive state I. As time evolves, inactive sites can be activated by their active nearest neighbors at a rate $\lambda m/(2d)$, where m is the number of active nearest neighbors, while active sites can spontaneously become inactive at a decay rate of μ. The behavior of the system is then determined by the ratio of the activation rate λ to the decay rate μ. It controls a nonequilibrium continuous phase transition between an active phase and an absorbing (inactive) phase, which is in the directed percolation (DP) [24] universality class. If $\lambda \gg \mu$, the activation process survives in an infinite system for infinite times, i.e., the system reaches a steady state in which the density of active sites is nonzero, defining the active phase. In the opposite case, $\lambda \ll \mu$, all the sites in the system eventually become and remain inactive, i.e., the system will reach a state that it cannot escape, with zero density of active sites, defining the absorbing (inactive) phase.

In the GCP introduced by Hinrichsen [25], each site can be in an active state A or in one of n inactive states I_k ($k = 1 \ldots n$). We define the time evolution of the GCP through the transition rates of pairs of nearest neighbors as follows:

$$w(AA \to AI_k) = w(AA \to I_k A) = \bar{\mu}_k/n\,, \tag{1}$$

$$w(AI_k \to I_k I_k) = w(I_k A \to I_k I_k) = \mu_k\,, \tag{2}$$

$$w(AI_k \to AA) = w(I_k A \to AA) = \lambda\,, \tag{3}$$

$$w(I_k I_l \to I_k A) = w(I_k I_l \to A I_l) = \sigma\,, \tag{4}$$

with $k, l = 1 \ldots n$ and $k \neq l$ (all other rates are zero). For $n = 1$ and $\bar{\mu}_k = \mu_k = \mu$, we retrieve the simple contact process with a proper rescaling of the parameters. The boundary activation rate σ generates activity at the boundary between domains of different inactive

states. This limits the number of absorbing macroscopic states to that of the inactive microscopic states n. In other words, the boundary activation rate σ defined by (4) prevents the trapping of the system in an inactive macroscopic state unless all sites are in the same inactive microscopic state. Without loss of generality, one can chose the time unit such that one of the rates equals unity, so we set $\sigma = 1$. Moreover, to keep the parameter space manageable, we set $\bar{\mu}_k = \mu_k$ and $\lambda = \sigma = 1$ [26], unless otherwise mentioned. In the following, our focus will be on $n = 2$ and dimensions $d = 1, 2$.

Consider the symmetric case, in which the decay rates toward the two inactive states I_1 and I_2 are equal, $\mu_1 = \mu_2 = \mu$. If μ is small enough (active phase), the system eventually reaches a steady state with nonzero density of active sites ρ. In this phase, the symmetry between I_1 and I_2 is not broken, since both states have identical occupation probabilities. In the opposite limit where μ is increased beyond the critical point μ_c^0 ($\mu_c^0 \approx 0.628$ for $d = 1$ and $\mu_c^0 \approx 1.000$ for $d = 2$ [25, 27, 28]) the system undergoes a nonequilibrium phase transition to an absorbing state with all sites either in state I_1 or all in state I_2, resulting in a spontaneous breaking of the symmetry between I_1 and I_2. Therefore, the critical behavior of the transition is not in the DP universality class but in the parity conserving (PC) universality class for $d = 1$ [25, 27, 29] and in the generalized voter (GV) universality class for $d = 2$ [28, 30, 31, 32]. In the asymmetric case, $\mu_1 \neq \mu_2$, the favored inactive state will asymptotically play the dominant role, and the critical behavior reverts back to the DP universality class.

To introduce random-field disorder, we need to break the symmetry between I_1 and I_2 locally. Therefore, we make $\mu_1(\mathbf{r})$ and $\mu_2(\mathbf{r})$, the decay rates at site $\mathbf{r}$ toward I_1 and I_2 respectively, independent random variables drawn from a probability distribution $W(\mu_1, \mu_2)$. A sufficient condition to preserve the symmetry globally (in the statistical sense) is $W(\mu_1, \mu_2) = W(\mu_2, \mu_1)$. Accordingly, the random variable $\alpha(\mathbf{r}) = \ln[\mu_2(\mathbf{r})/\mu_1(\mathbf{r})]$

has a symmetric probability distribution, $w(\alpha) = w(-\alpha)$. The value of α provides a dimensionless measure of the broken symmetry. The binary distribution

$$W(\mu_1, \mu_2) = \frac{1}{2}\delta(\mu_1 - \mu_h)\delta(\mu_2 - \mu_l) + \frac{1}{2}\delta(\mu_1 - \mu_l)\delta(\mu_2 - \mu_h) \tag{5}$$

is an example, where μ_h or μ_l are the possible local decay rate values. The corresponding random variable α has the symmetric probability distribution

$$W(\alpha) = \frac{1}{2}\delta(\alpha + \alpha_0) + \frac{1}{2}\delta(\alpha - \alpha_0), \tag{6}$$

where $\alpha_0 = \ln(\mu_h/\mu_l)$.

III. THEORY

A. Overview

Let us consider the GCP in the presence of binary random-field disorder defined by (5). If the boundary activation process is turned off ($\sigma = 0$), the difference between the two inactive states (I_1 , I_2) is no longer dynamically relevant, i.e., the system is in an inactive macroscopic state if each site is in any of the two inactive states (I_1 , I_2). In this case, the dynamics of the system is identical to that of the simple contact process with an effective decay rate $\mu_{eff} = \mu_h + \mu_l$. This results in a continuous phase transition between an active phase and an absorbing phase in which the system ends up in random combination of the states I_1 and I_2. Turning on the boundary activation rate ($\sigma > 0$) favors the active phase. Moreover, the only two inactive macroscopic states are those in which all sites of the system are in the same inactive state, either I_1 or I_2 (symmetry-broken phase). In this case, the question regarding the survival of the phase transition in the presence of random-field disorder is equivalent to asking whether a symmetry-broken phase exists if $\mu_h \neq \mu_l$.

To address this question, we consider the large-μ regime where all decay rates are much larger than the clean critical value μ_c^0. In this regime the decay processes (1) and (2) dominate over the activation process (3). In an initially active system, almost all sites quickly decay into one of the two inactive states I_1 and I_2. As a result, the system consists of a combination of domains of states I_1 and I_2. However, the domain walls can move as a result of a boundary activation process (4) followed quickly by a decay process (2) which results in the original site being in a different inactive state. The domain wall hopping rate at site $\mathbf{r}$ thus depends on the decay rates $\mu_1(\mathbf{r})$ and $\mu_2(\mathbf{r})$ which are random. Consequently, the left-right ($d = 1$) symmetry of the hopping rates is locally broken. However, their symmetry is preserved globally in a statistical sense because $W(\mu_1, \mu_2) = W(\mu_2, \mu_1)$. The resulting random walk of the domain walls with random hopping rates governs the dynamics of the system in the large-μ regime and long-time limit.

B. One space dimension, $d = 1$

A one-dimensional random walk with random hopping rates is a well-studied mathematical problem and is known as the Sinai walk [33]. The typical displacement of a Sinai walker grows as $[\ln(t/t_0)]^{1/\psi_i}$ with time t where $\psi_i = 1/2$. Here, t_0 is a microscopic time scale, and we use a subscript i on the exponent ψ to mark the inactive phase. This is much slower than the $t^{1/2}$ law of the conventional random walk (see Fig. 1). When two neighboring domain walls run into each other, they annihilate, resulting in a single domain instead of three domains. The typical distance between domain walls surviving at time t is therefore proportional to $[\ln(t/t_0)]^{1/\psi_i}$. Correspondingly, the density of surviving domains decays as $[\ln(t/t_0)]^{-1/\psi_i}$. As the domains grow without limit, eventually the symmetry between I_1 and I_2 will be spontaneously broken when a single domain dominates the entire system, i.e., all sites are in the same inactive state, either I_1 or I_2. The initial conditions and the details of the stochastic time evaluation of the system determine which of the two absorbing states will be the fate of the system. The existence of a symmetry broken phase

implies the persistence of the nonequilibrium transition in the presence of random-field disorder.

The time evolution of the density of active sites can also be estimated from the Sinai walk. In the large-μ regime, active sites can only exist in the vicinity of domain walls as a result of the boundary activation process. This implies that, asymptotically, the density of active sites ρ is proportional to the density of the domain walls. Thus we expect that

$$\rho(t) \sim [\ln(t/t_0)]^{-\bar{\alpha}_i} \tag{7}$$

with $\bar{\alpha}_i = 1/\psi_i = 2$. We have introduced the decay exponent $\bar{\alpha}_i$ in analogy to the critical density decay exponent α, i stands for the inactive phase, as above, and the bar corresponds to a logarithmic rather than a power-law time dependence.

To emphasize the importance of the absorbing nature of the inactive states (I_1, I_2) and its role in the survival of the nonequilibrium phase transition in the presence of a random-field disorder, we compare the domain wall dynamics in our system with that of an analogous equilibrium system, namely the random-field Ising chain.

At sufficiently low temperatures the macroscopic state of the random-field Ising model consists of domains of up and down spins. The domain wall dynamics in the random-field Ising chain is analogous to that of our system. In fact, the hopping rates of the domain walls in the two systems can be mapped onto each other, as we show in Appendix A. However, in the random-field Ising chain there is an additional process: A spin inside a domain of spin up (down) can flip down (up) due to a thermal fluctuation. This process breaks the original domain by creating two new domain walls inside it. As a result of such processes, the growth of a typical domain size is limited, preventing spontaneous symmetry breaking as suggested by the Imry-Ma criterion [12]. In contrast, in our system a site in an inactive state (I_1 or I_2) can be activated only if at least one of its nearest neighbors is in a different state (1)-(4). As a result, the interior of an inactive uniform domain (all sites

in state I_1 or all in state I_2) is dynamically dead, and the typical domain size growth is unlimited.

A more comprehensive understanding of the domain wall dynamics can be obtained from the real-space renormalization group of the random-field Ising chain developed by Fisher, Le Doussal and Monthus [34, 35, 36]. Translating their results into the language of the GCP, the asymptotic behavior of the linear size $R(t)$ of a domain and the density $\rho(t)$ of active sites after a quench from the active into the inactive phase (which corresponds to a decay run, i.e. a start from a completely active lattice in the Monte Carlo simulations) are found to be

$$R(t) \sim [\ln(t/t_0)]^{1/\psi_i}, \tag{8}$$

$$\rho(t) \sim [\ln(t/t_0)]^{-\bar{\alpha}_i} \tag{9}$$

with $\bar{\alpha}_i = 1/\psi_i = 2$. Similarly, starting from a single finite domain in the inactive state I_1 (I_2) that is embedded in an infinite system of the inactive state I_2 (I_1) (spreading runs in Monte Carlo simulations) and measuring the survival probability $P_s(t)$ of the finite domain yields

$$P_s(t) \sim [\ln(t/t_0)]^{-\bar{\delta}_i} \tag{10}$$

with $\bar{\delta}_i = 1/\psi_i - \phi = (3 - \sqrt{5})/2$. Here, the linear size of the surviving domain has the same scaling behavior [Eq.(8)] as the linear size $R(t)$ of a domain in the decay runs. Moreover, in the inactive phase of the GCP, active sites live only at domain walls, thus the number of active sites in a surviving system scales with the total domain wall size $R(t)^{d-1} \sim [\ln(t/t_0)]^{(d-1)/\psi_i}$. If we define an exponent $\bar{\Theta}_i$ via the scaling of the number N_s of active sites averaged over all systems via

$$N_s(t) \sim [\ln(t/t_0)]^{\bar{\Theta}_i}, \tag{11}$$

then the number of active sites in surviving systems must scale as $N_s/P_s \sim [\ln(t/t_0)]^{\bar{\Theta}_i+\bar{\delta}_i} \sim [\ln(t/t_0)]^{(d-1)/\psi_i}$. We thus obtain $\bar{\Theta}_i = (d-1)/\psi - \bar{\delta}_i$. In one dimension, $d = 1$, this implies that $\bar{\Theta}_i = -\bar{\delta}_i$.

C. Two space dimension, $d = 2$

In contrast to the one-dimensional case where the domain wall size in the inactive phase is fixed (it always consists of a single $I_1 I_2$ bond); in higher space dimensions domain walls may change size (i.e., length or area; see Fig. 2) as the hopping of a domain wall segment might result in the annihilation of existing segments or the creation of a new ones. Therefore, the theory developed in the last section does not directly apply. However, in $d = 2$, we can still map the domain wall hopping rates of the GCP with random-field disorder in the inactive phase onto those of the random-field Ising model in the low-temperature regime, as we show in Appendix A.

Grinstein and Fernandez investigated the domain growth dynamics of the random-field Ising model at low temperature following a quench from high temperature [37]. They found that the linear size R of a domain grows as $\ln^2(t)$ with time up to some crossover length R_x, beyond which R grows as $\ln(t)$. Eventually, the domain growth stops because thermal fluctuations prevent symmetry breaking in the random-field Ising model, in agreement with the Imry-Ma argument. As this mechanism does not exist in the GCP, we can ignore it. Based on their findings and the mapping (Appendix A) between the GCP and the random-field Ising model, we obtain that in the inactive phase of the GCP, the linear size of a domain R grows with time as

$$R(t) \sim \begin{cases} \alpha_0^{-2} \ln^2(t/t_0) & (t < t_x) \\ \\ \alpha_0^{-2} \ln(t/t_0) & (t > t_x) \end{cases}, \tag{12}$$

where t_x is the crossover time between the two regimes. In contrast to the Ising model where the crossover time t_x can be controlled independently by the temperature, in the GCP the

ratio of t_x/t_0 depends only on the lattice geometry in the small-σ limit, $\sigma \ll \mu$. (Specifically, from the Monte Carlo simulations in Sec. D we get an estimate of $\ln(t_x/t_0) \approx 8.3$.)

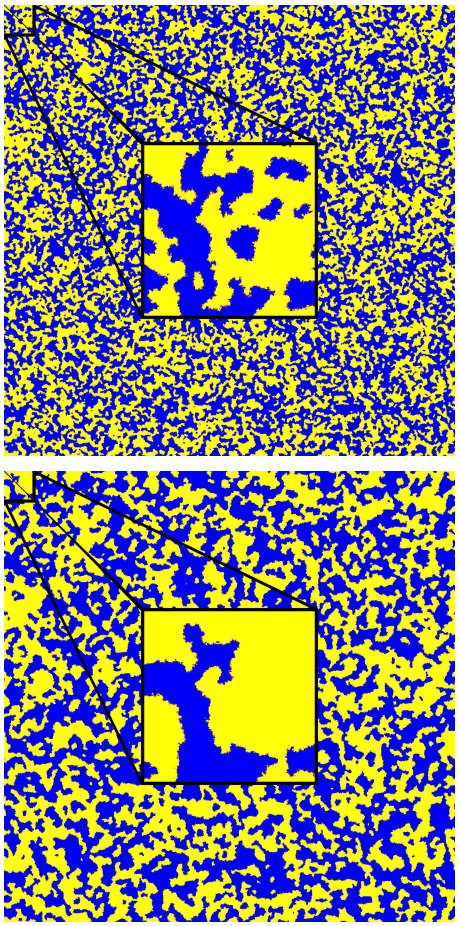

Fig. 2. Simulation snapshots of the two-dimensional GCP with random-field disorder, starting from a fully active lattice with size of 5000×5000 and $\mu \approx 3.0$. I_1 and I_2 are shown in yellow and blue (light and dark gray). There is a small number of active sites at domain walls that are marked in red (midtone gray). Top: Snapshot at $t = 3 \times 10^3$ (pre-asymptotic regime). Bottom: Snapshot at $t \approx 3.6 \times 10^4$ (asymptotic regime).

In the inactive phase of the GCP, active sites exist mainly due to the boundary activation process. Therefore, active sites can only exist in the vicinity of domains boundaries. This implies that, asymptotically, the number of active sites is proportional to the total size

(length) of domain walls. Accordingly the density of active sites ρ is proportional to R^{-1}. Thus we expect that

$$\rho(t) \sim \begin{cases} \alpha_0^2 \ln^{-2}(t/t_0) & (t < t_x) \\ \\ \alpha_0^2 \ln^{-1}(t/t_0) & (t > t_x) \end{cases} . \tag{13}$$

D. Scaling at the critical point

In this subsection, we give a brief summary of the scaling theory for an infinite-randomness fixed point with activated scaling. It was predicted to occur in the one-dimensional disordered contact process using a strong-disorder renormalization group [38] and later confirmed numerically in one, two, and three dimensions [39, 40, 41]. Here, we generalize it to the case where the exponents β and β' differ from each other.

As the decay rate μ approaches its critical value μ_c starting from the active phase, the steady-state density ρ_{stat} and the ultimate survival probability $P_s(\infty)$ approach zero, following power laws as

$$\rho_{\text{stat}} \sim \Delta^{\beta}, \tag{14}$$

$$P_s(\infty) \sim \Delta^{\beta'}, \tag{15}$$

where $\Delta = (\mu_c - \mu_c)/\mu_c$ is the dimensionless distance from criticality, β and β' are the order parameter and the survival probability critical exponents, respectively. Moreover, the divergence of the (spatial) correlation length $\xi_\perp$, approaching criticality follows the power-law

$$\xi_\perp \sim |\Delta|^{-\nu_\perp}, \tag{16}$$

where $\nu_\perp$ is the correlation length critical exponent. All the critical exponents defined so far describe the static behavior of observables near the critical point. The ultraslow dynamics

at an infinite-randomness fixed point is reflected in the activated scaling, i.e., the correlation time $\xi_\parallel$ scales with the correlation length $\xi_\perp$ as

$$\ln(\xi_\parallel/t_0) \sim \xi_\perp^\psi, \tag{17}$$

where ψ is the so-called tunneling exponent and t_0 is a nonuniversal microscopic time scale. This leads to

$$\ln(\xi_\parallel/t_0) \sim |\Delta|^{-\bar{\nu}_\parallel}. \tag{18}$$

Here $\bar{\nu}_\parallel = \psi\nu_\perp$ is the correlation time exponent. Generally, the four critical exponents β, β', $\nu_\perp$ and $\bar{\nu}_\parallel$, form a complete set that characterizes an absorbing state phase transition. For some special cases, e.g., the transition in the DP universality class, symmetry considerations reduce this set to only three exponent, because $\beta = \beta'$ [16]. In terms of these exponents we can write the finite-size (time) scaling of the density ρ of active sites in a decay experiment as function of Δ, $\ln(t/t_0)$, and system size L as

$$\rho(\Delta, \ln[t/t_0], L) = b^{\beta/\nu_\perp}\rho(\Delta b^{-1/\nu_\perp}, \ln[t/t_0]b^\psi, Lb). \tag{19}$$

Here b is an arbitrary dimensionless scale factor. Similarly, in a spreading experiment the survival probability P_s, number of active sites in the active cloud N_s and the mean-square radius of this cloud R have the scaling forms

$$P_s(\Delta, \ln[t/t_0], L) = b^{\beta'/\nu_\perp}P_s(\Delta b^{-1/\nu_\perp}, \ln[t/t_0]b^\psi, Lb), \tag{20}$$

$$\begin{aligned} &N_s(\Delta, \ln[t/t_0], L) \\ &\quad = b^{(\beta+\beta')/\nu_\perp - d}N_s(\Delta b^{-1/\nu_\perp}, \ln[t/t_0]b^\psi, Lb), \end{aligned} \tag{21}$$

and

$$R(\Delta, \ln[t/t_0], L) = b^{-1}R(\Delta b^{-1/\nu_\perp}, \ln[t/t_0]b^\psi, Lb). \tag{22}$$

We can find the asymptotic time dependencies of observables in the thermodynamic limit ($L \to \infty$) and at criticality ($\Delta = 0$) from the scaling relations above, by setting the scale factor b to $\ln(t/t_0)^{-1/\psi}$. This leads to a logarithmic time decay of the density of active sites and the survival probability as

$$\rho(t) \sim [\ln(t/t_0)]^{-\bar{\alpha}}, \tag{23}$$

$$P_s(t) \sim [\ln(t/t_0)]^{-\bar{\delta}}, \tag{24}$$

where $\bar{\alpha} = \beta/\bar{\nu}_\parallel$ and $\bar{\delta} = \beta'/\bar{\nu}_\parallel$. Analogously, the number of active sites in the active cloud and the mean-square radius of this cloud starting from a single active seed site increase logarithmically with time as

$$N_s(t) \sim [\ln(t/t_0)]^{\bar{\Theta}}, \tag{25}$$

$$R(t) \sim [\ln(t/t_0)]^{1/\psi} \tag{26}$$

with $\bar{\Theta} = (d\nu_\perp - \beta - \beta')/\bar{\nu}_\parallel$. This exponent relation can be rewritten in terms of the time dependence exponents as

$$\bar{\alpha} + \bar{\delta} + \bar{\Theta} = d/\psi. \tag{27}$$

It is similar to the hyperscaling relation for absorbing state transitions with conventional power-law scaling [16].

IV. MONTE CARLO SIMULATIONS

A. Method and overview

To test our predictions, we perform Monte Carlo simulations [27, 28] of the GCP defined by (1) to (4) in the presence of random-field disorder in one and two space dimensions. In the one-dimensional case, we perform the simulations with two different types of initial conditions: (i) decay runs and (ii) spreading runs. Decay runs start from a com-

pletely active lattice (all sites in state A), and we monitor the time evolution of the density ρ of active sites as well as the densities ρ_1 and ρ_2 of inactive sites I_1 and I_2, respectively. Spreading runs start from a fully inactive lattice with all sites in inactive state I_1 except a single active (seed) site in the active state A. Here, we measure the survival probability P_s, the number of active sites in the active cloud N_s and the mean-square radius R^2 of this cloud as functions of time. In the two-dimensional case we perform decay run simulations only. We implement the random-field disorder through the distribution (5) using $3\mu_l/2 = \mu_h \equiv \mu$.

In both types of runs, the simulation proceeds as a sequence of individual events. Each event consists of randomly selecting a pair of nearest-neighbor sites from the active region. In the spreading runs, the active region initially consists of the seed site and its nearest-neighbors. Its size increases as activity spreads in the system. In contrast, in the decay runs, the active region is the entire system. The selected pair is updated through one of the possible processes (1) to (4) with probability τw. The time step τ is fixed at a constant value which is chosen such that the total probability of an outcome of the process (1)-(4) with the highest total rate is unity. Each event result in a time increment of τ/N_{pair} where N_{pair} is the number of nearest-neighbor pairs in the active region.

B. Absorbing phase in one space dimension, $d = 1$

We studied systems with sizes up to $L = 10^5$ and times up to $t_{\max} = 2 \times 10^8$. An overview over the density decay runs is provided in Fig. 3 which shows the time evolution of the density of active sites. The inset of Fig. 3 shows that for systems with both decay rates $\mu_h = \mu$ and $\mu_l = 2\mu/3$ greater than the clean critical value $\mu_c^0 = 0.628$, the density ρ continues to decay up to the longest times studied. Still, the decay is obviously slower than a power law. Our theoretical arguments led to Eq. (7), which predicts that asymptotically $\rho^{-1/\bar{\alpha}_i}$ depends linearly on $\ln(t)$. This prediction is tested in Fig. 4. We see that all curves with $\mu > 1$ follow the predicted behavior over several orders of magnitude in time.

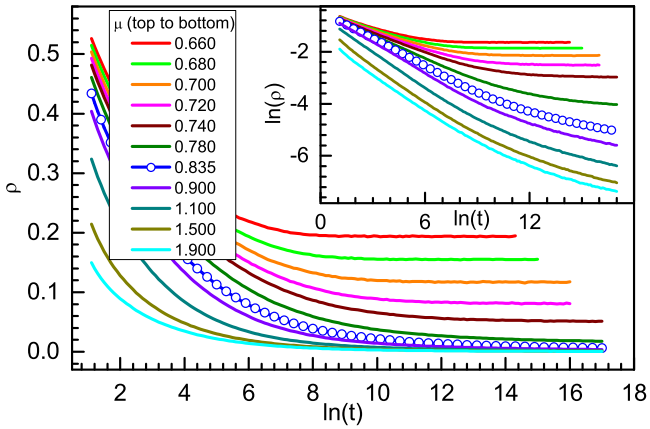

Fig. 3. Density ρ vs time t in one dimension for several values of the decay rate μ. The data are averages over 60 to 1000 disorder configurations. Inset: The log-log plot shows that the density decay is slower than a power law for all μ.

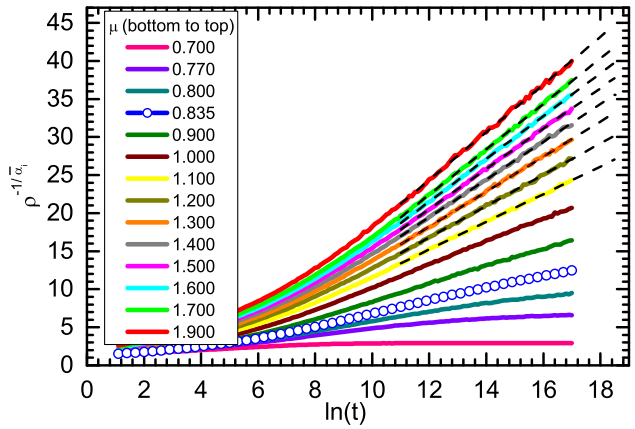

Fig. 4. $\rho^{-1/\bar{\alpha}_i}$ vs $\ln(t)$ for several values of the decay rate μ. The dashed straight lines are fits to the predicted behavior $\rho \sim [\ln(t/t_0)]^{-\bar{\alpha}_i}$ with $\bar{\alpha}_i = 2$.

Similarly, Eqs. (8) and (10) predict linear dependences of both $P_s^{-1/\bar{\delta}_i}$ and R^{ψ_i} on $\ln(t)$ (asymptotically for $t \to \infty$). To verify these predictions, we performed spreading simulations deep in the inactive phase with $\mu = 3$ and $\lambda = 0.01$ ($\mu/\lambda \gg 1$). Our simulation results are presented in Fig. 5. The figure shows that R^{ψ_i} meets the prediction over about one and half orders of magnitude in time. The behavior of $P_s^{-1/\bar{\delta}_i}$ seems to be pre-asymptotic, i.e., $P_s^{-1/\bar{\delta}_i}$ slowly approaches the predicted asymptotic linear dependence on $\ln(t)$ but has

not quite reached it at the end of our simulations. Increasing the time in order to reach the true asymptotic behavior, requires prohibitively large numerical effort.

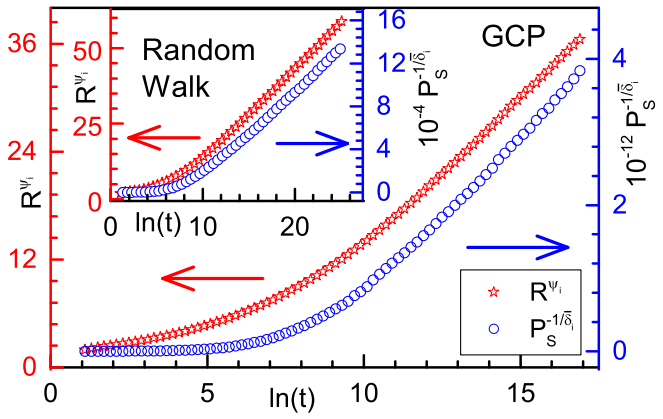

Fig. 5. $P_s^{-1/\bar{\delta}_i}$ and R^{ψ_i} vs $\ln(t)$, with $\bar{\delta}_i = (3-\sqrt{5})/2$ and $\psi_i = 1/2$. Main panel: GCP with random-field disorder, with $\mu = 3$ and $\lambda = 0.01$. The data are averages over 36000 samples with 4000 individual runs per sample. Inset: Toy model consisting of two random walkers with random hopping probabilities. The ratio between right and left hopping probabilities α_i at site i is drawn from a time-independent binary distribution with possible values of $(2/3)^{\pm 1}$. If the first walker see a ratio α_i, the second walker sees the inverted ratio α_i^{-1}. The data are averages over 600 samples with 1000 individual runs per sample.

As domain walls between the two inactive states are the only relevant degrees of freedom in the absorbing phase, we used a toy model in which we replace the two domain walls ($I_1 I_2$ and $I_2 I_1$) in the spreading simulation by two random walkers with random right and left hopping probabilities. The ratio between right and left hopping probabilities at a given site is proportional to the ratio between the decay rates toward the two inactive states (μ_1/μ_2 for the walker representing $I_1 I_2$ and μ_2/μ_1 for the other walker representing $I_2 I_1$). This toy model is numerically simpler and allows us to reach longer times. The inset of Fig. 5 shows that the data for P_s and R obtained from the random walk toy model follow the predictions of Eqs. (8) and (10) over several orders of magnitude in time.

C. Criticality in one space dimension, $d = 1$

We now turn to the critical point in one space dimension. In a previous work [22], we obtained a rough estimate of the critical decay rate μ_c. The more detailed simulations reported here have led to a better estimate of μ_c as well as a complete set of critical exponents.

Because the critical point separates an active system from an ultimately dead one (in the absorbing state), the dynamics at criticality is expected to be slower than the dynamics in the inactive phase. Since, observables in the inactive phase evolve as power laws of $\ln(t/t_0)$, a simple power law dependent on t time evolution at criticality can be ruled out. Instead, let us assume that the critical behavior follows the activated scaling scenario outlined in Sec. III D.

In simulations of absorbing state transitions, the critical point is often identified by plotting the data such that the critical time dependence leads to a straight line. In the case of activated scaling, this is hampered by the unknown microscopic scale t_0 which acts as a strong correction to scaling.

However, Vojta *et al.* [40] provided a method to overcome the absence of a t_0 value by observing that t_0 should be the same for all observables measured in the same simulation run because t_0 is related to the time scale of the underlying strong-disorder renormalization group. Therefore, asymptotically, observables have power-law dependencies on each other. For example, combining Eqs. (24) and (25) gives $N_s \sim P_s^{-\bar{\Theta}/\bar{\delta}}$. Using this method, the data plotted in Fig. 6 indicate a critical decay rate of $\mu_c = 0.835(3)$ and yield a value of $\bar{\Theta}/\bar{\delta} = -0.27(5)$. The numbers in parentheses give the error estimate of the last digits. Our error estimate contains the statistical and the systematic errors as well as the error due to the uncertainty of μ_c. (Possible correlations between errors from different sources have been ignored.) To obtain the exponents $\bar{\alpha}$, $\bar{\delta}$ and ψ, we search for values that yield linear dependencies of each of $\rho^{-1/\bar{\alpha}}$, $P_s^{-1/\bar{\delta}}$ and R^{ψ} [see Eqs. (23), (24), and (26)] on $\ln(t/t_0)$ at the critical $\mu_c = 0.835$. We find values of $\bar{\alpha} = 1.4(1)$, $\bar{\delta} = 0.225(8)$ and $\psi = 0.62(7)$

(Fig. 7). Moreover, using the measured values of $\bar{\Theta}/\bar{\delta}$ and $\bar{\delta}$, we find $\bar{\Theta} = -0.060(12)$. The hyperscaling relation, Eq. (27), is satisfied by the obtained critical exponents $\bar{\alpha}$, $\bar{\delta}$, ψ, and $\bar{\Theta}$, within the given errors.

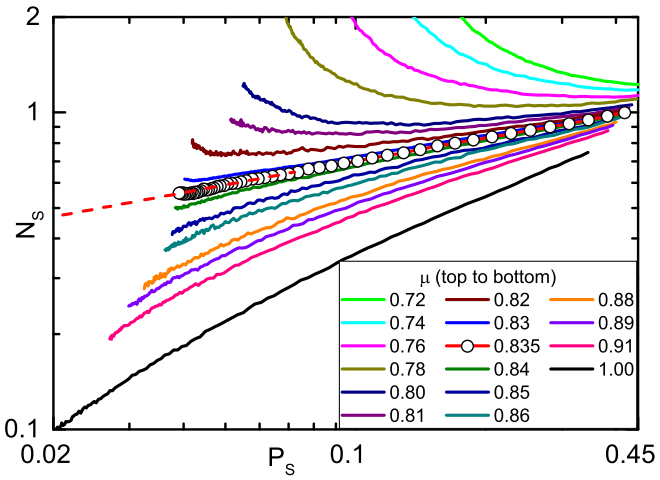

Fig. 6. Double-log plot of N_s vs P_s for several values of the decay rate μ. The data are averages over 1000 to 8000 disorder configurations with 100 to 400 trials each. The straight dashed line is a power-law fit of the asymptotic part of the critical curve ($\mu = 0.835$) yielding $\bar{\theta}/\bar{\delta} = -0.27(5)$.

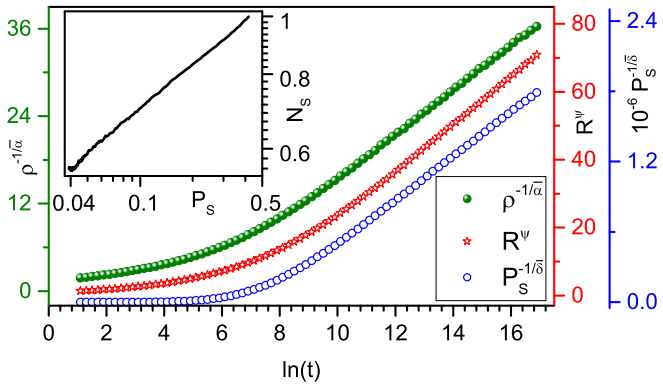

Fig. 7. $\rho^{-1/\bar{\alpha}}$, R^{ψ}, and $P_s^{-1/\bar{\delta}}$ vs $\ln(t)$ at criticality. Here, $\psi = 0.62(7)$, $\bar{\alpha} = 1.4(1)$ and $\bar{\delta} = 0.225(8)$ are determined from the data by requiring that the corresponding curves become straight lines asymptotically. Inset: Double-log plot of N_s vs P_s at criticality as in Fig. 6.

So far, we obtained only three independent critical exponents. In order to find a complete set of critical exponents that is required to characterize the universality class of the transition, we need to find one more critical exponent independently. Thus, we turn to the density scaling relation, Eq. (19). Setting the scale factor $b = \ln(t/t_0)^{-1/\psi}$ and in the limit $L \to \infty$, we get

$$\rho \ln(t/t_0)^{\bar{\alpha}} = \tilde{X}[\Delta^{\bar{\nu}_\parallel} \ln(t/t_0)]. \tag{28}$$

Here $\tilde{X}$ is a scaling function. At the critical point ($\Delta = 0$), the quantity $\rho \ln(t/t_0)^{\bar{\alpha}}$ asymptotically approaches a constant value [$\tilde{X}(0) = \text{const.}$]. As we deviate from the critical point toward the active phase, the quantity $\rho \ln(t/t_0)^{\bar{\alpha}}$ represents the scaling function $\tilde{X}$ with an argument that is scaled by $\Delta^{\bar{\nu}_\parallel}$ as shown in Fig. 8.

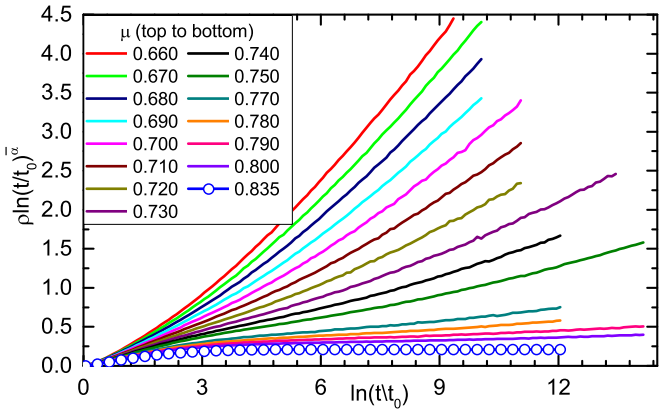

Fig. 8. $\rho \ln(t/t_0)^{\bar{\alpha}}$ vs $\ln(t/t_0)$ for several decay rates μ at and below the critical decay rate $\mu_c = 0.835$. The quantity $\rho \ln(t/t_0)^{\bar{\alpha}}$ has zero scale dimension. Thus, asymptotically it is time independent at criticality, $\mu_c = 0.835$.

In Fig. 9, we rescale the abscissa of each of the off-critical curves with a scaling factor x until they all collapse onto a reference curve. According to Eq. (28), a fit of the scaling factor x to the power-law dependence $x = (\Delta/\Delta_{ref})^{-\bar{\nu}_\parallel}$ (see upper inset in Fig. 9), yields the correlation time critical exponent $\bar{\nu}_\parallel = 1.78(4)$.

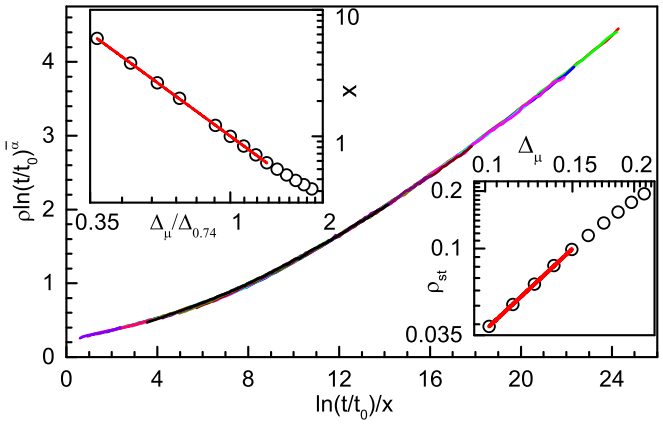

Fig. 9. Scaling plot of $\rho \ln(t/t_0)^{\bar{\alpha}}$ vs $\ln(t/t_0)/x$ for several decay rates μ below the critical decay rate $\mu_c = 0.835$ (the same off-critical decay rate values listed in Fig. 8). x is the scaling factor necessary to scale the data onto the curve of $\mu = \mu_{ref} = 0.74$. Upper inset: Double-log plot of the scaling factor x vs $\Delta_\mu/\Delta_{0.74}$ where $\Delta_\mu = (\mu_c - \mu)/\mu_c$. The straight solid line is a power-law fit yielding $\bar{\nu}_\parallel = 1.78(4)$. Lower inset: Double-log plot of the stationary density ρ_{st} vs Δ_μ. The straight solid line is a power-law fit yielding $\beta = 2.42(8)$.

With the help of the scaling relations [Eqs. (19)-(22)], other critical exponents can be calculated (Table I), e.g., the scaling relation $\beta = \bar{\alpha}\bar{\nu}_\parallel$ gives the order parameter critical exponent $\beta = 2.5(2)$. The steady-state density ρ_{stat} [Eq. (14)] yields another independent estimate of the exponent $\beta = 2.42(8)$ (see lower inset in Fig. 9).

We conclude that all the Monte Carlo simulations data are well described within the activated scaling scenario.

D. Two space dimension, $d = 2$

In two dimensions our simulations focused on the inactive phase. We studied systems with sizes of up to 2000×2000 sites and times up to $t_{\max} = 5 \times 10^4$. Figure 10 shows an overview of the time evolution of the density of active sites from decay runs. Similar to the one-dimensional case, in two-dimensional systems with both decay rates $\mu_h = \mu$ and $\mu_l = 2\mu/3$ greater than the clean critical value $\mu_c^0 = 1.000$, the density ρ continues to decay slowly (slower than a power law) up to the longest times studied, as shown in the inset of Fig. 10.

Table I. Critical and inactive phase exponents for the one dimensional generalized contact process with two symmetric inactive states in the presence random-field disorder. The values for the inactive phase are found analytically. The values for the generic transition emerge from fits of our data (above the horizontal line) and from scaling relations (below the horizontal line). The numbers in parentheses gives the estimated error of the last given digits, where possible correlations between errors from different sources are ignored.

Critical point		**Inactive phase**	
$\bar{\alpha}$	1.4(1)	$\bar{\alpha}_i$	2
ψ	0.62(7)	ψ_i	1/2
$\bar{\delta}$	0.225(8)	$\bar{\delta}_i$	$(3-\sqrt{5})/2$
$\bar{\nu}_{\parallel}$	1.78(4)		
β	2.42(8)		
$\bar{\Theta}$	-0.060(12)	$\bar{\Theta}_i$	$(\sqrt{5}-3)/2$
$\nu_{\perp}$	2.9(4)		
β'	0.40(2)		

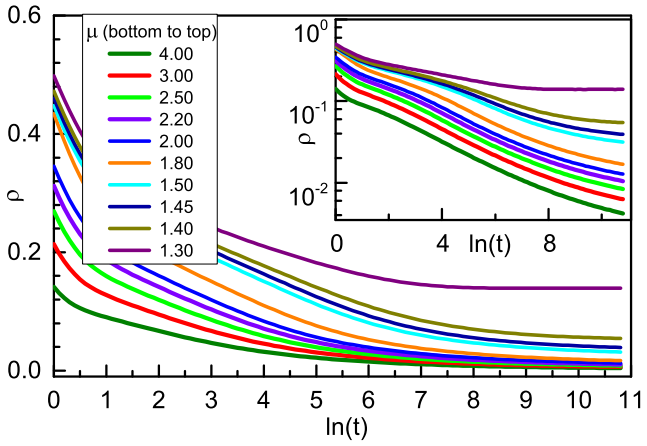

Fig. 10. Density ρ vs time t in two dimensions for several values of the decay rate μ. The data are averages over 100 disorder configurations. Inset: The log-log plot shows that the density decay is slower than a power law for all μ.

According to our theory [Eq. (13)] the time evolution of the density of active sites ρ is predicted to consist of two regimes, a pre-asymptotic regime and an asymptotic regime. In the pre-asymptotic regime $\rho^{-1/2}$ depends linearly on $\ln(t)$ up to a crossover time t_x, after which ρ^{-1} depends linearly on $\ln(t)$. The prediction of Eq. (13) is tested in Fig. 11, which

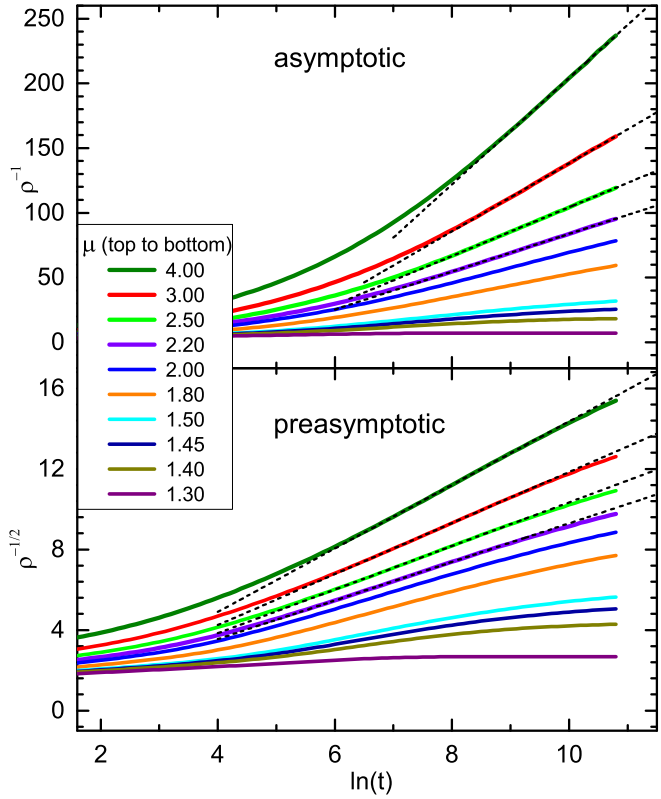

Fig. 11. Upper panel: ρ^{-1} vs time t for several values of the decay rate μ. The solid straight lines are fits to the predicted asymptotic behavior $\rho \sim \ln^{-1}(t/t_0)$. Lower panel: $\rho^{-1/2}$ vs time t for several values of the decay rate μ. The solid straight lines are fits to the predicted pre-asymptotic behavior $\rho \sim \ln^{-2}(t/t_0)$.

it shows that for all curves with $\mu > 2$, the predicted behavior is evident up to the longest times studied. Moreover, our results give an estimate of $\ln(t_x/t_0) \approx 8.3$.

V. CONCLUSIONS

To summarize, we have studied the effects of random-field disorder on the nonequilibrium phase transitions of the one- and two-dimensional GCP. We have found that these transitions survive the presence of random-field disorder, in contrast to equilibrium transitions in one and two space dimensions that are destroyed by such disorder. Moreover, we have investigated in detail the critical behavior of the one-dimensional GCP with random-

field disorder by means of large-scale Monte Carlo simulations. We have found that the scaling is of activated type comparable to that of the infinite-randomness critical point in the disordered contact process, but with different values of the exponents.

The main difference between the effects of random-field disorder in the GCP and in equilibrium systems such as random-field Ising model, is the absorbing nature of the inactive states I_1 and I_2 in the former. The interior of a uniform domain in an equilibrium system (e.g., a spin-up or spin-down domain in the Ising model) can give rise to a new domain of a different state, due to thermal fluctuations. This splits the original domain. Thus, the growth of the typical domain size is limited to its Imry-Ma equilibrium size, resulting in the destruction of the equilibrium transition in sufficiently low dimensions. In contrast, no new domains (nor active sites) can ever, spontaneously, appear in the interior of an I_1 or I_2 domain. We thus expect that our results are qualitatively valid for all nonequilibrium phase transitions with random-field disorder that locally breaks the symmetry between two *absorbing* states. Actually, Pigolotti and Cencini [42] have observed spontaneous symmetry breaking using a model of two competing biological species in a two-dimensional landscape with local habitat preference. The response of other nonequilibrium transitions may be different. For example our theory does not apply to transitions with random fields that break the symmetry between two active states. Furthermore, destabilizing the absorbing character of an inactive state by spontaneous fluctuations, even with small rates, results in the destruction of the phase transition [43].

The dynamics in the inactive phase of the GCP with random-field disorder is ultraslow. In one dimension, it is controlled by the Sinai walk of domain walls between the two inactive states. As a result, the densities of domain walls and active sites decay logarithmically with time. The dynamics in two dimensions can be mapped to that of the well-studied low-temperature random-field Ising model in the regime before the Imry-Ma limit for the domain size is reached. In this regime, the domain wall density decays logarithmically with time. Because an Imry-Ma limit is absent in our system (due to the

absorbing nature of the inactive states), this logarithmic time decay of the densities of domain walls and active sites continues for infinite time. Let us also mention the well-studied voter model. In this model each voter (site) can have one of two opinions (I_1, I_2), and two neighboring voters can convince one another of their own opinion with equal chances. Here, random-field disorder can be introduced in terms of local preference of one opinion over the other. Analogous to the GCP, the dynamics in the random-field one-dimensional voter model is solely controlled by the Sinai walk of domain walls. We therefore expect its dynamics to be, asymptotically, similar to that of the inactive phase of the one-dimensional GCP with random-field disorder.

We also note that the survival of a nonequilibrium continuous phase transitions in the presence of random-field disorder, implies the survival of the corresponding nonequilibrium first-order phase transition between the two *absorbing* states. (This transition can be tuned through a global preference of one of the two absorbing states.) In contrast, Martín *et al.* [44] have illustrated that nonequilibrium first-order phase transitions between fluctuating and absorbing states are destroyed by quenched disorder, in agreement with the Imry-Ma criterion.

In the higher-dimensional ($d > 2$) GCP, the mapping of domain wall hopping rates onto the random-field Ising model at low-temperatures still holds, but only qualitatively [45]. In addition, the interior of a uniform absorbing state domain, is still free of any spontaneous fluctuations. Furthermore, the Imry-Ma argument predicts weaker effects of random fields on equilibrium transitions in higher dimensions. All of the above suggests that domain formation will not be able to destroy the absorbing state transition in higher dimensions. However, other unrelated mechanisms may destroy the transition. For example, to the best of our knowledge, not even the clean GCP in dimensions $d > 2$ has been studied in detail. Its transition could be destroyed in analogy with the related voter model that never reaches an absorbing state where one opinion dominates, for $d > 2$ [46].

While straightforward experimental realizations of absorbing state transitions were lacking for a long time [47], appealing examples were recently found in driven suspensions [48, 49], turbulent liquid crystals [50], and superconducting vortices [51]. Moreover, the nonequilibrium nature of biological systems suggests them as potential candidates for observing nonequilibrium transitions. For example experiments in colony biofilms [52] are accurately represented by a model of two competing strains of bacteria [53] reveling a transition in the GV universality class (the same class as the clean two-dimensional GCP).

ACKNOWLEDGEMENTS

This work has been supported in part by the NSF under Grant No. DMR-1205803.

APPENDIX A: DOMAIN WALL HOPPING RATES

In this Appendix, we map the domain wall hopping rates of the random-field Ising chain in the low-temperature regime onto those of the GCP with random-field disorder in the inactive phase, in one and two space dimensions. We first define state variables s_i for the GCP in analogy to the Ising variables, such that $s_i = -1$ and $s_i = +1$ correspond to site i being in the inactive state I_1 and I_2, respectively. Also, we denote the decay rates toward the states I_1 and I_2 at any site i as $\mu_i^{(-1)}$ and $\mu_i^{(+1)}$, respectively. Since we are considering only the absorbing phase of the GCP, we can chose the activation rate λ to be much smaller than any other rate in the system such that the activation process (3) can be ignored.

First we consider the mapping in one space dimension. Figure 12 shows a schematic of the $(+-)$ domain wall dynamics. As shown in the figure, the hopping of the domain wall across site i from left to right and from right to left is based on two consecutive processes, an activation of site i through the boundary activation process (4) with probability rate σ, followed by a decay toward an inactive states (I_1or I_2) with a total decay rate $\mu_i^{(-1)} + \mu_i^{(+1)}$. The total effective probability rate w of the two consecutive processes behaves as the

inverse of their typical total time $\tau_1 + \tau_2$ where $\tau_1 = 1/\sigma$ and $\tau_2 = 1/(\mu_i^{(-1)} + \mu_i^{(+1)})$. i.e., $w = 1/(\tau_1 + \tau_2)$. The outcome of this combined process is the hopping of the domain wall from the right (left) to the left (right) of site i with probability of $\mu_i^{(-1)}\tau_2$ ($\mu_i^{(+1)}\tau_2$) provided that the active site i decays to an inactive state that is different than the initial one. However, with probability of $\mu_i^{(+1)}\tau_2$ ($\mu_i^{(-1)}\tau_2$) the decay process leaves site i in the same initial inactive state, i.e., the domain wall does not move. The hopping rates $w(\leftarrow)$ and

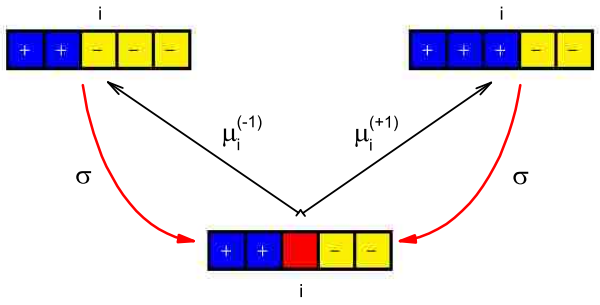

Fig. 12. Schematics of the dynamics of a +− domain wall in one space dimension. Red, yellow and blue (midtone, light, and dark gray) squares represent a site in the active state A, and inactive states I_1 and I_2 respectively.

$w(\rightarrow)$ to the left (right) can be found by multiplying w with the probability that the active site i ends up in a different inactive state than the initial one. Doing so we get

$$w(\leftarrow) = \frac{\sigma \mu_i^{(-1)}}{\sigma + \mu_i^{(-1)} + \mu_i^{(+1)}}, \tag{A1}$$

$$w(\rightarrow) = \frac{\sigma \mu_i^{(+1)}}{\sigma + \mu_i^{(+1)} + \mu_i^{(-1)}}. \tag{A2}$$

In general we can write

$$w(\leftarrow) = \frac{\sigma \mu_i^{(-s_i)}}{\sigma + \mu_i^{(-s_i)} + \mu_i^{(s_i)}}, \tag{A3}$$

$$w(\rightarrow) = \frac{\sigma \mu_i^{(s_i)}}{\sigma + \mu_i^{(-s_i)} + \mu_i^{(s_i)}}, \tag{A4}$$

where s_i is the state of site i when it is to the left of the domain wall. The ratio of the hopping rates is

$$\frac{w(\rightarrow)}{w(\leftarrow)} = \frac{\mu_i^{(s_i)}}{\mu_i^{(-s_i)}}. \tag{A5}$$

Using the variable $\alpha_i = \ln(\mu_i^{(+1)}/\mu_i^{(-1)})$, we can write $s_i\alpha_i = \ln(\mu_i^{(s_i)}/\mu_i^{(-s_i)})$. This lead to

$$\frac{w(\rightarrow)}{w(\leftarrow)} = \exp(s_i\alpha_i). \tag{A6}$$

Now, we turn to the case of the random-field Ising model defined by the Hamiltonian

$$H = -J \sum_{<i,j>} s_i s_j - \sum_i h_i s_i, \tag{A7}$$

where $J > 0$ and h_i is a random variable drawn from a symmetric distribution such that $< h_i >= 0$. The transition rates ratio can be found from the detailed balance equation as

$$\frac{w(\rightarrow)}{w(\leftarrow)} = \exp(-\Delta E/T) = \exp(2s_i h_i/T), \tag{A8}$$

where ΔE is the change in the system energy as the spin at site i flips from $-s_i$ to s_i. From Eq. (A6) and Eq. (A8) the two systems have equal hopping rate ratios if

$$\alpha_i = 2h_i/T. \tag{A9}$$

For the binary distribution (5) and (6), this implies

$$\ln(\mu_h/\mu_l) = \alpha_0 = 2h_0/T, \tag{A10}$$

where h_i is drawn from a symmetric binary distribution with possible values of $\pm h_0$.

We now turn to two dimensions. In contrast to the one-dimensional case where the domain wall size is fixed (it always consists of a single +− bond); domain walls in two space dimensions may change size length as the hopping of a domain wall segment might result in the creation of new segments or the annihilation of existing ones (Fig. 13).

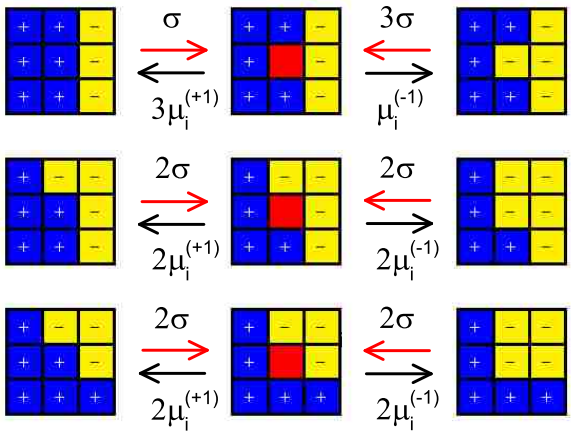

Fig. 13. Schematics of the dynamics of a +− domain wall in two space dimensions. Red, yellow, and blue (midtone, light, and dark gray) squares represent a site in an active state A and inactive states I_1 and I_2 respectively.

Therefore, the domain wall geometry must be taken into account. We consider the domain wall motion due to a single site changing from +1 to −1 or from −1 to +1, as sketched in Fig. 13. As in the one-dimensional case, the hopping consists of two consecutive processes. First the inactive site i in the inactive state s_i must be activated with probability rate of $n_{\rm dif}\sigma$ followed by a decay toward an inactive states $-s_i$ or s_i with a total decay rate $n_{\rm dif}\mu_i^{(-s_i)} + (4 - n_{\rm dif})\mu_i^{(s_i)}$. Here, $n_{\rm dif}$ is the number of inactive neighbors in a different state than s_i, i.e., in state $-s_i$. (In order to suppress any activation of one of the neighbors of site

i before the decay of site i to an inactive state, we work in the limit $\mu_i^{\pm s_i}/\sigma \gg 1$.) The effective probability rate w of the two consecutive processes is

$$w = \frac{n_{\rm dif}\sigma[n_{\rm dif}\mu_i^{(-s_i)} + (4-n_{\rm dif})\mu_i^{(s_i)}]}{n_{\rm dif}\sigma + n_{\rm dif}\mu_i^{(-s_i)} + (4-n_{\rm dif})\mu_i^{(s_i)}}. \tag{A11}$$

The probability that site i will end up in a different inactive state than the initial one at the end of this process is $n_{\rm dif}\mu_i^{(-s_i)}/(n_{\rm dif}\mu_i^{(-s_i)} + (4-n_{\rm dif})\mu_i^{(s_i)})$. As a result, the hopping rate $w_{s_i\to -s_i}$ from state s_i to $-s_i$ is

$$w_{s_i\to -s_i} = \frac{n_{\rm dif}^2\sigma\mu_i^{(-s_i)}}{n_{\rm dif}\sigma + n_{\rm dif}\mu_i^{(-s_i)} + (4-n_{\rm dif})\mu_i^{(s_i)}} \ . \tag{A12}$$

The hopping rate of site i back to its initial state $w_{-s_i\to s_i}$ can simply be found by interchanging s_i with $-s_i$ and $n_{\rm dif}$ with $4-n_{\rm dif}$ in Eq. (A12):

$$w_{-s_i\to s_i} = \frac{(4-n_{\rm dif})^2\sigma\mu_i^{(s_i)}}{(4-n_{\rm dif})\sigma + (4-n_{\rm dif})\mu_i^{(s_i)} + n_{\rm dif}\mu_i^{(-s_i)}} \ . \tag{A13}$$

The ratio between $s_i \to -s_i$ and $-s_i \to s_i$ hopping rates is

$$\begin{aligned}\frac{w_{s_i\to -s_i}}{w_{-s_i\to s_i}} &= \left(\frac{n_{\rm dif}}{4-n_{\rm dif}}\right)^2\left(\frac{\mu_i^{(-s_i)}}{\mu_i^{(s_i)}}\right) \\ &\times\left[\frac{(4-n_{\rm dif})\sigma + (4-n_{\rm dif})\mu_i^{(s_i)} + n_{\rm dif}\mu_i^{(-s_i)}}{n_{\rm dif}\sigma + n_{\rm dif}\mu_i^{(-s_i)} + (4-n_{\rm dif})\mu_i^{(s_i)}}\right].\end{aligned} \tag{A14}$$

In the limit $\mu_i^{\pm s_i}/\sigma \gg 1$, the right most factor of Eq. (A14) is equal to unity, the middle factor is similar to the random-field factor in the one-dimensional case [Eq. (A5)] and the first factor encodes the geometry. Therefore, we can write,

$$\frac{w_{s_i\to -s_i}}{w_{-s_i\to s_i}} = \left(\frac{n_{\rm dif}}{4-n_{\rm dif}}\right)^2 \exp(s_i\alpha_i). \tag{A15}$$

Considering the possible values of n_{dif} for a site at a domain wall, we get:

$$\frac{w_{s_i \to -s_i}}{w_{-s_i \to s_i}} = \begin{cases} 1/9 \exp(s_i \alpha_i) & (n_{\mathrm{dif}} = 1) \\ \exp(s_i \alpha_i) & (n_{\mathrm{dif}} = 2) \\ 9 \exp(s_i \alpha_i) & (n_{\mathrm{dif}} = 3) \end{cases}. \tag{A16}$$

In the case of two-dimensional random-field Ising model, the transition rates ratio can be found from the detailed balance equation as

$$\frac{w_{s_i \to -s_i}}{w_{-s_i \to s_i}} = \exp[4(n_{\mathrm{dif}} - 2)J/T + 2 s_i h_i / T], \tag{A17}$$

substituting for the possible values of n_{dif} we get:

$$\frac{w_{s_i \to -s_i}}{w_{-s_i \to s_i}} = \begin{cases} \exp(-4J/T + s_i h_i / T) & (n_{\mathrm{dif}} = 1) \\ \exp(s_i h_i / T) & (n_{\mathrm{dif}} = 2) \\ \exp(4J/T + s_i h_i / T) & (n_{\mathrm{dif}} = 3) \end{cases}. \tag{A18}$$

The comparison between Eq. (A16) and Eq. (A18), suggests the same mapping of the random-field term as in the one-dimensional case,

$$h_i / T = \alpha_i / 2, \tag{A19}$$

while the ratio J/T is constant,

$$J/T = \ln(3)/2. \tag{A20}$$

APPENDIX B:DOMAIN WALL DYNAMICS IN THE RFIM

Here we consider the random-field Ising model defined by the Hamiltonian,

$$H = -J \sum_{<i,j>} s_i s_j - \sum_i h_i s_i, \tag{B1}$$

where $\langle h_i \rangle = 0$ and $\langle h_i h_j \rangle = h^2 \delta_{i,j}$ in the limit $h \ll J$. (The results in this appendix have been derived in Refs. [37, 54, 55], we summarize them for the convenience of the reader.)

1. Interface roughening in the RFIM

In the absence of disorder ($h = 0$) the interface between spin-up and spin-down domains will tend to be flat in order to minimize the surface energy E_J. However, random-field disorder prefers an interface profile that follows the random-field fluctuations in order to minimize the field energy E_h. Let $z(\mathbf{r}_\perp)$ be the interface profile function (Fig. 14). The increase of the surface energy compared to its flat interface value can be estimated as

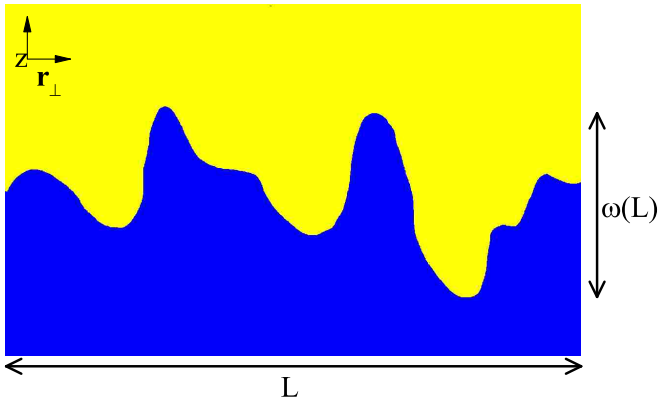

Fig. 14. Interface separating domains of spin-up [blue (dark gray)] and spin-down [yellow (light gray)] with interface profile $z(\mathbf{r}_\perp)$.

$$\Delta E_J \sim J \int d^{d-1}\mathbf{r}_\perp \left[1 + (\nabla z)^2\right]^{1/2} - J \int d^{d-1}\mathbf{r}_\perp. \tag{B2}$$

If $z(\mathbf{r}_\perp)$ fluctuates on a scale of $\omega(L)$, where $\omega(L) \ll L$, we can approximate $\left(1 + (\nabla z)^2\right)^{1/2}$ by $1 + 1/2[\omega(L)/L]^2$ to obtain

$$\Delta E_J \sim J L^{d-3} \omega^2(L). \tag{B3}$$

The gain in random field due to reshaping the interface to a favorable profile is (based on a central limit theorem argument) proportional to the square root of the interface volume and h such that

$$\Delta E_h \sim -h \left[L^{d-1} \omega(L)\right]^{1/2}. \tag{B4}$$

If we minimize the total energy change $\Delta E = \Delta E_J + \Delta E_h$ with respect to $\omega(L)$, we get

$$\omega_{\min} \sim (h/J)^{2/3} \, L^{(5-d)/3}, \tag{B5}$$

which corresponds to energy gain of

$$\Delta E_{\min} \sim J \, (h/J)^{4/3} \, L^{(d+1)/3}. \tag{B6}$$

Based on Eq. (B5) the interface width ($\omega_{\min}$) is bounded (smooth) for $d > 5$ and infinitely increasing for $d < 5$, where

$$\lim_{L\to\infty} \omega_{\min} = \begin{cases} 0 & (d > 5) \\ \infty & (d < 5) \end{cases}, \tag{B7}$$

However, the ratio

$$\frac{\omega_{\min}}{L} \sim (h/J)^{2/3} \, L^{(2-d)/3} \tag{B8}$$

is bounded for $d > 2$, where

$$\lim_{L\to\infty} \frac{\omega_{\min}}{L} = \begin{cases} 0 & (d > 2) \\ \infty & (d < 2) \end{cases} . \tag{B9}$$

Accordingly, the interface is rough on scale of $w(L) \ll L$ for $2 < d < 5$.

2. Asymptotic Interface Dynamics

Consider a spherical d-dimensional spin-up (spin-down) domain of radius R embedded in a much larger spin-down (spin-up) domain. Also, consider that the interface profile minimizes the random-field energy locally (the interface is in a favorable position w.r.t. the random field). According to the above results, the interface is rough on a scale $w \ll R$ for $2 < d < 5$. The embedded domain wishes to reduce the surface energy by shrinking but the random-field creates an energy barrier against the interface motion.

In order to estimate the energy barrier height, we assume that the radius of the embedded domain shrinks from R to $R - \Delta r$. As a result, the surface energy will decrease as

$$\Delta E_J \sim -JR^{d-2}\Delta r. \tag{B10}$$

As the interface moves it covers a volume proportional to $R^{d-1}\Delta r$. The typical value of the random-field energy in an unfavorable configuration is

$$\Delta E_h \sim h\left(R^{d-1}\Delta r\right)^{1/2}. \tag{B11}$$

The total energy change is then

$$\Delta E \sim -JR^{d-2}\Delta r + h\left(R^{d-1}\Delta r\right)^{1/2}, \tag{B12}$$

where proportionality factors are suppressed. As Δr starts to increase from zero, the random-field term ΔE_h initially dominates over the surface term ΔE_J in Eq. (B12). As Δr

continues to increase the surface term will win eventually, and the interface reaches a new favorable position w.r.t. the random field. The typical height of the energy barrier can be found by maximizing ΔE given in Eq. (B12). This leads to a barrier height of

$$\Delta E_{\max} \sim h^2 R/(4J), \tag{B13}$$

with a typical width of

$$\Delta r_{\max} \sim h^2 R^{3-d}/(4J^2). \tag{B14}$$

The time taken to overcome an energy barrier of height ΔE at temperature T depends exponentially on the ratio $\Delta E/T$, i.e.,

$$t = t_0 \exp(\Delta E/T), \tag{B15}$$

where t_0 is a microscopic time scale. This means that at time t, energy barriers lower than $T \ln(t/t_0)$ have been overcome, while energy barriers higher than $T \ln(t/t_0)$ have not yet been overcome. Therefore, the typical domain radius R [based on Eq. (B13)] at time t is

$$R \sim (JT/h^2) \ln(t/t_0). \tag{B16}$$

Note that smaller domains have been eliminated by shrinking; (when a domain starts shrinking, it collapses because the smaller the radius the lower the barrier).

3. Pre-asymptotic Interface Dynamics

The previous results are in the asymptotic regime $R \gg 1$, where all energies are much greater than the microscopic scales J and h. In this case, treating ΔE as continuous is justified. However, the change in the interface energy ΔE_J cannot be less than J. This means that Eq. (B13), which governs the dependence of the barrier height $\Delta E_{\max}$ on R, break down as R decreases below the crossover value $R_x \sim J^2/h^2$.

In this regime($R \ll R_x$), microscopic considerations must be taken into account. First, we consider this regime in two dimensions. Start with a domain wall that is flat except for a double kink as shown in Fig. 15. Only spins right next to the kink can flip without

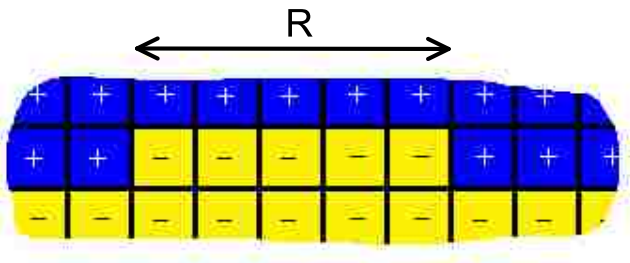

Fig. 15. Interface separating domains of spin-up [blue (dark gray)] and spin-down [yellow (light gray)] with a double kink of spin-down on top of otherwise flat interface.

increasing the interface length . A spin flip that increases the interface length costs energy of order of $J \gg h$. Therefore, it is unlikely to happen. Instead, sides of the double kink can move left and right, with probabilities that depend only on the random-field values, until they meet and cancel each other. Before the sides of the double kink meet there is no gain in the interface energy ΔE_J . However, there is energy cost (barrier) of $\Delta E_h \sim hR^{1/2}$ where R is the distance between the kinks. The characteristic decay time is $t = t_0 \exp(\Delta E_h/T)$, which leads to

$$R \sim (T^2/h^2) \ln^2(t/t_0). \tag{B17}$$

In higher dimensions ($d > 2$), we consider an island of size R^{d-1} on top of otherwise flat interface. In this case the elimination of such an island can be done by eliminating one-dimensional rows in any of the $(d-1)$ directions at a time. Each row elimination

involves a barrier of $hR^{1/2}$ and result in an energy gain of $\sim J$. Therefore, two-dimensional results applies for all $d \geq 2$. In summary, the typical domain radius behaves as

$$R \sim \begin{cases} (T^2/h^2)\ln^2(t/t_0) & (t < t_x) \\ \\ (JT/h^2)\ln(t/t_0) & (t > t_x) \end{cases}, \tag{B18}$$

where

$$\ln(t_x/t_0) \sim J/T. \tag{B19}$$

BIBLIOGRAPHY

[1] A. B. Harris and T. C. Lubensky. *Phys. Rev. Lett.*, 33:1540, 1974.

[2] G. Grinstein and A. Luther. *Phys. Rev. B*, 13:1329, 1976.

[3] T. Vojta. Disorder-induced rounding of certain quantum phase transitions. *Phys. Rev. Lett.*, 90:107202, 2003; Smearing of the phase transition in Ising systems with planar defects. *J. Phys. A*, 36:10921, 2003; Broadening of a nonequilibrium phase transition by extended structural defects. *Phys. Rev. E*, 70:026108, 2004;

[4] Yoseph Imry and Michael Wortis. Influence of quenched impurities on first-order phase transitions. *Phys. Rev. B*, 19:3580–3585, Apr 1979.

[5] Kenneth Hui and A. Nihat Berker. Random-field mechanism in random-bond multi-critical systems. *Phys. Rev. Lett.*, 62:2507–2510, May 1989.

[6] Michael Aizenman and Jan Wehr. Rounding of first-order phase transitions in systems with quenched disorder. *Phys. Rev. Lett.*, 62:2503–2506, May 1989.

[7] S. M. A. Tabei, M. J. P. Gingras, Y.-J. Kao, P. Stasiak, and J.-Y. Fortin. Induced random fields in the $LiHo_xY_{1-x}F_4$ quantum ising magnet in a transverse magnetic field. *Phys. Rev. Lett.*, 97(23):237203, 2006.

[8] D. M. Silevitch, D. Bitko, J. Brooke, S. Ghosh, G. Aeppli, and T. F. Rosenbaum. A ferromagnet in a continuously tunable random field. *Nature*, 448:567, 2007.

[9] Moshe Schechter. $Liho_xy_{1-x}f_4$ as a random-field ising ferromagnet. *Phys. Rev. B*, 77(2):020401, 2008.

[10] Amos Maritan, Marek Cieplak, Tommaso Bellini, and Jayanth R. Banavar. Nematic-isotropic transition in porous media. *Phys. Rev. Lett.*, 72:4113–4116, Jun 1994.

[11] E. W. Carlson, K. A. Dahmen, E. Fradkin, and S. A. Kivelson. Hysteresis and noise from electronic nematicity in high-temperature superconductors. *Phys. Rev. Lett.*, 96:097003, Mar 2006.

[12] Yoseph Imry and Shang-keng Ma. Random-field instability of the ordered state of continuous symmetry. *Phys. Rev. Lett.*, 35:1399–1401, Nov 1975.

[13] This holds for discrete symmetry. For continuous symmetry the surface energy behaves as L^{d-2} resulting in a marginal dimension of 4.

[14] B. Schmittmann and R. K. P. Zia. Statistical mechanics of driven diffusive systems. In C. Domb and J. L. Lebowitz, editors, *Phase Transitions and Critical Phenomena*, volume 17, page 1. Academic, New York, 1995.

[15] J. Marro and R. Dickman. *Nonequilibrium Phase Transitions in Lattice Models*. Cambridge University Press, Cambridge, 1999.

[16] H. Hinrichsen. Nonequilibrium critical phenomena and phase transitions into absorbing states. *Adv. Phys.*, 49:815, 2000.

[17] G. Odor. Universality classes in nonequilibrium lattice systems. *Rev. Mod. Phys.*, 76:663, 2004.

[18] U. C. Täuber, M. Howard, and B. P. Vollmayr-Lee. Applications of field-theoretic renormalization group methods to reaction-diffusion problems. *J. Phys. A*, 38:R79, 2005.

[19] T. Vojta. Rare region effects at classical, quantum, and non-equilibrium phase transitions. *J. Phys. A*, 39:R143, 2006.

[20] Ahmed K. Ibrahim, Hatem Barghathi, and Thomas Vojta. Enhanced rare-region effects in the contact process with long-range correlated disorder. *Phys. Rev. E*, 90:042132, Oct 2014.

[21] Hatem Barghathi and Thomas Vojta. Phase transitions on random lattices: How random is topological disorder? *Phys. Rev. Lett.*, 113:120602, Sep 2014.

[22] Hatem Barghathi and Thomas Vojta. Random fields at a nonequilibrium phase transition. *Phys. Rev. Lett.*, 109:170603, Oct 2012.

[23] T. E. Harris. Contact interactions on a lattice. *Ann. Prob.*, 2:969, 1974.

[24] P. Grassberger and A. de la Torre. *Ann. Phys. (NY)*, 122:373, 1979.

[25] H. Hinrichsen. Stochastic lattice models with several absorbing states. *Phys. Rev. E*, 55:219, 1997.

[26] According to Ref. [27], the qualitative behavior for $\bar{\mu}_k \neq \mu_k$ is identical to that for $\bar{\mu}_k = \mu_k$. Moreover, the precise value of σ is not important as long as it is nonzero.

[27] M. Y. Lee and T. Vojta. Phase transitions of the generalized contact process with two absorbing states. *Phys. Rev. E*, 81:061128, 2010.

[28] Man Young Lee and Thomas Vojta. Generalized contact process with two symmetric absorbing states in two dimensions. *Phys. Rev. E*, 83:011114, Jan 2011.

[29] P. Grassberger, F. Krause, and T. von der Twer. A new type of kinetic critical phenomenon. *J. Phys. A*, 17:L105, 1984.

[30] Ivan Dornic, Hugues Chaté, Jérôme Chave, and Haye Hinrichsen. Critical coarsening without surface tension: The universality class of the voter model. *Phys. Rev. Lett.*, 87(4):045701, Jul 2001.

[31] Michel Droz, Antonio L. Ferreira, and Adam Lipowski. Splitting the voter potts model critical point. *Phys. Rev. E*, 67(5):056108, May 2003.

[32] Omar Al Hammal, Hugues Chaté, Ivan Dornic, and Miguel A. Muñoz. Langevin description of critical phenomena with two symmetric absorbing states. *Phys. Rev. Lett.*, 94(23):230601, Jun 2005.

[33] F. Solomon. Random walks in random environment. *Ann. Prob.*, 3:1, 1975; H. Kesten, M. Kozlov, and F. Spitzer. A limit law for random walk in a random environment. *Compositio Math.*, 30:145, 1975; Y. G. Sinai. Limit behaviour of one-dimensional random walks in random environments. *Theor. Probab. Appl.*, 27:256, 1982.

[34] D. S. Fisher, P. Le Doussal, and C. Monthus. Random walks, reaction-diffusion, and nonequilibrium dynamics of spin chains in one-dimensional random environments. *Phys. Rev. Lett*, 80:3539, 1998.

[35] D. S. Fisher, P. Le Doussal, and C. Monthus. *Phys. Rev. E*, 64:066107, 2001.

[36] P. Le Doussal, C. Monthus, and D. S. Fisher. Random walkers in one-dimensional random environments: Exact renormalization group analysis. *Phys. Rev. E*, 59:4795, 1999.

[37] G. Grinstein and J. F. Fernandez. Equilibration of random-field ising systems. *Phys. Rev. B*, 29:6389–6392, Jun 1984.

[38] J. Hooyberghs, F. Iglói, and C. Vanderzande. Strong-disorder fixed point in absorbing-state phase transitions. *Phys. Rev. Lett.*, 90:100601, 2003.

[39] T. Vojta and M. Dickison. Critical behavior and Griffiths effects in the disordered contact process. *Phys. Rev. E*, 72:036126, 2005.

[40] T. Vojta, A. Farquhar, and J. Mast. Infinite-randomness critical point in the two-dimensional disordered contact process. *Phys. Rev. E*, 79:011111, 2009.

[41] Thomas Vojta. Monte carlo simulations of the clean and disordered contact process in three dimensions. *Phys. Rev. E*, 86:051137, Nov 2012.

[42] S. Pigolotti and M. Cencini. Coexistence and invasibility in a two-species competition model with habitat-preference. *J. Theor. Biology*, 265:609, 2010.

[43] Claudio Borile, Amos Maritan, and Miguel A. Muñoz. The effect of quenched disorder in neutral theories. *Journal of Statistical Mechanics: Theory and Experiment*, 2013(04):P04032, 2013.

[44] Paula Villa Martín, Juan A. Bonachela, and Miguel A. Muñoz. Quenched disorder forbids discontinuous transitions in nonequilibrium low-dimensional systems. *Phys. Rev. E*, 89:012145, Jan 2014.

[45] In dimensions $d > 2$ the number of different configurations of nearest-neighbors in states I_1 vs I_2 increases. As a result the number of nontrivial hopping rates ratios is more than one and increases with the dimensionality of the system. In the Ising model there is only one parameter to fine tune map these ratios, specifically, the ratio J/T.

[46] E. Ben-Naim, L. Frachebourg, and P. L. Krapivsky. Coarsening and persistence in the voter model. *Phys. Rev. E*, 53:3078–3087, Apr 1996.

[47] H. Hinrichsen. On possible experimental realizations of directed percolation. *Braz. J. Phys.*, 30:69, 2000.

[48] L. Corte, P. M. Chaikin, J. P. Gollub, and D. J. Pine. Random organization in periodically driven systems. *Nature Physics*, 4:420, 2008.

[49] Alexandre Franceschini, Emmanouela Filippidi, Elisabeth Guazzelli, and David J. Pine. Transverse alignment of fibers in a periodically sheared suspension: An absorbing phase transition with a slowly varying control parameter. *Phys. Rev. Lett.*, 107:250603, Dec 2011.

[50] K. A. Takeuchi, M. Kuroda, H. Chate, and M. Sano. Directed percolation criticality in turbulent liquid crystals. *Phys. Rev. Lett.*, 99:234503, 2007.

[51] S. Okuma, Y. Tsugawa, and A. Motohashi. Transition from reversible to irreversible flow: Absorbing and depinning transitions in a sheared-vortex system. *Phys. Rev. B*, 83:012503, Jan 2011.

[52] K. S. Korolev, Joao B. Xavier, David R. Nelson, and Kevin R. Foster. A quantitative test of population genetics using spatiogenetic patterns in bacterial colonies. *The American Naturalist*, 178:538, 2011.

[53] K. S. Korolev and David R. Nelson. Competition and cooperation in one-dimensional stepping-stone models. *Phys. Rev. Lett.*, 107:088103, Aug 2011.

[54] J. Villain. Nonequilibrium "critical" exponents in the random-field ising model. *Phys. Rev. Lett.*, 52:1543–1546, Apr 1984.

[55] G. Grinstein and Shang-keng Ma. Surface tension, roughening, and lower critical dimension in the random-field ising model. *Phys. Rev. B*, 28:2588–2601, Sep 1983.

IV. ENHANCED RARE-REGION EFFECTS IN THE CONTACT PROCESS WITH LONG-RANGE CORRELATED DISORDER

Ahmed K. Ibrahim, Hatem Barghathi, and Thomas Vojta

Department of Physics, Missouri University of Science and Technology, Rolla, MO 65409, USA

ABSTRACT[*]

We investigate the nonequilibrium phase transition in the disordered contact process in the presence of long-range spatial disorder correlations. These correlations greatly increase the probability for finding rare regions that are locally in the active phase while the bulk system is still in the inactive phase. Specifically, if the correlations decay as a power of the distance, the rare region probability is a stretched exponential of the rare region size rather than a simple exponential as is the case for uncorrelated disorder. As a result, the Griffiths singularities are enhanced and take a non-power-law form. The critical point itself is of infinite-randomness type but with critical exponent values that differ from the uncorrelated case. We report large-scale Monte-Carlo simulations that verify and illustrate our theory. We also discuss generalizations to higher dimensions and applications to other systems such as the random transverse-field Ising model, itinerant magnets and the superconductor-metal transition.

[*]Published in Physical Review E **90**, 042132 (2014).

I. INTRODUCTION

The effects of quenched spatial disorder on phase transitions have been a topic of great interest for several decades. Initially, research concentrated on classical (thermal) transitions for which many results can be obtained by using perturbative methods adapted from the theory of phase transitions in clean systems (see, e.g., Ref. [1]).

Later, it became clear, however, that many transitions are dominated by the non-perturbative effects of strong, rare disorder fluctuations and the rare spatial regions that support them. Such rare regions can be locally in one phase while the bulk system is in the other. The resulting slow dynamics leads to thermodynamic singularities, now known as the Griffiths singularities [2, 3], not just at the transition point but in an entire parameter region around it. Griffiths singularities at generic classical (thermal) phase transitions are very weak and probably unobservable in experiment [4]. In contrast, at many quantum and nonequilibrium phase transitions, the rare regions lead to strong Griffiths effects characterized by non-universal power-law singularities of various observables. The critical point itself is of exotic infinite-randomness type and characterized by activated rather than power-law dynamical scaling. This was first demonstrated in the random-transverse field Ising chain using a strong-disorder renormalization group [5, 6] as well as heuristic optimal fluctuation arguments and computer simulations [7, 8, 9]. Similar power-law Griffiths singularities were also found at the nonequilibrium transition of the disordered contact process [10, 11, 12] and at many other quantum and nonequilibrium transitions. In some systems, the rare region effects are even stronger and destroy the sharp phase transition by smearing [13]. Recent reviews and a classification of rare region effects can be found, e.g., in Refs. [14].

The majority of the literature on rare regions and Griffiths singularities focuses on uncorrelated disorder. In many physical situations, we can expect, however, that the disorder is correlated in space, for example if it caused by charged impurities. It is

intuitively clear that sufficiently long-ranged spatial disorder correlations must enhance the rare region effects because they greatly increase the probability for finding large atypical rare regions. Rieger and Igloi [15] studied a random transverse-field Ising chain with power-law disorder correlations. They indeed found that sufficiently long-ranged correlations change the universality class of the transition. They also predicted that the Griffiths singularities take the same power-law form as in the case of uncorrelated disorder, but with changed exponents.

In this paper, we investigate the nonequilibrium phase transition in the disordered one-dimensional contact process with power-law disorder correlations by means of optimal fluctuation theory and computer simulations. Our paper is organized as follows. We define the contact process with correlated disorder in Sec. II. In Sec. III, we develop our theory of the nonequilibrium phase transition and the accompanying Griffiths phase. Specifically, we show that the probability of finding a large rare region is a stretched exponential of its size rather than a simple exponential as for uncorrelated disorder. As a result, the Griffiths singularities are enhanced and take a non-power-law form. The critical point itself is of infinite-randomness type but its exponents differ from the uncorrelated case. Section IV is devoted to Monte-Carlo simulations that verify and illustrate our theory. In Sec. V, we generalize our results to higher dimensions and other physical systems. We also discuss the relation between the present work and Ref. [15]. We conclude in Sec. VI.

II. CONTACT PROCESS WITH CORRELATED DISORDER

The contact process [16] is a prototypical nonequilibrium many-particle system which can be understood as a model for the spreading of an epidemic. Consider a one-dimensional regular lattice of L sites. Each site can be in one of two states, either inactive (healthy) or active (infected). The time evolution of the contact process is given by a continuous-time Markov process during which active lattice sites infect their nearest

neighbors or heal spontaneously. Specifically, an active site becomes inactive at rate μ, while an inactive site becomes active at rate $n\lambda/2$ where n is the number of its active nearest neighbors. The healing rate μ and the infection rate λ are the external control parameters of the contact process. Without loss of generality, μ can be set to unity, thereby fixing the unit of time.

The qualitative behavior of the contact process is easily understood. If healing dominates over infection, $\mu \gg \lambda$, the epidemic eventually dies out completely, i.e., all lattices sites become inactive. At this point, the system is in a fluctuationless state that it can never leave. This absorbing state constitutes the inactive phase of the contact process. In the opposite limit, $\mu \ll \lambda$, the infection never dies out (in the thermodynamic limit $L \to \infty$). The system eventually reaches a steady state in which a nonzero fraction of lattices sites is active. This fluctuating steady state constitutes the active phase of the contact process. The active and inactive phases are separated by a nonequilibrium phase transition in the directed percolation universality class [17, 18, 19]. The order parameter of this absorbing-state transition is given by the steady state density $\rho_{\rm stat} = \lim_{t\to\infty} \rho(t)$ which is the long-time limit of the density of infected sites at time t,

$$\rho(t) = \frac{1}{L}\sum_i \langle n_i(t)\rangle \ . \tag{1}$$

Here, $n_i(t)$ is the occupation of site i at time t, i.e., $n_i(t) = 1$ if the site is infected and $n_i(t) = 0$ if it is healthy. $\langle \ldots \rangle$ denotes the average over all realizations of the Markov process.

So far, we have discussed the clean contact process for which λ and μ are spatially uniform. Quenched spatial disorder is introduced by making the infection rate λ_i of site

i and/or its healing rate μ_i random variables. The correlations of the randomness can be characterized by the correlation function

$$G_\lambda(i,j) = [\lambda_i \lambda_j]_{\rm dis} - [\lambda_i]_{\rm dis}\,[\lambda_j]_{\rm dis} \tag{2}$$

where $[\ldots]_{\rm dis}$ denotes the disorder average. The correlation function G_μ of the healing rates μ_i can be defined analogously. The existing literature on the disordered contact process mostly considered the case of uncorrelated disorder, $G_\lambda(i,j) \sim G_\mu(i,j) \sim \delta_{ij}$. In the present paper, we are interested in long-range correlations whose correlation function decays as a power of the distance r_{ij} between the two sites,

$$G_\lambda(i,j) \sim G_\mu(i,j) \sim r_{ij}^{-\gamma}\,, \tag{3}$$

for large r_{ij}. For our analytical calculations we will often use a correlated Gaussian distribution

$$P_G(\lambda_1,\ldots,\lambda_L) \sim \exp\left[-\frac{1}{2}\sum_{i,j}(\lambda_i-\bar\lambda)A_{ij}(\lambda_j-\bar\lambda)\right] \tag{4}$$

of average $\bar\lambda = [\lambda_i]_{\rm dis}$ and covariance matrix $(A^{-1})_{ij} = G_\lambda(i,j)$ [20]. Alternatively, we will also use a correlated binary distribution in which λ_i can take values λ and $c\lambda$ with overall probabilities $(1-p)$ and p, respectively. Here, p and c are constants between 0 and 1.

III. THEORY

A. Rare region probability

The Griffiths phase in the disordered contact process is caused by rare large spatial regions whose effective infection rate is larger than the bulk average $\bar\lambda$. For weak disorder

and outside the asymptotic critical region, the effective infection rate can be approximated by

$$\lambda_{RR} \approx \frac{1}{L_{RR}} \sum_{i \in RR} \lambda_i \tag{5}$$

To estimate how the probability distribution of λ_{RR} depends on the rare region size L_{RR}, we start from the correlated Gaussian (4), introduce λ_{RR} as a new variable and then integrate out all other random variables. For large L_{RR} and up to subleading boundary terms, this leads to the distribution

$$P(\lambda_{RR}, L_{RR}) \sim \exp\left[-\frac{L_{RR}}{2\tilde{G}(L_{RR})}(\lambda_{RR} - \bar{\lambda})^2\right] \tag{6}$$

where $\tilde{G}(L_{RR})$ is the sum over the correlation function

$$\tilde{G}(L_{RR}) \sim \sum_{j=0}^{L_{RR}/2} G_\lambda(0, j) \; . \tag{7}$$

Two cases need to be distinguished, depending on the value of the decay exponent γ in the correlation function (3). If $\gamma > 1$, the sum $\tilde{G}(L_{RR})$ converges in the limit $L_{RR} \to \infty$. The probability distribution of the effective infection rate λ_{RR} thus takes the asymptotic form

$$P(\lambda_{RR}, L_{RR}) \sim \exp\left[-\frac{1}{2b^2} L_{RR} \, (\lambda_{RR} - \bar{\lambda})^2\right] \tag{8}$$

where b is a constant. This form is identical to the result for uncorrelated or short-range correlated disorder (and agrees with the prediction of the central limit theorem). For $0 < \gamma < 1$, in contrast, the sum $\tilde{G}(L_{RR})$ behaves as $L_{RR}^{1-\gamma}$ for large L_{RR}. Consequently, the probability distribution of λ_{RR} reads

$$P(\lambda_{RR}, L_{RR}) \sim \exp\left[-\frac{1}{2b^2} L_{RR}^{\gamma} \, (\lambda_{RR} - \bar{\lambda})^2\right] \; . \tag{9}$$

This is a stretched exponential decay in L_{RR} rather than the simple exponential obtained in (8). In other words, for $0 < \gamma < 1$, the probability for finding a large deviation of λ_{RR} from the average $\bar{\lambda}$ decays much more slowly with rare region size than in the uncorrelated case.

We have also considered a correlated binary disorder distribution instead of the Gaussian (4). In this case, rare regions can be defined as regions of L_{RR} consecutive sites having the larger of the two infection rates. For uncorrelated disorder, the probability for finding such a region decays as a simple exponential of its size L_{RR}. We have confirmed numerically that the corresponding probability for the power-law correlations (3) with $0 < \gamma < 1$ follows a stretched exponential

$$w(L_{RR}) \sim \exp(-cL_{RR}^{\gamma}) \tag{10}$$

with the same exponent γ as in eq. (9).

B. Griffiths phase

We now use the results of Sec. III A to analyze the time evolution of the density of active sites $\rho(t)$ in the Griffiths phase on the inactive side of the nonequilibrium transition. This calculation is a generalization to the case of correlated disorder of the approach of Refs. [21, 22].

The rare region contribution to $\rho(t)$ can be obtained by summing over all regions that are locally in the active phase, ie., all regions having $\lambda_{RR} > \lambda_c$. For the correlated Gaussian distribution (4), $\rho(t)$ reads

$$\begin{aligned} \rho(t) \quad \sim \quad & \int_{\lambda_c}^{\infty} d\lambda_{RR} \int_0^{\infty} dL_{RR}\, P(\lambda_{RR}, L_{RR}) \times \\ & \times L_{RR} \exp[-t/\tau(\lambda_{RR}, L_{RR})] \end{aligned} \tag{11}$$

Here, $P(\lambda_{RR}, L_{RR})$ is the rare region distribution (8) or (9), depending on the value of γ; and $\tau(\lambda_{RR}, L_{RR})$ denotes the lifetime of the rare region. It can be estimated as follows. As

the rare region is locally in the active phase, $\lambda_{RR} > \lambda_c$, it can only decay via an atypical coherent fluctuation of all its sites. The probability for this to happen is exponentially small in the rare region size [10], resulting in an exponentially large life time

$$\tau(\lambda_{RR}, L_{RR}) = t_0 \exp\left[a L_{RR}\right] \tag{12}$$

where t_0 is a microscopic time scale. The coefficient a vanishes at $\lambda_{RR} = \lambda_c$ and increases with increasing λ_{RR}, i.e., the deeper the region is in the active phase, the larger a becomes. Because a has the dimension of an inverse length, it scales as $\xi_\perp^{-1}$ (where $\xi_\perp$ is the correlation length) according to finite-size scaling [23],

$$a = a'(\lambda_{RR} - \lambda_c)^{\nu_{0\perp}} \, . \tag{13}$$

Note that $\nu_{0\perp}$ is the *clean* correlation length exponent unless the rare region is very close to criticality (inside the narrow asymptotic critical region) [24].

In the long-time limit $t \gg t_0$, the integral (11) can be solved in saddle-point approximation. The saddle point equations read

$$\frac{\partial}{\partial L_{RR}} \left[\frac{L_{RR}^\gamma}{2b^2} (\lambda_{RR} - \bar{\lambda})^2 + \frac{t}{t_0} e^{-a'(\lambda_{RR}-\lambda_c)^{\nu_{0\perp}} L_{RR}} \right] = 0 \, , \tag{14}$$

$$\frac{\partial}{\partial \lambda_{RR}} \left[\frac{L_{RR}^\gamma}{2b^2} (\lambda_{RR} - \bar{\lambda})^2 + \frac{t}{t_0} e^{-a'(\lambda_{RR}-\lambda_c)^{\nu_{0\perp}} L_{RR}} \right] = 0 \, , \tag{15}$$

and yield the saddle point values

$$\lambda_{sp} - \lambda_c = \frac{\gamma \nu_{0\perp}}{2 - \gamma \nu_{0\perp}} (\lambda_c - \bar{\lambda}) \, , \tag{16}$$

$$L_{sp} \sim (\lambda_c - \bar{\lambda})^{-\nu_{0\perp}} \ln(t/t_0) \, . \tag{17}$$

Equations (14) to (17) apply to the long-range correlated case $\gamma < 1$; the corresponding relations for the short-range correlated case follow by formally setting $\gamma = 1$.

For the method to be valid, λ_{sp} must be within the integration range of the integral (11). The bulk system is in the inactive phase implying $\bar{\lambda} < \lambda_c$. Moreover, the clean correlation length exponent of the one-dimensional contact process takes the value $\nu_{0\perp} \approx 1.097$ [25]. Consequently, the saddle-point value λ_{sp} is larger than λ_c, as required. Inserting the saddle-point values into the integrand yields

$$\rho(t) \sim \exp\left[-\frac{1}{z'}\left(\ln\frac{t}{t_0}\right)^{\gamma}\right] \tag{18}$$

where

$$z' \sim (\lambda_c - \bar{\lambda})^{\gamma\nu_{0\perp}-2} \tag{19}$$

plays the role of a dynamical exponent in the Griffiths phase. In the short-range correlated case, γ is formally 1. Thus, eq. (18) reproduces the well-known power-law Griffiths singularity of density in this case [10, 11, 12]. In contrast, in the long-range correlated case, $\gamma < 1$, the decay of the density is slower than any power. Long-range disorder correlations thus lead to a qualitatively enhanced Griffiths singularity.

The above derivation started from the correlated Gaussian distribution (4). However, an analogous calculation can be performed for a correlated binary distribution by combining the rare region probability (10) with the rare region life time (12). Solving the resulting integral over L_{RR} in saddle-point approximation leads to the same functional form (18) of the Griffiths singularity, with

$$z' = a^{\gamma}/c\ . \tag{20}$$

If the rare regions are not in the active phase but right a the critical point, their decay time depends on their size via the power law $\tau(\lambda_c, L_{RR}) \sim L_{RR}^{z_0}$ rather than the exponential (12). Here, $z_0 \approx 1.581$ is the clean dynamical exponent. For a correlated binary disorder distribution, this can be achieved by tuning the stronger of the two infection rates to the

clean critical value. Repeating the saddle-point integration for this case gives a stretched exponential density decay

$$\ln \rho(t) \sim -t^{\gamma/(\gamma+z_0)} \; . \tag{21}$$

As before, the short-range correlated case is recovered by formally setting $\gamma = 1$.

Griffiths singularities in other quantities can be derived in an analogous manner. Consider, for example, systems that start from a single active site in an otherwise inactive lattice. In this situation, the central quantity is the survival probability $P_s(t)$ that measures how likely the system is to be still active (i.e., to contain at least one active site) at time t. For directed percolation problems such as the contact process, the survival probability behaves in the same way as the density of active sites [17]. Thus, the time-dependencies (18) and (21) derived for $\rho(t)$ also hold for $P_s(t)$.

We emphasize that the dependencies of the Griffiths dynamical exponent z' on the distance from criticality given in (19) and (20) hold outside the asymptotic critical region of the disordered contact process. The analysis of the critical region itself requires more sophisticated methods that will be discussed in the next section.

C. Critical point

After discussing the Griffiths phase, we now turn to the critical point of the disordered contact process itself. The contact process with spatially *uncorrelated* disorder features an exotic infinite-randomness critical point in the universality class of the (uncorrelated) random transverse-field Ising chain [11, 12]. Is this critical point stable or unstable against the long-range power-law disorder correlations (3)? According to Weinrib and Halperin's generalization [26] of the Harris criterion, power-law disorder correlations are irrelevant if the decay exponent γ fulfills the inequality

$$\gamma > 2/\nu_\perp^{unc} \tag{22}$$

where $\nu_\perp^{unc}$ is the correlation length exponent for uncorrelated disorder. If this inequality is violated, the correlations are relevant, and the critical behavior must change. The correlation length exponent of the contact process with uncorrelated disorder takes the value $\nu_\perp^{unc} = 2$ [5, 11]. The long-range correlations are thus irrelevant if $\gamma > 1$ and relevant if $\gamma < 1$. Interestingly, this is the same criterion as we derived for the Griffiths phase in Secs. III A and III B.

What is the fate of the transition in the long-range correlated case $\gamma < 1$? As long-range correlations tend to further enhance the disorder effects, we expect the critical behavior to be of infinite-randomness type, but with modified critical exponents that produce stronger singularities. In the strong-disorder regime close to criticality, the behavior of the contact process is identical to that of a random transverse-field Ising chain as both are governed by the same strong-disorder renormalization group recursion relations [5, 11]. Note that the application of these recursion is justified even in the presence of disorder correlations provided that the distributions of the *logarithms* of μ and λ become infinitely broad. The transverse-field Ising chain with long-range correlated disorder was solved by Rieger and Igloi [15] who mapped the problem onto fractional Brownian motion. They found an exact result for the tunneling exponent ψ which relates correlation length $\xi_\perp$ and correlation time ξ_t via $\ln(\xi_t/t_0) \sim \xi_\perp^\psi$. For $\gamma > 1$, it takes the uncorrelated value $\psi = 1/2$ while it is given by $\psi = 1 - \gamma/2$ for $\gamma < 1$. The correlation length exponent $\nu_\perp$ takes the value 2 for $\gamma > 1$ as for uncorrelated disorder. For $\gamma < 1$, it reads $\nu_\perp = 2/\gamma$ in agreement with general arguments by Weinrib and Halperin [26]. A third exponent is necessary to define a complete set; Rieger and Igloi numerically calculated the scale dimension $\beta/\nu_\perp$ of the order parameter and found it to decay continuously from its uncorrelated value $(3 - \sqrt{5})/4$ (taken for all $\gamma > 1$) to 0 (for $\gamma = 0$).

A qualitative understanding of these results in the context of the contact process can be obtained from simple arguments based on the strong-disorder recursion relations [11] even though a closed form solution of the renormalization group does not exist for

the case of long-range correlated disorder [27]. Imagine performing a (large) number of strong-disorder renormalization group steps, iteratively removing the largest decay rates μ_i and infection rates λ_i. The resulting chain will consist of surviving sites (representing clusters of original sites) whose effective decay rate can be estimated as

$$\mu_{\text{eff}} = C_\mu \frac{\mu_1 \dots \mu_L}{\lambda_1 \dots \lambda_{L-1}} \tag{23}$$

and long bonds with effective infection rates

$$\lambda_{\text{eff}} = C_\lambda \frac{\lambda_1 \dots \lambda_L}{\mu_1 \dots \mu_{L-1}} \tag{24}$$

where L is the size of the cluster or bond. In the strong-disorder limit, the prefactors C_μ and C_λ provide subleading corrections only. $\ln \mu_{\text{eff}}$ and $\ln \lambda_{\text{eff}}$ can thus be understood as the displacements of correlated random walks

$$\ln \mu_{\text{eff}} \sim \sum_{i=1}^{L-1} \ln(\mu_i/\lambda_i)\,, \qquad \ln \lambda_{\text{eff}} \sim \sum_{i=1}^{L-1} \ln(\lambda_i/\mu_i)\,. \tag{25}$$

Right at criticality, these random walks have to be (asymptotically) unbiased because healing and infection remain competing in the limit $L \to \infty$. The typical values $\ln \mu_{\text{typ}}$ and $\ln \lambda_{\text{typ}}$ of the cluster healing and infection rates can be estimated from the variance of the random walk displacements giving

$$|\ln \mu_{\text{typ}}| \sim |\ln \lambda_{\text{typ}}| \sim \sqrt{L\,\tilde{G}(L)} \sim \begin{cases} L^{1/2} & (\gamma > 1) \\ L^{1-\gamma/2} & (\gamma < 1) \end{cases} \tag{26}$$

for large L. Here, $\tilde{G}(L)$ is the sum over the disorder correlation function defined in eq. (7). This estimate thus reproduces the values of ψ quoted above [28].

Moving away from criticality introduces a bias into the random walks. The crossover from critical to off-critical behavior occurs when the displacement due to the bias becomes

larger than the displacement (26) due to the randomness. The bias term scales as $|\lambda - \lambda_c|L$. We thus obtain a crossover length

$$L_x \sim \begin{cases} |\lambda - \lambda_c|^{-2} & (\gamma > 1) \\ |\lambda - \lambda_c|^{-2/\gamma} & (\gamma < 1) \end{cases} \tag{27}$$

in agreement with the quoted values of $\nu_\perp$.

IV. MONTE-CARLO SIMULATIONS

A. Overview

We now turn to large-scale Monte-Carlo simulations of the one-dimensional contact process with power-law correlated disorder. We use the same numerical implementation of the contact process as in earlier studies with uncorrelated disorder in one, two, three, and five dimensions in Refs. [12, 22, 29, 30]. It is based on an algorithm suggested by Dickman [31]: The simulation starts at time $t = 0$ from an initial configuration of active and inactive sites and consists of a sequence of events. During each event an active site i is chosen at random from a list of all N_a active sites. Then a process is selected, either infection of a neighbor with probability $\lambda_i/(1 + \lambda_i)$ or healing with probability $1/(1 + \lambda_i)$. For infection, either the left or the right neighbor are chosen with probability 1/2. The infection succeeds if this neighbor is inactive. The time is then incremented by $1/N_a$.

Using this algorithm, we have simulated long chains for times up to $t = 10^7$. All production runs use $L = 2^{20} \approx 10^6$ sites with periodic boundary conditions, and the results are averages over large numbers of disorder configurations; precise data will be given below.

The random infection rates λ_i are drawn from a correlated binary distribution in which λ_i can take values λ and $c\lambda$ with overall probabilities $(1 - p)$ and p, respectively. Here, p and c are constants between 0 and 1. To generate these correlated random variables, we employ the Fourier-filtering method [32]. It starts from uncorrelated Gaussian random

numbers u_i and turns them into correlated Gaussian random numbers v_i characterized by the (translationally invariant) correlation function $G_\lambda(i,j)$. This is achieved by transforming the Fourier components $\tilde{u}_q$ of the uncorrelated random numbers according to

$$\tilde{v}_q = \left[\tilde{G}(L,q)\right]^{1/2} \tilde{u}_q, \tag{28}$$

where $\tilde{G}(L,q)$ is the Fourier transform of $G_\lambda(i,j)$. We parameterize our long-range correlations by the function

$$G_\lambda(i,j) = \left[1 + (i-j)^2\right]^{-\gamma/2} \tag{29}$$

with periodic boundary conditions using the minimum image convention. Simulations are performed for $\gamma = 1.5, 0.8, 0.6$ and 0.4. To arrive at binary random variables, the correlated Gaussian random numbers v_i then undergo binary projection: the infection rate λ_i takes the value λ ("strong site") if v_i is greater than a composition-dependent threshold and the value $c\lambda$ with $0 < c < 1$ ("weak site") if v_i is less than the threshold. We chose a concentration $p = 0.8$ of weak sites and a strength $c = 0.2$ in all simulations. While the binary projection changes the details of the disorder correlations, the functional form of the long-distance tail remains unchanged.

Most of our simulations are spreading runs that start from a single active site in an otherwise inactive lattice; we monitor the survival probability $P_s(t)$, the number of sites $N_s(t)$ of the active cluster, and its (mean-square) radius $R(t)$. Within the activated scaling scenario [11, 12] associated with an infinite-randomness critical point, these quantities are expected to display logarithmic time dependencies,

$$P_s \sim [\ln(t/t_0)]^{-\bar{\delta}}, \tag{30}$$

$$N_s \sim [\ln(t/t_0)]^{\bar{\Theta}}, \tag{31}$$

$$R \sim [\ln(t/t_0)]^{1/\psi}. \tag{32}$$

The exponents $\bar{\delta}$ and $\bar{\Theta}$ can be expressed in terms of the scale dimension $\beta/\nu_\perp$ of the order parameter and the tunneling exponent ψ as $\bar{\delta} = \beta/(\nu_\perp\psi)$ and $\bar{\Theta} = 1/\psi - 2\bar{\delta}$ [12].

B. Results: critical behavior

We start be considering the case $\gamma = 1.5$. According to the theory laid out in Sec. III, the power-law disorder correlations are irrelevant for $\gamma > 1$. We therefore expect the critical behavior for $\gamma = 1.5$ to be identical to that of the random contact process with uncorrelated disorder which features an infinite-randomness critical point in the universality class of the (uncorrelated) random transverse-field Ising chain [11, 12]. Its critical exponents are known exactly, their numerical values read $\beta = 0.38197$, $\nu_\perp = 2$, $\psi = 0.5$, $\bar{\delta} = 0.38197$, and $\bar{\Theta} = 1.2360$ [5, 6].

To test these predictions, we analyze the time evolution of P_s, N_s and R in Fig. 1. Specifically, the figure presents plots of $P_s^{-1/\bar{\delta}}$, $N_s^{1/\bar{\Theta}}$ and R^ψ vs. $\ln(t)$ using the theoretically predicted exponent values. In such plots, the critical time dependencies (30) to (32) correspond to straight lines independent of the unknown value of the microscopic time scale t_0. The plots show that the data for infection rate $\lambda = 11.44$ follow the predicted time dependencies (30) to (32) over more than four orders of magnitude in time. We thus identify $\lambda_c = 11.44(6)$ as the critical infection rate (the number in brackets is an estimate of the error of the last digit); and we conclude that the critical behavior for $\gamma = 1.5$ is indeed identical to that of the contact process with uncorrelated disorder.

We now turn to $\gamma < 1$, for which the long-range correlations are expected to change the critical behavior. A complete set of exponents is not known analytically in this case; the data analysis is therefore more complicated than for $\gamma > 1$. As we do have an analytical value for the tunneling exponent, $\psi = 1 - \gamma/2$, we can graph R^ψ vs. $\ln(t)$, to find the critical point. Figure 2 shows the corresponding plot for $\gamma = 0.4$. The data at $\lambda = 11.6$ follow the predicted time dependence (32) for more than three orders of magnitude in time. We thus identify $\lambda_c = 11.6(2)$ as the critical infection rate. Analogous plots for $\gamma = 0.8$ and 0.6 give infection rates of $\lambda_c = 11.3(2)$ and $\lambda_c = 11.4(2)$, respectively.

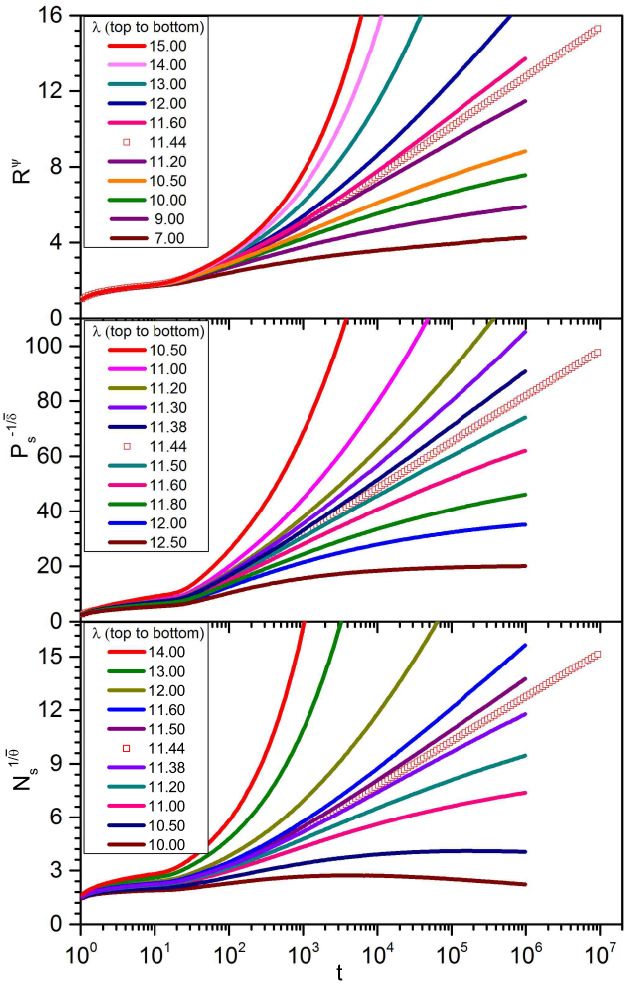

Fig. 1. Time evolution of the number of active sites N_s, the survival probability P_s, and the radius of the active cloud R for the disordered contact process with power-law disorder correlations characterized by a decay exponent $\gamma = 1.5$. The data are averages over up to 40000 samples with 100 individual runs per sample. The critical exponents are fixed at their uncorrelated values $\psi = 0.5$, $\bar{\delta} = 0.38197$, and $\bar{\Theta} = 1.2360$.

Alternatively, we can employ a version of the method used in Refs. [29, 30] that allows us to eliminate the unknown microscopic time scale t_0 from the analysis. It is based on the observation that t_0 takes the same value in all of the quantities (because it is related to the basic energy scale of the underlying renormalization group). Thus, if we plot $N_s(t)$ versus $P_s(t)$, the critical point corresponds to power-law behavior, and t_0 drops out. The same is true for other combinations of observables. Specifically, by combining eqs. (30),

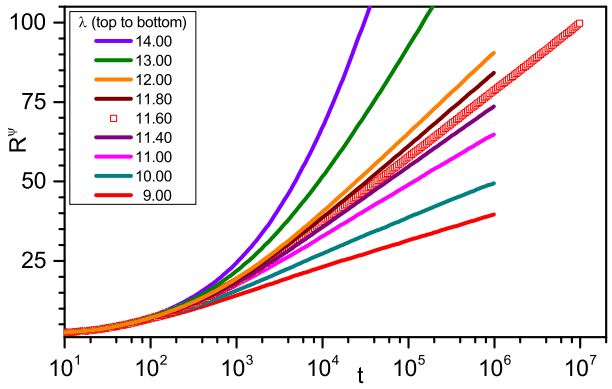

Fig. 2. Time evolution of the radius of the active cloud R for $\gamma = 0.4$. The data are averages over about 30000 samples with 100 individual runs per sample. The tunneling exponent is set to its analytical value $\psi = 1 - \gamma/2 = 0.8$.

(31) and (32), we see that $N_s/P_s^2 \propto R$ at criticality. Thus, identifying straight lines in plots of N_s/P_s^2 versus R allows us to find the critical point without needing a value for t_0. Figure 3 shows such a plot for $\gamma = 0.8$; and we have created analogous plots of $\gamma = 0.6$ and

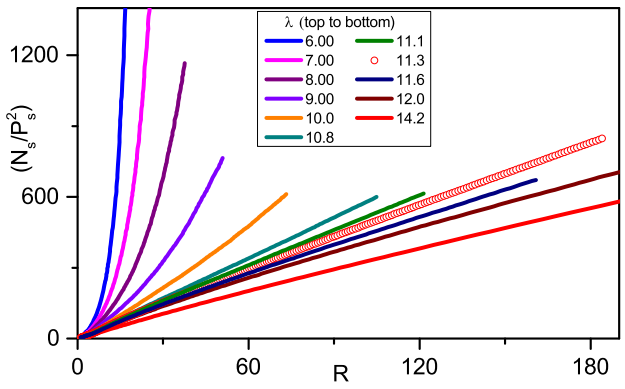

Fig. 3. N_s/P_s^2 vs. R for a correlation decay exponent $\gamma = 0.8$. The data are averages over about 20000 samples with 100 individual runs per sample. The maximum time is 10^6 for all curves except the critical one, $\lambda = 11.3$, for which it is 10^7.

0.4. They give the same critical infection rates, $\lambda_c = 11.3(2)$ (for $\gamma = 0.8$), $\lambda_c = 11.4(2)$ (for $\gamma = 0.6$), and $\lambda_c = 11.6(2)$ (for $\gamma = 0.4$) as the plots of R^{ψ} vs. $\ln(t)$. Interestingly, within their numerical errors, λ_c does not depend on the decay exponent γ of the disorder correlations.

Once the critical point is identified, we can verify and/or find critical exponents by analyzing the time evolutions of P_s, N_s and R. Figure 4 displays $P_s^{-1/\bar{\delta}}$, $N_s^{1/\bar{\Theta}}$ and R^{ψ} versus $\ln(t)$ at criticality for $\gamma = 0.8$. The tunneling exponent ψ is set to its theoretical value

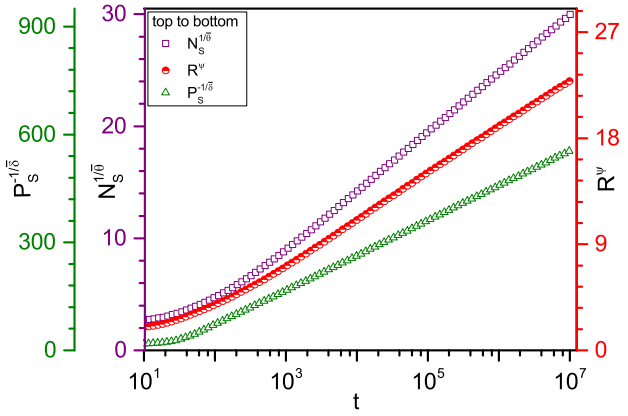

Fig. 4. $N_s^{1/\bar{\Theta}}$, $P_s^{-1/\bar{\delta}}$, and R^{ψ} versus $\ln(t)$ at criticality for a correlation decay exponent $\gamma = 0.8$. Here, $\psi = 0.6$ is set to its theoretical value while $\bar{\delta} = 0.269$ and $\bar{\Theta} = 0.982$ are determined from the data by requiring that the corresponding curves become straight lines for large times.

$1 - \gamma/2$ while $\bar{\delta}$ and $\bar{\Theta}$ are determined from the data by requiring that the corresponding curves become straight lines for large times. The data follow the predicted logarithmic time dependencies (30), (31) and (32) over about four orders of magnitude in time. This not only confirms the theoretical value of ψ, it also allows us to extract estimates the scale dimension $\beta/\nu_{\perp}$ of the order parameter from both $\bar{\delta}$ and $\bar{\Theta}$. We have performed the same analysis also for $\gamma = 0.6$ and $\gamma = 0.4$.

Table I. Critical exponents of the one-dimensional contact process with power-law correlated disorder. The exponents $\nu_\perp$ and ψ (above the horizontal line) are known analytically, as are all exponents in the short-range case $\gamma > 1$. The exponents $\bar{\delta}$ and $\bar{\Theta}$ for $\gamma < 1$ stem from fits of our data. The scale dimension $\beta/\nu_\perp$ of the order parameter can be extracted from both $\bar{\delta}$ and $\bar{\Theta}$, the data in the table are averages of the two values.

exponent	$\gamma > 1$	$\gamma = 0.8$	$\gamma = 0.6$	$\gamma = 0.4$
$\nu_\perp$	2	2.5	3.33	5
ψ	0.5	0.6	0.7	0.8
$\bar{\delta}$	0.3820	0.27	0.20	0.13
$\bar{\Theta}$	1.2360	0.98	0.98	1.01
$\beta/\nu_\perp$	0.1910	0.18	0.14	0.10

The resulting exponent values are summarized in Table I. The uncertainty of $\bar{\delta}$ and $\bar{\Theta}$ can be roughly estimated from the hyperscaling relation $\bar{\Theta} + 2\bar{\delta} = 1/\psi$. The exponents for $\gamma = 0.6$ and $\gamma = 0.4$ fulfill this relation in good approximation (less than 4% difference between the left and the right sides). For $\gamma = 0.8$, the agreement is not quite as good. As $\gamma = 0.8$ is close to the marginal value of 1, this may be caused by a slow crossover from the short-range correlated fixed point to the long-range correlated one.

The values of the scale dimension of the order parameter, $\beta/\nu_\perp$, are in reasonable agreement with those calculated by Rieger and Igloi from the average persistence of a Sinai random walker (see inset of Fig. 1 of Ref. [15]).

To obtain a complete set of exponents, we also analyze off-critical data. Fig. 5 shows a double-logarithmic plot of P_s vs. R for decay exponent $\gamma = 0.8$. The plot allows us to determine the crossover radius R_x at which the survival probability of slightly off-critical curves has dropped to half of its critical value. According to scaling, the crossover radius must depend on the distance from criticality via $R_x \sim |\lambda - \lambda_c|^{-\nu_\perp}$. The inset of Fig. 5 shows that our data indeed follow this power law with the predicted exponent $\nu_\perp = 2/\gamma = 2.5$.

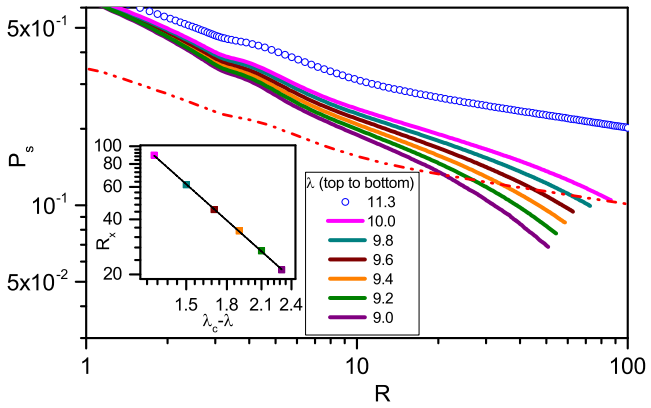

Fig. 5. Double-log plot of P_s vs. R for decay exponent $\gamma = 0.8$ and several infection rates λ at and below the critical rate $\lambda_c = 11.3$. The dash-dotted line shows $P_s/2$ for $\lambda = \lambda_c$. The crossing points of the dash-dotted line with the off-critical data determines the crossover radius R_x. Inset: R_x vs. $|\lambda - \lambda_c|$. The solid line is a power-law fit to $R_x \sim |\lambda - \lambda_c|^{-\nu_\perp}$ with an exponent $\nu_\perp = 2.5$.

C. Results: Griffiths phase

We now turn to the Griffiths phase $\lambda_{c0} \leq \lambda < \lambda_c$ where $\lambda_{c0} \approx 3.298$ is the critical infection rate of the clean contact process containing only "strong" sites ($p = 0$).

Right at the clean critical point, $\lambda = \lambda_{c0}$, the time evolution of the survival probability is predicted to follow the stretched exponential (21) in the long-time limit. Our corresponding data for $\gamma = 0.8$, 0.6, and 0.4 are plotted in Fig. 6. For all γ, the data indeed follow stretched exponentials over more than six orders of magnitude in P_s. The exponent y decreases with decreasing γ, as predicted in (21). The actual numerical values of y are somewhat larger than the prediction $y = \gamma/(\gamma + z_0)$. We attribute this to the fact that, due to the rapid decay of P_s, the data are taken at rather short times ($t \lessapprox 10^3$). Thus, they probably have not reached the true asymptotic regime, yet.

We now move into the bulk of the Griffiths phase, $\lambda_{c0} < \lambda < \lambda_c$. Here, we wish to contrast the conventional power-law Griffiths singularity with the unusual non-power-law form (18). Fig. 7 shows the survival probability as a function of time for a decay exponent $\gamma = 1.5$ and several infection rates inside the Griffiths phase. After initial transients, all

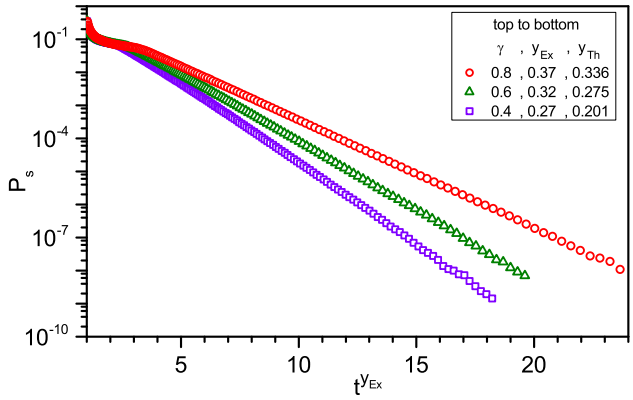

Fig. 6. Time evolution of the survival probability P_s at the clean critical infection rate $\lambda_{c0} = 3.298$ for decay exponents $\gamma = 0.8$, 0.6, and 0.4. The data are averages over 2×10^4 to 10^5 samples with at least 10^4 individual runs per sample. The experimental values y_{Ex} are determined by requiring that the respective curves become straight lines for large times, implying a stretched exponential time dependence, $\ln P_s \sim t^y$. The theoretical values follow from eq. (21) which gives $y_{Th} = \gamma/(\gamma + z_0)$.

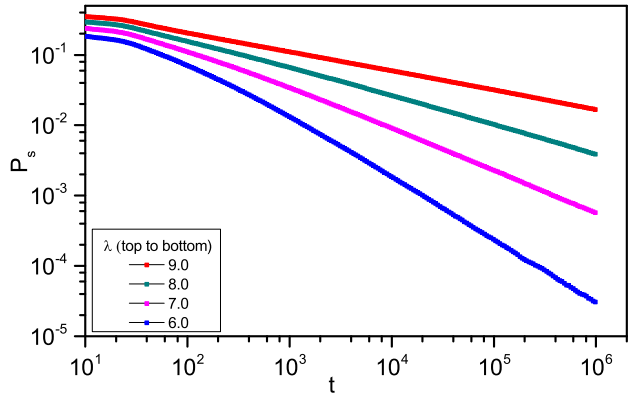

Fig. 7. Double-log plot of the survival probability P_s vs. time t for decay exponent $\gamma = 1.5$ at several infection rates inside the Griffiths phase, $\lambda_{c0} < \lambda < \lambda_c$. The data are averages over up to 40000 samples with 100 individual runs per sample.

data follow power laws (represented by straight lines) over serval orders of magnitude in P_s and/or t. For $\gamma = 1.5$, we thus find the same type of power-law Griffiths singularity as in the case of uncorrelated or short-range correlated disorder.

In the long-range correlated regime, $\gamma < 1$, we expect the survival probability to follow eq. (18) rather than a power-law. This prediction is tested in Fig. 8 which shows of P_s vs. t for decay exponent $\gamma = 0.4$. In the double-logarithmic plot in the inset, all data

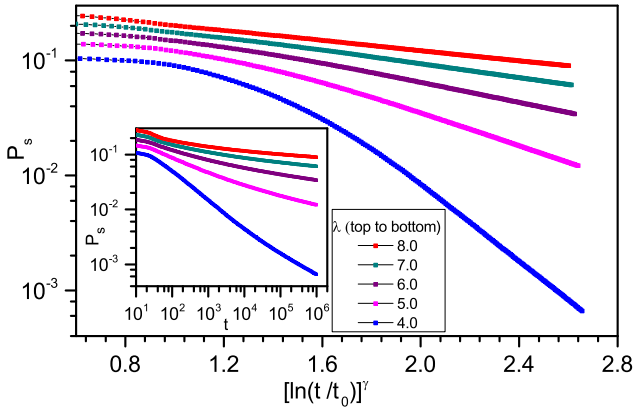

Fig. 8. Survival probability P_s vs. time t for decay exponent $\gamma = 0.4$ at several infection rates inside the Griffiths phase, $\lambda_{c0} < \lambda < \lambda_c$, plotted such that eq. (18) yields straight lines (the values of t_0 are fit parameters). The data are averages over up to 20000 samples with 100 individual runs per sample. Inset: Double-log plot of the same data to test for power-law behavior.

show pronounced upward curvatures rather than the straight lines expected for power laws. In contrast, when plotted as $\ln P_s$ vs. $[\ln(t/t_0)]^\gamma$ (where t_0 is a fit parameter) in the main panel of the figure, all curves become straight for sufficiently long times implying that the long-time behavior of P_s indeed follows eq. (18).

We have produced analogous plots for decay exponents $\gamma = 0.6$ and 0.8. As γ decreases from 1 towards 0, the upward curvature in the double-logarithmic plots becomes bigger, reflecting stronger and stronger deviations from power-law behavior, as expected. In contrast, eq. (18) describes the long-time behavior of all data very well, confirming our theory.

V. GENERALIZATIONS

A. Higher dimensions

It this section, we generalize our results to the contact process in higher dimensions $d > 1$. The theory of Sec. A can be easily adapted, yielding the rare-region distribution

$$P(\lambda_{RR}, L_{RR}) \sim \begin{cases} \exp\left[-\dfrac{1}{2b^2}\, L_{RR}^{d}\, (\lambda_{RR} - \bar{\lambda})^2\right] & (\gamma > d) \\ \exp\left[-\dfrac{1}{2b^2}\, L_{RR}^{\gamma}\, (\lambda_{RR} - \bar{\lambda})^2\right] & (\gamma < d) \end{cases} . \tag{33}$$

This means that the functional form of the rare-region distribution is identical to the case of uncorrelated disorder as long as $\gamma > d$. For $\gamma < d$, the probability for finding a rare-region decays more slowly with its size. In terms of the volume L_{RR}^{d}, it is given by a stretched exponential rather than a simple one.

Using this result, we now repeat the calculation of Sec. B for general d. For $\gamma < d$, the resulting long-time behavior of the density of active sites in the Griffiths phase reads

$$\rho(t) \sim \exp\left[-\frac{d}{z'}\left(\ln\frac{t}{t_0}\right)^{\gamma/d}\right] \tag{34}$$

with

$$z' \sim d(\lambda_c - \bar{\lambda})^{\gamma\nu_{0\perp}-2} \tag{35}$$

As in one dimension, the decay described by eq. (34) is slower than any power. For $\gamma > d$, in contrast, we find the usual power-law behavior. Equation (34) also holds for a correlated binary distribution with $z' = d\, a^{\gamma/d}/c$. The behavior right at the boundary of the Griffiths phase (when the stronger of the two infection rates of the binary distribution is tuned to the clean critical value) takes the form (21) for all dimensions.

The behavior of the critical point itself will again be of infinite-randomness type, but for a sufficiently small correlation decay exponent $\gamma < 2/\nu_{\perp}^{unc}$, the critical exponents will differ from those of the contact process with uncorrelated disorder (which were found

numerically in Ref. [29] for two dimensions and in Ref. [30] for three dimensions). The correlation length exponent will take the value $\nu_\perp = 2/\gamma$ [26]; other exponents need to be found numerically [15].

It is interesting to compare the relevance criteria of the long-range correlations in the Griffiths phase and at the critical point. In one dimension, the long-range correlations become relevant for $\gamma < 1$ both in the Griffiths phase and at criticality (because the correlation length exponent of the one-dimensional contact process with uncorrelated disorder has the value $\nu_\perp^{unc} = 2$, saturating the Harris criterion). In dimensions $d > 1$, the two criteria differ. The uncorrelated correlation length exponent is larger than $2/d$ [29, 30]. Thus, the long-range correlations do not become relevant for $\gamma < d$ but only if $\gamma < 2/\nu_\perp^{unc} < d$. In contrast, the long-range correlations become relevant for $\gamma < d$ in the Griffiths phase. Consequently, for $d > 1$, we expect a (narrow) range of decay exponents γ for which the long-range correlations are relevant in the Griffiths phase but irrelevant at criticality. The fate of the system in this subtle regime remains a task for the future.

B. Other systems

The theory of Secs. III A and III B and its generalization to higher dimensions have produced enhanced *non-power-law* Griffiths singularities for sufficiently long-ranged disorder correlations. Are these results restricted to the contact process or do they apply to other systems as well? In this section, we show that they hold for a broad class of systems in which the charateristic energy or inverse time scale of a rare region depends exponentially on its volume (class B of the rare region classification of Refs. [14, 33]). In addition to the contact process, this class contains, e.g., the random transverse-field Ising model, Hertz' model of the itinerant antiferromagnetic quantum phase transition, and the pair-breaking superconductor-metal quantum phase transition.

To demonstrate the enhanced Griffiths singularities, we generalize the calculation of the rare region density of states developed in Ref. [21] to the case of our power-law

correlated disorder. Consider a disordered system with rare regions whose characteristic energy ϵ depends on their volume via

$$\epsilon(\lambda_{RR}, L_{RR}) = \epsilon_0 \exp[-aL_{RR}^d] \,. \tag{36}$$

Here, ϵ_0 is a microscopic energy scale, and $a = a'(\lambda_{RR} - \lambda_c)^{d\nu_{0\perp}}$ with λ representing the parameter that tunes the system through the phase transition. In the contact process, $\epsilon = 1/\tau$ is the inverse life time of a rare region; in the transverse-field Ising model, it represents its energy gap. We can derive a rare-region density of states by summing over all values of λ_{RR} and L_{RR},

$$\tilde{\rho}(\epsilon) \sim \int_{\lambda_c}^{\infty} \int_0^{\infty} dL_{RR}\, P(\lambda_{RR}, L_{RR})\, \delta[\epsilon - \epsilon(\lambda_{RR}, L_{RR})] \tag{37}$$

with the Gaussian rare-region probability $P(\lambda_{RR}, L_{RR})$ from eq. (33). After carrying out the integral over L_{RR} with the help of the δ function, the remaining λ_{RR}-integral can be performed in saddle-point approximation in the limit $\epsilon \to 0$. For $\gamma < d$, the resulting density of states takes the form

$$\tilde{\rho}(\epsilon) \sim \frac{1}{\epsilon} \exp\left[-\frac{d}{z'}\left(\ln \frac{\epsilon_0}{\epsilon}\right)^{\gamma/d}\right] \tag{38}$$

with z' given by eq. (35). For $\gamma > d$, in contrast, we recover the usual power-law behavior $\tilde{\rho}(\epsilon) \sim \epsilon^{d/z'-1}$. If we start from correlated binary disorder rather than a Gaussian distribution, we arrive at the same expression (38) for the density of states with $z' = da^{\gamma/d}/c$. Equation (38) shows that the Griffiths singularities are qualitatively enhanced for $\gamma < d$ as the density of states diverges as $1/\epsilon$ times a function that is slower than any power law.

Griffiths singularities in other observables can be calculated from appropriate integrals of $\tilde{\rho}(\epsilon)$. For example, our results for the density of active sites in the contact process can be reproduced by $\rho(t) \sim \int d\epsilon\, \tilde{\rho}(\epsilon) \exp(-\epsilon t)$. In the case of the random transverse-field

Ising model, we can calculate (see, e.g., Ref. [14]) the temperature dependence of observables such as the entropy $S(T) \sim \int_0^T d\epsilon \tilde{\rho}(\epsilon)$, the specific heat $C(T) = T(\partial S/\partial T)$, and the susceptibility $\chi(T) \sim (1/T) \int_0^T d\epsilon \tilde{\rho}(\epsilon)$. For $\gamma < d$, we find

$$S(T) \sim C(T) \sim T\chi(T) \sim \exp\left[-\frac{d}{z'}\left(\ln\frac{\epsilon_0}{T}\right)^{\gamma/d}\right] . \tag{39}$$

Analogously, the magnetization in a longitudinal field H scales as

$$M(H) \sim \exp\left[-\frac{d}{z'}\left(\ln\frac{\epsilon_0}{H}\right)^{\gamma/d}\right] . \tag{40}$$

Let us compare these results with those obtained in Ref. [15]. Equations (38), (39), and (40) yield Griffiths singularities that are qualitatively stronger than power laws. In contrast, Rieger and Igloi obtained the usual power-law Griffiths singularities, albeit with changed exponents. We believe that this discrepancy arises from the fact that Rieger and Igloi assumed that the probability for finding a strongly coupled cluster of size L_{RR} in d dimensions takes the same functional form, $\exp(-cL_{RR}^d)$, as for uncorrelated disorder. Our calculations show that this assumption is justified for $\gamma > d$. For $\gamma < d$, however, the rare region probability decays as $\exp(-cL_{RR}^\gamma)$, i.e., more slowly than in the uncorrelated case.

VI. CONCLUSIONS

To summarize, we have studied the effects of long-range spatial disorder correlations on the critical behavior and the Griffiths singularities in the disordered one-dimensional contact process. As long as the correlations decay faster as $1/r_{ij}$ with the distance r_{ij} between the sites, the correlations are irrelevant both at criticality and in the Griffiths phase. This means that both the critical and the Griffiths singularities are identical to those of the contact process with uncorrelated disorder. If the correlations decay more slowly than

$1/r_{ij}$, the universality class of the critical point changes, and the Griffiths singularities take an enhanced, non-power-law form.

What is the reason for the enhanced singularities? As positive spatial correlations imply that neighboring sites have similar infection rates, it is intuitively clear that sufficiently long-ranged correlations must increase the probability for finding large atypical regions. This is borne out in our calculations in Sec. III A: If the disorder correlations decay more slowly than $1/r_{ij}$, the probability for finding a rare region behaves as a stretched exponential of its size (rather than the simple exponential found for uncorrelated and short-range correlated disorder). Note that similar stretched exponentials have also been found in the distributions of rare events in long-range correlated time series [34, 35].

Our theory of the Griffiths phase is easily generalized to higher dimensions. In general dimension d, the rare-region probability decays exponentially with the rare-region volume as long as the disorder correlations decay faster than $1/r_{ij}^d$. As a result, the Griffiths singularities take the usual power-law form. For correlations decaying slower than $1/r_{ij}^d$, the rare region probability becomes a stretched exponential of the volume, leading to enhanced, non-power-law Griffiths singularities.

Moreover, as shown in Sec. V B, the theory is not restricted to the contact process. It holds for all systems for which the characteristic energy (or inverse time) of a rare region depends exponentially on its volume, i.e., for all systems in class B of the rare region classification of Refs. [14, 33]. The random transverse-field Ising model is a prototypical example in the class. Our theory predicts that the character of its Griffiths singularities changes from the usual power-law behavior for correlations decaying faster than $1/r_{ij}^d$ to the enhanced non-power-law forms (39) and (40) for correlations decaying slower than $1/r_{ij}^d$.

What about systems in the other classes, class A and class C, of the rare region classification of Refs. [14, 33]? The rare regions in systems belonging to class A have characteristic energies that decrease as a power of their sizes. Using this power-law dependence rather than the exponential (36) in the calculation of Sec. V B yields an exponentially small

density of states. We conclude that rare regions effects in class A remain very weak, even in the presence of long-range disorder correlations. Rare regions in systems belonging to class C can undergo the phase transition by themselves, independently from the bulk system. This results in a smearing of the global phase transition. Svoboda et al. [36] considered the effects of spatial disorder correlations on such smeared phase transitions. They found that even short-range correlations can have dramatic effects and qualitatively change the behavior of observable quantities compared to the uncorrelated case. This phenomenon may have been observed in $Sr_{1-x}Ca_xRuO_3$ [37].

ACKNOWLEDGEMENTS

This work was supported by the NSF under Grant Nos. DMR-1205803 and PHYS-1066293. We acknowledge the hospitality of the Aspen Center for Physics.

BIBLIOGRAPHY

[1] G. Grinstein. Phases and phase transitions of quneched disordered systems. In E. G. D. Cohen, editor, *Fundamental Problems in Statistical Mechanics VI*, page 147. Elsevier, New York, 1985.

[2] R. B. Griffiths. Nonanalytic behavior above the critical point in a random Ising ferromagnet. *Phys. Rev. Lett.*, 23:17, 1969.

[3] B. M. McCoy. Incompleteness of the critical exponent description for ferromagnetic systems containing random impurities. *Phys. Rev. Lett.*, 23:383, 1969.

[4] Y. Imry. Griffiths singularity in finite macroscopically large dilute Ising models. *Phys. Rev. B*, 15:4448, 1977.

[5] D. S. Fisher. Random transverse field Ising spin chains. *Phys. Rev. Lett.*, 69:534, 1992.

[6] D. S. Fisher. Critical behavior of random transverse-field Ising spin chains. *Phys. Rev. B*, 51:6411, 1995.

[7] M. Thill and D. A. Huse. Equilibrium behaviour of quantum Ising spin glass. *Physica A*, 214:321, 1995.

[8] A. P. Young and H. Rieger. Numerical study of the random transverse-field Ising spin chain. *Phys. Rev. B*, 53:8486, 1996.

[9] Partial results on the related McCoy-Wu model had already been obtained much earlier [38, 39] but they were only fully understood after Fisher's strong-disorder renormalization group calculation [5, 6].

[10] A. J. Noest. New universality for spatially disordered cellular automata and directed percolation. *Phys. Rev. Lett.*, 57:90, 1986; Power-law relaxation of spatially disordered stochastic automata and directed percolation. *Phys. Rev. B*, 38:2715, 1988.

[11] J. Hooyberghs, F. Iglói, and C. Vanderzande. Strong-disorder fixed point in absorbing-state phase transitions. *Phys. Rev. Lett.*, 90:100601, 2003; Absorbing state phase transitions with quenched disorder. *Phys. Rev. E*, 69:066140, 2004.

[12] T. Vojta and M. Dickison. Critical behavior and Griffiths effects in the disordered contact process. *Phys. Rev. E*, 72:036126, 2005.

[13] T. Vojta. Disorder-induced rounding of certain quantum phase transitions. *Phys. Rev. Lett.*, 90:107202, 2003; Smearing of the phase transition in Ising systems with planar defects. *J. Phys. A*, 36:10921, 2003; Broadening of a nonequilibrium phase transition by extended structural defects. *Phys. Rev. E*, 70:026108, 2004.

[14] T. Vojta. Rare region effects at classical, quantum, and non-equilibrium phase transitions. *J. Phys. A*, 39:R143, 2006; Quantum Griffiths effects and smeared phase transitions in metals: theory and experiment. *J. Low Temp. Phys.*, 161:299, 2010.

[15] H. Rieger and F. Igloi. Random quantum magnets with long-range correlated disorder: Enhancement of critical and Griffiths-McCoy singularities. *Phys. Rev. Lett.*, 83:3741, 1999.

[16] T. E. Harris. Contact interactions on a lattice. *Ann. Prob.*, 2:969, 1974.

[17] P. Grassberger and A. de la Torre. *Ann. Phys. (NY)*, 122:373, 1979.

[18] H. K. Janssen. *Z. Phys. B*, 42:151, 1981.

[19] P. Grassberger. *Z. Phys. B*, 47:365, 1982.

[20] The negative tail of the Gaussian has to be truncated appropriately because the infection rate λ_i must be positive.

[21] Thomas Vojta and José A. Hoyos. Criticality and quenched disorder: Harris criterion versus rare regions. *Phys. Rev. Lett.*, 112:075702, Feb 2014.

[22] Thomas Vojta, John Igo, and José A. Hoyos. Rare regions and griffiths singularities at a clean critical point: The five-dimensional disordered contact process. *Phys. Rev. E*, 90:012139, Jul 2014.

[23] M. N. Barber. Finite-size scaling. In C. Domb and J. L. Lebowitz, editors, *Phase Transitions and Critical Phenomena*, volume 8, pages 145–266. Academic, New York, 1983.

[24] The scaling behavior of a also follows from the fact that the term aL_{RR} in the exponent of (12) represents the number $(L_{RR}/\xi_\perp)$ of independent correlation volumes that need to decay coherently.

[25] I. Jensen. Low-density series expansions for directed percolation: I. a new efficient algorithm with applications to the square lattice. *J. Phys. A*, 32:5233, 1999.

[26] Abel Weinrib and B. I. Halperin. Critical phenomena in systems with long-range-correlated quenched disorder. *Phys. Rev. B*, 27:413–427, Jan 1983.

[27] This mainly stems from the fact that the strong-disorder renormalization group cannot be formulated in terms of single-site distributions if the disorder is long-range correlated.

[28] Note that this argument is not rigorous as it neglects the subtle correlations involved in picking which μ_i or λ_i to decimate in the strong-disorder renormalization group step.

[29] T. Vojta, A. Farquhar, and J. Mast. Infinite-randomness critical point in the two-dimensional disordered contact process. *Phys. Rev. E*, 79:011111, 2009.

[30] Thomas Vojta. Monte carlo simulations of the clean and disordered contact process in three dimensions. *Phys. Rev. E*, 86:051137, Nov 2012.

[31] R. Dickman. Reweighting in nonequilibrium simulations. *Phys. Rev. E*, 60:R2441, 1999.

[32] H. A. Makse, S. Havlin, M. Schwartz, and H. E. Stanley. Method for generating long-range correlations for large systems. *Phys. Rev. E*, 53:5445–5449, 1996.

[33] T. Vojta and J. Schmalian. Quantum Griffiths effects in itinerant Heisenberg magnets. *Phys. Rev. B*, 72:045438, 2005.

[34] Armin Bunde, Jan F. Eichner, Jan W. Kantelhardt, and Shlomo Havlin. Long-term memory: A natural mechanism for the clustering of extreme events and anomalous residual times in climate records. *Phys. Rev. Lett.*, 94:048701, Jan 2005.

[35] Eduardo G. Altmann and Holger Kantz. Recurrence time analysis, long-term correlations, and extreme events. *Phys. Rev. E*, 71:056106, May 2005.

[36] C. Svoboda, D. Nozadze, F. Hrahsheh, and T. Vojta. Disorder correlations at smeared phase transitions. *EPL (Europhysics Letters)*, 97(2):20007, 2012.

[37] L. Demkó, S. Bordács, T. Vojta, D. Nozadze, F. Hrahsheh, C. Svoboda, B. Dóra, H. Yamada, M. Kawasaki, Y. Tokura, and I. Kézsmárki. Disorder promotes ferromagnetism: Rounding of the quantum phase transition in $Sr_{1-x}Ca_xRuO_3$. *Phys. Rev. Lett.*, 108:185701, May 2012.

[38] B. M. McCoy and T. T. Wu. Random impurities as the cause of smooth specific heats near the critical temperature. *Phys. Rev. Lett.*, 21:549, 1968.

[39] B. M. McCoy and T. T. Wu. Theory of a two-dimensional Ising model with random impurities. i. thermodynamics. *Phys. Rev.*, 176:631, 1968.

V. CONTACT PROCESS ON GENERALIZED FIBONACCI CHAINS: INFINITE-MODULATION CRITICALITY AND DOUBLE-LOG PERIODIC OSCILLATIONS

Hatem Barghathi[1], David Nozadze[1,2], and Thomas Vojta[1]

[1]*Department of Physics, Missouri University of Science and Technology, Rolla, MO 65409, USA*

[2]*Department of Physics, The Ohio State University, Columbus, OH 43210, USA*

ABSTRACT[*]

We study the nonequilibrium phase transition of the contact process with aperiodic transition rates using a real-space renormalization group as well as Monte-Carlo simulations. The transition rates are modulated according to the generalized Fibonacci sequences defined by the inflation rules A $\rightarrow$ AB^k and B $\rightarrow$ A. For $k = 1$ and 2, the aperiodic fluctuations are irrelevant, and the nonequilibrium transition is in the clean directed percolation universality class. For $k \geq 3$, the aperiodic fluctuations are relevant. We develop a complete theory of the resulting unconventional "infinite-modulation" critical point which is characterized by activated dynamical scaling. Moreover, observables such as the survival probability and the size of the active cloud display pronounced double-log periodic oscillations in time which reflect the discrete scale invariance of the aperiodic chains. We illustrate our theory by extensive numerical results, and we discuss relations to phase transitions in other quasiperiodic systems.

[*]Published in Physical Review E **89**, 012112 (2014).

I. INTRODUCTION

Many-particle systems far from equilibrium can display abrupt transitions between different nonequilibrium steady states that share many characteristics with equilibrium phase transitions. Examples of such nonequilibrium phase transitions occur in turbulence, catalytic reactions, interface growth, and in the dynamics of epidemics and other biological populations [1, 2, 3, 4, 5, 6, 7, 8].

Absorbing-state transitions constitute a particularly well-studied subclass of nonequilibrium phase transitions. They separate active, fluctuating steady states from absorbing states which are completely inactive and do not display any fluctuations. Generically, absorbing-state transitions are in the directed percolation (DP) universality class [9], provided they feature a scalar order parameter and short-range interactions but no extra symmetries or conservation laws [10, 11]. The contact process [12] is a prototypical model in the DP universality class. Experimental examples of absorbing state transitions were found in turbulent liquid crystals [13], periodically driven suspensions [14, 15], and in systems of superconducting vortices [16].

Many realistic experimental systems contain various types of spatial inhomogeneities. For this reason, the effects of such inhomogeneities on absorbing state transitions have attracted considerable attention. Random disorder was shown to destabilize the clean DP critical point [17] because its correlation length critical exponent $\nu_\perp$ violates the Harris criterion [18] $d\nu_\perp > 2$ in space dimensions $d = 1, 2$ and 3. Early numerical simulations of the disordered contact process [19, 20, 21, 22] showed unusually slow dynamics but the ultimate fate of the transition was only resolved by means of a strong-disorder renormalization group analysis [23] of the one-dimensional disordered contact process. It yielded an exotic infinite-randomness critical point accompanied by power-law Griffiths singularities [24]. The renormalization group predictions were confirmed by Monte-

Carlo simulations [25], and analogous behavior was also found in two and three dimensions [26, 27] as well as in diluted systems at the lattice percolation threshold [28].

Spatial inhomogeneities can arise not just from random disorder but also from deterministic but aperiodic (quasiperiodic) modulations of the transition rates defining the nonequilibrium process. The stability of a clean critical point against such aperiodic fluctuations can be tested by means of a generalization of the Harris criterion, the Harris-Luck criterion [29], which relates the clean correlation length exponent $\nu_\perp$ and the wandering exponent ω of the aperiodic structure.

In this paper, we use a real-space renormalization group as well as Monte-Carlo simulations to study the one-dimensional contact process with aperiodic transition rates modulated according to the generalized Fibonacci sequences defined by the inflation rules $A \to AB^k$ and $B \to A$. For $k = 1$ and 2, the aperiodic fluctuations are irrelevant according to the Harris-Luck criterion. Correspondingly, we find the nonequilibrium transition to be in the clean directed percolation universality class. For $k \geq 3$, the aperiodic fluctuations are relevant. We develop a complete theory of the resulting "infinite-modulation" critical point. It is characterized by a diverging strength of the inhomogeneities and features activated dynamical scaling similar to the disordered contact process. Moreover, observables display double-log periodic oscillations in time which reflect the discrete scale invariance of the aperiodic chains. We also confirm and illustrate the renormalization group predictions by extensive numerical simulations.

The paper is organized as follows. In Sec. II, we introduce the contact process and the generalized Fibonacci chains. We also discuss the Harris-Luck criterion. The renormalization group theory is developed in Sec. III. Section IV is devoted to the Monte-Carlo simulations. We conclude in Sec. V.

II. CONTACT PROCESS ON APERIODIC CHAINS

A. Generalized Fibonacci chains

We consider a family of aperiodic two-letter sequences generated by the inflation rules

$$\begin{aligned} \mathrm{A} &\rightarrow \mathrm{AB}^k \\ \mathrm{B} &\rightarrow \mathrm{A} \end{aligned} \tag{1}$$

where k is a positive integer and B^k stands for a sequence of k letters B. The case $k = 1$ corresponds to the famous Fibonacci sequence. For $k = 2$, the fourth-generation sequence (starting from a single letter A) reads ABBAAABBABB. In general, the sequences created by eq. (1) contain groups of k letters B separated by either single letters A or groups of $k + 1$ letters A. Many properties of these sequences can be obtained from the substitution matrix

$$\mathbf{M}_k = \begin{pmatrix} 1 & 1 \\ k & 0 \end{pmatrix} \tag{2}$$

which describes how the numbers N_A and N_B of letters A and B evolve under the inflation (see, e.g., Ref. [30] and references therein). Its eigenvalues read

$$\zeta_\pm = \frac{1}{2}\left(1 \pm \sqrt{1+4k}\right) . \tag{3}$$

The larger eigenvalue ζ_+ controls how the total length $N(i) = N_A(i) + N_B(i)$ increases with the inflation step i. In the limit of large i, one obtains $N_i \sim \zeta_+^i$. The smaller eigenvalue ζ_- governs the fluctuations of the numbers N_A and N_B. Specifically, $\Delta N_A(i) = |N_A(i) - x_A N(i)| \sim |\zeta_-|^i$ for large i. Here $x_A = \lim_{i\to\infty} N_A(i)/N(i)$ is the fraction of letters A in the infinite chain. The same relation also holds for N_B. The wandering exponent ω relates the fluctuations to the length of the chain, $\Delta N_A(i) \sim N(i)^\omega$. This yields the equation

$$\omega = \ln|\zeta_-|/\ln\zeta_+ . \tag{4}$$

For the generalized Fibonacci chains defined in (1), the specific values are $\omega_1 = -1$, $\omega_2 = 0$ and $\omega_3 \approx 0.3171$ for $k = 1, 2$ and 3. Upon further increasing k, ω increases monotonically and reaches 1 for $k \to \infty$.

B. Contact process

The (clean) contact process [12] is one of the simplest systems undergoing an absorbing state transition. It can be understood as model for the spreading of an epidemic. Each lattice site can be in one of two states, active (infected) or inactive (healthy). Over time, active sites can infect their neighbors or they can heal spontaneously. More precisely, the time evolution is a continuous-time Markov process during which infected sites heal at a rate μ while healthy sites become infected by their neighbors at a rate $\lambda n/(2d)$. Here, n is the number of sick nearest neighbors of the given site.

The long-time behavior of the system is controlled by the ratio of the infection rate λ and the healing rate μ. For $\lambda \ll \mu$, healing dominates over infection, and the epidemic eventually dies out completely. Thus, the model ends up in the absorbing state without any infected sites. This is the inactive phase. In contrast, the density of infected sites remains nonzero in the long-time limit if the infection rate λ is sufficiently large, i.e., the model is in the active phase. The nonequilibrium transition separating these two phases belongs to the DP universality class.

Spatial inhomogeneity can be introduced into the contact process by making the infection and/or healing rates dependent on the lattice site. We are interested in aperiodic (quasiperiodic) inhomogeneities. Specifically, we consider a chain of sites that have equal healing rates μ but two different the infection rates λ_A and λ_B [31]. They are arranged on the bonds of the chain according to the generalized Fibonacci sequences discussed in the last section. An example ($k = 2$) is shown in Fig. 1. For $\lambda_A = \lambda_B$, the system coincides with the usual (clean) one-dimensional contact process.

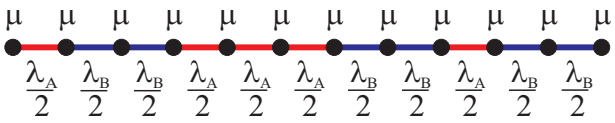

Fig. 1. Sequence of transition rates for the contact process on a generalized Fibonacci chain, showing the 4th generation of the $k = 2$ chain.

C. Harris-Luck criterion

Luck [29] derived a criterion for the stability of a clean critical point against weak aperiodic inhomogeneities. The basic idea is analogous to that of the Harris criterion for random disorder: The clean critical point is stable of the fluctuations Δr of the local distance from criticality between different correlation volumes are smaller than the global distance r to criticality. For aperiodic inhomogeneities characterized by a wandering exponent ω, the fluctuations behave as $\Delta r \sim N^{\omega-1} \sim \xi^{d(\omega-1)}$ while the global distance from criticality scales as $r \sim \xi^{-1/\nu_\perp}$. The condition $\Delta r < r$ for $\xi \to \infty$ leads to the exponent inequality

$$\omega < 1 - \frac{1}{d\nu_\perp} \,. \tag{5}$$

This is the Harris-Luck criterion. In the case of random disorder, $\omega = 1/2$, it reduces to the usual Harris criterion [18]. If the inequality (5) is fulfilled, weak inhomogeneities are irrelevant, otherwise they are relevant and change the character of the phase transition.

The correlation length exponent of the one-dimensional clean contact process takes the value $\nu_\perp \approx 1.097$. The Harris-Luck criterion thus simplifies to $\omega < 1 - 1/\nu_\perp \approx 0.0884$. This implies that aperiodic fluctuations of the transition rates are irrelevant for $k = 1$ and 2 while they are relevant for $k \geq 3$.

III. REAL-SPACE RENORMALIZATION GROUP

A. Overview

This section is devoted to a real-space renormalization group for the contact process on generalized Fibonacci chains. Our method is inspired by a similar calculation for the transverse-field Ising chain [32]. There are, however, some important differences.

Let us start by assuming that the transition rates fulfill the condition $\lambda_A \ll \mu \ll \lambda_B$. We can then perform a renormalization group step which consists of two parts:

(i) Combine the $(k+1)$ consecutive sites connected by the large λ_B infection rate into a single new site with a renormalized healing rate $\tilde{\mu} \ll \mu$. Structurally, this reverses one inflation step, as the result is a system with uniform infection rates λ_A but two different healing rates, μ and $\tilde{\mu}$, modulated according to a Fibonacci chain of one generation earlier.

(ii) Integrate out the sites with the original healing rate μ which is now the largest transition rate in the system. This generates renormalized infection rates (bonds) $\tilde{\lambda}$ between the remaining sites and reverses another inflation step. The system now has uniform healing rate $\tilde{\mu}$ and two different infection rates λ_A and $\tilde{\lambda}$ modulated according to a Fibonacci chain of two generations earlier than the original chain.

After renaming $\lambda_A \to \lambda_B$, $\tilde{\lambda} \to \lambda_A$ and $\tilde{\mu} \to \mu$ we arrive at a system equivalent to the original one, but with renormalized transition rates. As long as the renormalized rates still fulfill the condition $\lambda_A \ll \mu \ll \lambda_B$, this renormalization group step can be iterated.

In the opposite limit, $\lambda_A \gg \mu \gg \lambda_B$, an analogous renormalization group step does *not* preserve the structure of the system and can thus not be iterated. However, we will study the fate of systems in this regime numerically at the end of Sec. IV. If the healing rate μ is much larger (or smaller) than *both* infection rates, the system can never reach criticality, instead it is deep in the inactive (or active) phase.

B. Recursion relations

We now analyze the renormalization group step outlined above in a quantitative manner. The infection rate λ_B is the largest transition rate in the system. Thus, sites coupled by λ_B-bonds will quickly reinfect each other when one of them heals. Consequently, all $k+1$ sites coupled by the k consecutive λ_B bonds can be merged into a single new site of "moment" (number of sites)

$$\tilde{m} = (k+1)m \tag{6}$$

where m is the moment of the original sites (in the bare system, $m = 1$). The renormalized healing rate $\tilde{\mu}$ of these new sites can be found either by directly enumerating all possible healing paths of the cluster or by analyzing the eigenvalues of the generator of the Markov process in the Hamiltonian formalism (see, e.g., Ref. [23]). Both methods give the same result,

$$\tilde{\mu} = \alpha_k \frac{\mu^{k+1}}{(\lambda_B/2)^k} \tag{7}$$

with $\alpha_1 = 2$, $\alpha_2 = 4$, and $\alpha_3 = 8$. If $\mu \ll \lambda_B$, the renormalized healing rate is strongly reduced, $\tilde{\mu} \ll \mu$.

After the first part of the renormalization group step, the system has uniform infection rates λ_A but two types of sites, original sites having healing rate μ and new sites having healing rate $\tilde{\mu}$. If the rates fulfill the condition $\tilde{\mu} \ll \lambda_A \ll \mu$, we can perform the second part of the renormalization group step and integrate out the original sites which occur in groups of k. This leads to new effective bonds of length $k+1$ and renormalized infection rate

$$\tilde{\lambda}/2 = \frac{(\lambda_A/2)^{k+1}}{\mu^k} \,. \tag{8}$$

The renormalization group step is finished after renaming $\lambda_A \to \lambda_B$, $\tilde{\lambda} \to \lambda_A$ and $\tilde{\mu} \to \mu$. Equations (7) and (8) are similar to the corresponding relations for the transverse fields and

interactions in the transverse-field Ising model on generalized Fibonacci chains [32]. The main difference is the extra factor α_k in (7).

If we now iterate the renormalization group step, we obtain the following recursion relations

$$\lambda_{A,j+1}/2 = \frac{(\lambda_{A,j}/2)^{k+1}}{\mu_j^k}, \qquad \lambda_{B,j+1} = \lambda_{A,j}, \tag{9}$$

$$\mu_{j+1} = \alpha_k \frac{\mu_j^{k+1}}{(\lambda_{B,j}/2)^k}, \tag{10}$$

$$m_{j+1} = (k+1)\, m_j, \tag{11}$$

where j is the index of the renormalization group step. For the further analysis, it is convenient to introduce variables R_j and S_j that characterize the ratios of the transition rates,

$$R_j = \ln(2\mu_j/\lambda_{B,j}), \qquad S_j = \ln(\lambda_{A,j}/(2\mu_j)). \tag{12}$$

In terms of these variables, the recursion relations (9) and (10) turn into an inhomogeneous linear recurrence

$$R_{j+1} = kR_j - S_j + A_k, \tag{13}$$

$$S_{j+1} = -kR_j + (k+1)S_j - A_k \tag{14}$$

where $A_k = \ln(\alpha_k)$.

C. Renormalization-group flow

The general solution of the inhomogeneous recurrence (13,14) is the sum of a particular solution and the general solution of the corresponding homogeneous recurrence.

To find a particular solution, we use the ansatz $R_j = \bar{R} = \text{const}$ and $S_j = \bar{S} = \text{const}$. Inserting this into eqs. (13) and (14) yields

$$\bar{R} = -\frac{k-1}{k(k-2)} A_k \,, \qquad \bar{S} = -\frac{1}{k(k-2)} A_k \,. \tag{15}$$

The ansatz fails for the case $k = 2$ which thus requires a separate calculation. It will be given in the appendix.

The general solution of the homogeneous recurrence

$$R_{j+1} = kR_j - S_j \,, \tag{16}$$

$$S_{j+1} = -kR_j + (k+1)S_j \tag{17}$$

can be easily found by diagonalizing the coefficient matrix

$$\mathbf{T}_k = \begin{pmatrix} k & -1 \\ -k & k+1 \end{pmatrix} . \tag{18}$$

Its eigenvalues, ζ_+^2 and ζ_-^2, are the squares of the eigenvalues of the substitution matrix (2), and the corresponding right eigenvectors read

$$\begin{pmatrix} 1 \\ -\zeta_+ \end{pmatrix}, \qquad \begin{pmatrix} 1 \\ -\zeta_- \end{pmatrix} . \tag{19}$$

By decomposing the initial conditions $R_0 - \bar{R}$ and $S_0 - \bar{S}$ into the eigenvectors and multiplying with the j-th power of the matrix $\mathbf{T}_k$, we obtain the solution

$$R_j = \frac{1}{\zeta_+ - \zeta_-} \left(-\eta_- \zeta_+^{2j} + \eta_+ \zeta_-^{2j} \right) - \frac{k-1}{k(k-2)} A_k \,, \tag{20}$$

$$S_j = \frac{1}{\zeta_+ - \zeta_-} \left(\eta_- \zeta_+^{2j+1} - \eta_+ \zeta_-^{2j+1} \right) - \frac{1}{k(k-2)} A_k \,. \tag{21}$$

The coefficients η_+ and η_- are determined by the initial ratios R_0 and S_0 via

$$\eta_\pm = \zeta_\pm R_0 + S_0 + \frac{A_k}{k(k-2)}[1 + \zeta_\pm(k-1)] \,. \tag{22}$$

Let us analyze the solution (20), (21) to find the critical point. In the limit $j \to \infty$, the behavior of R_j and S_j is dominated by the larger of the two eigenvalues as $R_j \sim -\eta_- \zeta_+^{2j}$ and $S_j \sim \eta_- \zeta_+^{2j+1}$. If η_- is negative, R_j flows to $+\infty$ while S_j flows to $-\infty$. The healing rate μ thus becomes larger than both infection rates, putting the system into the inactive phase. In contrast, if η_- is positive, R_j flows to $-\infty$ while S_j flows to $+\infty$. In this case, the system is in the active phase because the healing rate becomes smaller than both infection rates. The critical point is therefore given by the condition $\eta_- = 0$. This can be rewritten in terms of the initial (bare) values of the transition rates as

$$\left(\frac{2\mu}{\lambda_B}\right)^{1-\zeta_-} = \frac{\lambda_A}{\lambda_B}\,\alpha_k^{\frac{1+\zeta_-(k-1)}{k(k-2)}} \,. \tag{23}$$

D. Critical behavior

At criticality, $\eta_- = 0$, the asymptotic behavior of R_j and S_j is determined by the smaller eigenvalue ζ_-. Specifically,

$$R_j = \frac{1}{\zeta_+ - \zeta_-}\eta_+ \zeta_-^{2j} - \frac{k-1}{k(k-2)} A_k \,, \tag{24}$$

$$S_j = -\frac{1}{\zeta_+ - \zeta_-}\eta_+ \zeta_-^{2j+1} - \frac{1}{k(k-2)} A_k \,. \tag{25}$$

Both quantities are negative because η_+ and ζ_- are negative. If $|\zeta_-| > 1$, both R_j and S_j diverge towards $-\infty$ with increasing j, i.e, the modulation of the transition rates becomes infinitely strong. At the resulting "infinite-modulation" critical point, the condition $\lambda_{A,j} \ll \mu_j \ll \lambda_{B,j}$ is better and better fulfilled with increasing j implying that the renormalization group becomes asymptotically exact.

To determine the critical behavior, we first analyze the flow of the inverse time scale Ω under the renormalization group. Ω can be identified with the largest transition rate in the system, $\Omega_j = \lambda_{B,j}$. Its recursion relation thus reads

$$\frac{\Omega_j}{\Omega_{j-1}} = \frac{\lambda_{A,j-1}}{\lambda_{B,j-1}} = \exp(R_{j-1} + S_{j-1}) \; . \tag{26}$$

Inserting the critical solutions (24) and (25), and iterating the recursion gives

$$\Omega_j = \alpha_k^{j/(k-2)} \exp\left[\frac{\eta_+(1-\zeta_-)(1-\zeta_-^{2j})}{(\zeta_+ - \zeta_-)(1-\zeta_-^2)}\right] \Omega_0 \tag{27}$$

To relate the inverse time scale Ω_j to the length scale ℓ_j, we recall that the length of the generalized Fibonacci chain increases as $N \sim \zeta_+^i$ with inflation step i. As each renormalization group step corresponds to two inflation steps, this means that the length scale ℓ_j behaves as $\ell_j \sim N \sim \zeta_+^{2j}$. Inserting this relation into (27), we obtain activated dynamical scaling of the form

$$\ln(\Omega_0/\Omega_j) \sim \ell_j^{\psi} \; . \tag{28}$$

The tunneling exponent is identical to the wandering exponent of the underlying Fibonacci chain, i.e., it takes the value

$$\psi = \omega = \ln|\zeta_-|/\ln\zeta_+ \; . \tag{29}$$

We now turn to the decay of the density ρ of active sites with time at criticality. Sites (clusters) that survive the renormalization group to step j, survive the real time evolution to time $t_j \sim 1/\Omega_j$. The density of sites after renormalization group step j is easily estimated as $\rho_j = n_j m_j$ where $n_j \sim 1/\ell_j$ is the density of surviving clusters and $m_j = (k+1)^j$ is their moment. Combining this with eq. (27), we obtain

$$\rho(t_j) \sim \left[\ln(t_j/t_0)\right]^{-\bar{\delta}} \tag{30}$$

with the critical exponent given by

$$\bar{\delta} = \frac{1}{\psi} - \phi = \frac{1}{\psi} - \frac{\ln(k+1)}{2\ln|\zeta_-|} \,. \tag{31}$$

(ϕ characterizes the relation between cluster moment and inverse time scale, $m_j \sim [\ln(\Omega_0/\Omega_j)]^{\phi}$.)

Experiments starting from a single active seed site embedded in an otherwise inactive system can be characterized by the survival probability P_s and the average number N_s of sites in the active cloud. Within the renormalization group approach, a run survives to time t if the seed site belongs to a cluster surviving at renormalization scale $\Omega \sim 1/t$. As the density of (original) sites surviving after renormalization group step j is given by $n_j m_j$, we find that the survival probability decays with the same critical exponent as the density, $P_s(t_j) \sim \left[\ln(t_j/t_0)\right]^{-\bar{\delta}}$. In each of the surviving runs, the number of infected sites is simply the current size of the renormalization group cluster. Thus, $N_s(t_j) = n_j m_j^2$. Expressing j in terms of the time scale yields

$$N_s(t_j) \sim \left[\ln(t_j/t_0)\right]^{\bar{\Theta}} \tag{32}$$

with the so-called critical initial slip exponent given by

$$\bar{\Theta} = -\frac{1}{\psi} + 2\phi = -\frac{1}{\psi} + \frac{\ln(k+1)}{\ln|\zeta_-|} \,. \tag{33}$$

Note that $\bar{\Theta}$, $\bar{\delta}$ and ψ fulfill the hyperscaling relation $\bar{\Theta} + 2\bar{\delta} - 1/\psi = 0$.

Finally, we turn to the off-critical behavior. Consider a system slightly on the inactive side of the transition, $\eta_- < 0$. According to the general solution (20), R_j increases under renormalization. The character of the flow changes from critical to that of the inactive

phase when R_j reaches 0. This happens at the crossover step j^*. If both $\zeta_+ > 1$ and $|\zeta_-| > 1$, the constant term in (20) can be neglected. This yields a crossover step

$$j^* = \frac{1}{2} \frac{\ln(\eta_-/\eta_+)}{\ln|\zeta_-/\zeta_+|} . \tag{34}$$

The corresponding crossover length scale is given by $\ell_{j^*} \sim \zeta_+^{2j^*} \sim \eta_-^{-\nu_\perp}$ with the correlation length critical exponent

$$\nu_\perp = \frac{1}{1-\psi} = \frac{\ln(\zeta_+)}{\ln(\zeta_+) - \ln|\zeta_-|} . \tag{35}$$

Interestingly, $\nu_\perp$ exactly saturates the Harris-Luck inequality (5).

The critical exponents ψ, $\bar{\delta}$ and ν (or, alternatively, ψ, $\bar{\Theta}$ and ν) constitute a complete set of exponents. All other exponents can therefore be calculated from scaling relations, for example, $\beta = \bar{\delta}\nu_\perp\psi$.

E. Log-periodic oscillations

If the renormalized transition rates of consecutive renormalization group steps are well separated, $\mu_{j+1} \ll \mu_j$ and $\lambda_{A,j+1} \ll \lambda_{A,j}$, the time evolution of the system proceeds in pronounced steps. For example, each downward step in density of active sites is associated with a time given by one of the renormalized decays rates, $1/t \sim \mu_j$.

The generalized Fibonacci sequences are invariant under the inflation rules (1), i.e., they feature *discrete* scale invariance. The steps in various observables are manifestations of the log-periodic oscillations usually associated with such discrete scale invariance (see, e.g., Ref. [33] for a review).

Within the real-space renormalization group approach, the steps can be analyzed by comparing the values of an observable at two consecutive renormalization group steps. The density ρ of active sites and the survival probability P_s behave as $\rho_j \sim P_{s,j} \sim m_j/\ell_j \sim (k+1)^j \zeta_+^{-2j}$. The step in $\ln\rho$ and $\ln P_s$ is therefore given by

$$\Delta\ln(\rho) = \Delta\ln(P_s) = \ln[(k+1)/\zeta_+^2] . \tag{36}$$

Because of the activated scaling, the oscillations are not log-periodic but double-log periodic in time, i.e.,

$$\Delta \ln[\ln(t/t_0)] = 2 \ln |\zeta_-| \, . \tag{37}$$

The size N_s of the active cluster growing out of a single seed has analogous steps of magnitude

$$\Delta \ln(N_s) = \ln[(k+1)^2/\zeta_+^2] \, . \tag{38}$$

F. Explicit predictions for $k = 1, 2$ and 3

We now apply the general renormalization group theory developed above to the specific cases $k = 1, 2$ and 3.

$k = 1$*: Fibonacci chain.* The eigenvalues of the substitution matrix $\mathbf{M}_1$ are given by $\zeta_\pm = (1 \pm \sqrt{5})/2$. Their numerical values are $\zeta_+ = 1.618$ and $\zeta_- = -0.6180$. As $|\zeta_-| < 1$, the (logarithmic) ratio variables R_j and S_j at criticality do not approach $-\infty$ under the renormalization group. Instead R_j approaches 0 and S_j goes to a constant. The renormalized transition rates thus eventually violate the condition $\lambda_A \ll \mu \ll \lambda_B$ (even if the bare rates fulfill it). This implies that the renormalization group method does not describe the correct asymptotic critical behavior for $k = 1$.

$k = 2$*:* The eigenvalues of the substitution matrix $\mathbf{M}_2$ are $\zeta_+ = 2$ and $\zeta_- = -1$. As $|\zeta_-| = 1$, the system is right at the boundary between the renormalization group method working and failing, and a more detailed analysis is required. Although the general solution (20,21) is not valid for $k = 2$, we have solved this case in the appendix. At criticality, both R_j and S_j go towards large positive values with $j \to \infty$. This means that the renormalization group method eventually fails for $k = 2$ even if the bare inhomogeneities are strong.

$k = 3$*:* The substitution matrix $\mathbf{M}_3$ has eigenvalues $\zeta_\pm = (1 \pm \sqrt{13})/2$ with numerical values $\zeta_+ = 2.303$ and $\zeta_- = -1.303$. Because $|\zeta_-| > 1$, the renormalization group is asymptotically exact in this case. Inserting ζ_+ and ζ_- into eqs. (29), (31), (33), and (35), we obtain the following values for the critical exponents: $\psi = \omega_3 = 0.3171$, $\bar{\delta} = 0.5330$,

$\bar{\Theta} = 2.086$, and $\nu = 1.464$. The steps in the observables can be determined from eqs. (36) to (38) yielding $\Delta \ln(\rho) = \Delta \ln(P_s) = 0.2819$, $\Delta \ln(N_s) = 1.104$, and $\Delta \ln[\ln(t/t_0)] = 0.5290$.

$k \geq 4$: Because $|\zeta_-|$ increases with increasing k, the renormalization group method is valid for all $k \geq 4$. Critical exponents and step sizes can be calculated analogously to the $k = 3$ case.

IV. MONTE-CARLO SIMULATIONS

A. Simulation method and overview

To test the predictions of the Harris-Luck criterion and the renormalization group approach of Sec. III, we performed extensive Monte-Carlo simulations. Our system is characterized by three transition rates, the uniform healing rate μ and the infection rates λ_A and λ_B which are modulated according to the generalized Fibonacci chain. We set the healing rate to $\mu = 1$ and tune the transition by changing λ_B. The ratio λ_A/λ_B is treated as a fixed external parameter that determines the strength of the aperiodic inhomogeneity.

Our numerical implementation of the contact process is similar to Ref. [34] but adapted to the case of nonuniform infection rates. The algorithm starts at time $t = 0$ from some configuration of infected and healthy sites and consists of a sequence of events. During each event an infected site is randomly chosen from a list of all N_a infected sites, then a process is selected, either healing with probability $1/[1+\max(\lambda_A, \lambda_B)]$, infection of the left neighbor with probability $(1/2)\lambda_{\text{left}}/[1 + \max(\lambda_A, \lambda_B)]$ or infection of the right neighbor with probability $(1/2)\lambda_{\text{right}}/[1 + \max(\lambda_A, \lambda_B)]$. ($\lambda_{\text{left}}$ and λ_{right} denote the infection rates of the bonds left and right of the given site.) The infection succeeds if this neighbor is healthy. The time is then incremented by $1/N_a$.

Employing this algorithm, we studied the cases $k = 1, 2$ and 3 using systems of up to 35 generations of the generalized Fibonacci chain (more than 10^7 sites). We used several different values of the parameter characterizing the strength of the inhomogeneity,

$\lambda_A/\lambda_B = 0.001,\ 0.004,\ 0.01,\ 0.04,\ 0.1,\ 2/3,\ 1$, and 25. To cope with the slow dynamics at criticality, we simulated long times up to 1.4×10^9. Most of our simulations were spreading runs that start from a single infected seed site and measure the survival probability P_s and the size N_s of the active cloud. The data are averaged over up to 500,000 trials. For comparison, we have also performed a few density decay runs that start from a fully active lattice.

B. Results for $k = 1$

According to the Harris-Luck criterion, weak inhomogeneities are irrelevant in the $k = 1$ case because the wandering exponent $\omega_1 = -1$ fulfills the inequality $\omega < 1 - 1/\nu_\perp \approx 0.0884$. Moreover, the renormalization group of Sec. III predicts that strong inhomogeneities decrease under renormalization. We therefore expect the contact process to display clean DP critical behavior even for strong bare inhomogeneities.

To test this prediction, we performed spreading simulations of a system having strong inhomogeneities characterized by $\lambda_A/\lambda_B = 0.01$. The resulting survival probability P_s and size N_s of the active cloud are presented in Fig. 2. The figure shows that the critical behavior is of conventional power-law type. The critical exponents extracted from fits to $P_s \sim t^{-\delta}$ and $N_s \sim t^{\Theta}$ take the values $\delta = 0.160$ and $\Theta = 0.314$ in excellent agreement with the clean DP values $\delta_{\rm DP} = 0.159464$ and $\Theta_{\rm DP} = 0.313686$ [35]. We thus conclude that the contact process with aperiodic transition rates modulated according to the $k = 1$ Fibonacci chain is indeed in the clean DP universality class. The same conclusion was reached in Ref. [36] based on simulations of the steady-state density ρ for smaller systems.

C. Results for $k = 2$

The wandering exponent $\omega_2 = 0$ fulfills the Harris-Luck criterion $\omega < 1 - 1/\nu_\perp \approx 0.0884$, but just barely. This implies that the inhomogeneities are asymptotically irrelevant but their magnitude will decrease only slowly with increasing length scale. The same picture also emerges from the renormalization group solution given in the appendix: If the bare

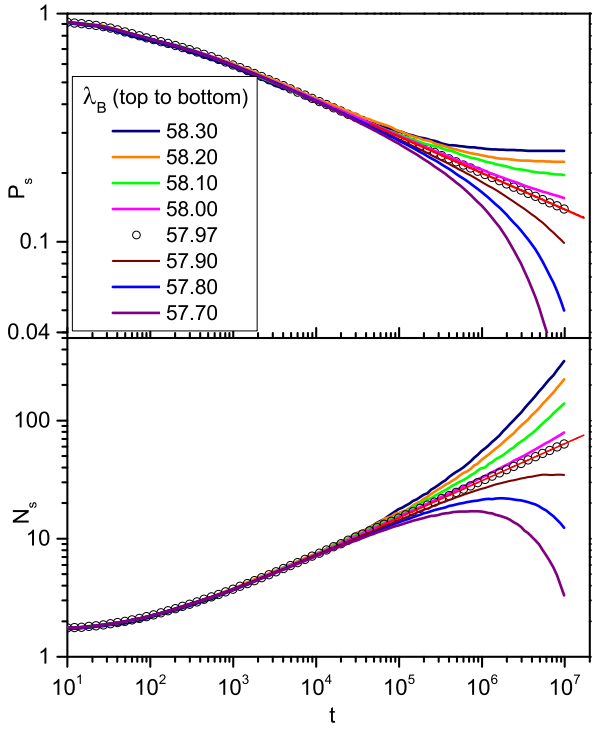

Fig. 2. Survival probability P_s and size N_s of the active cloud vs. time t for $k = 1$ and strong inhomogeneity $\lambda_A/\lambda_B = 0.01$. The data are averages of 100,000 (away from criticality) to 500,000 (at criticality) trials. The critical point is located at $\lambda_B = 57.97$. The solid straight lines represent power-law fits giving the critical exponents $\delta = 0.160$ and $\Theta = 0.314$.

inhomogeneities are strong, the renormalization group works for a number of steps until the rates leave the region of validity $\lambda_A \ll \mu \ll \lambda_B$. For strong bare inhomogeneities, we therefore expect unconventional behavior in a transient time regime while the asymptotic behavior should be in the DP universality class. For sufficiently weak inhomogeneities, the transient regime will be missing.

To verify these predictions, we performed spreading simulations for two different inhomogeneity strengths, $\lambda_A/\lambda_B = 0.01$ and 2/3. Figure 3 shows the survival probability P_s and size N_s of the active cloud for the weak inhomogeneity case. The figure yields conventional power-law critical behavior with exponents $\delta = 0.158$ and $\Theta = 0.311$ in excellent agreement with the clean DP values $\delta_{\rm DP} = 0.159464$ and $\Theta_{\rm DP} = 0.313686$.

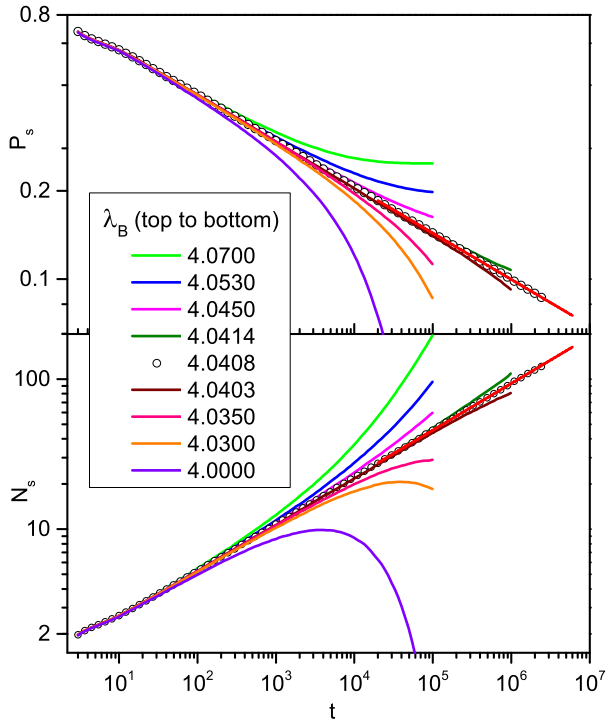

Fig. 3. Survival probability P_s and size N_s of the active cloud vs. time t for the case $k = 2$ and weak inhomogeneity $\lambda_A/\lambda_B = 2/3$. The data are averages of 100,000 to 150,000 trials. The critical point is located at $\lambda_B = 4.0408$. The solid straight lines represent power-law fits giving the critical exponents $\delta = 0.158$ and $\Theta = 0.311$.

In the case of strong inhomogeneities, $\lambda_A/\lambda_B = 0.01$, the behavior at early times is different as both N_s and P_s feature oscillations reminiscent of the steps discussed in Sec. III E. This becomes particularly clear if one plots N_s vs P_s as is done in Fig. 4. The strength of the oscillations decreases with time, but only slowly. Therefore, we have not been able to reach the asymptotic regime within the available simulation times. However, the emerging critical behavior for $\lambda_A/\lambda_B = 0.01$ is compatible with the clean DP universality class, as indicated by the dashed line in the lower panel of Fig. 4.

To summarize, we conclude that the asymptotic critical behavior of the $k = 2$ chain is in clean DP universality class for weak inhomogeneities. The same is likely true for strong inhomogeneities. However, the asymptotic behavior is approached very slowly,

giving rise to an extended transient regime of unconventional behavior that is controlled by the real-space renormalization group.

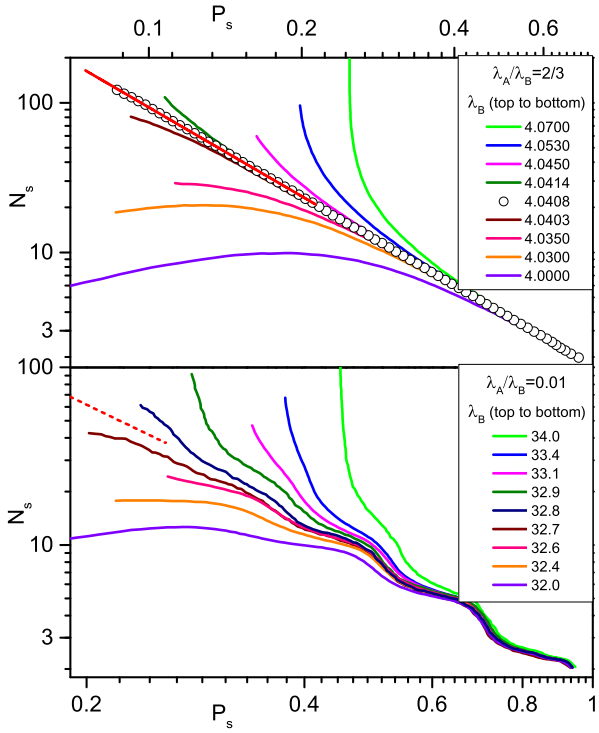

Fig. 4. N_s versus P_s for the case $k = 2$ and two different inhomogeneity strengths, $\lambda_A/\lambda_B = 2/3$ (upper panel) and $\lambda_A/\lambda_B = 0.01$ (lower panel). The data are averages of 100,000 to 150,000 trials. The solid line in the upper panel is a power-law fit of the critical curve ($\lambda_B = 4.0408$) yielding $\Theta/\delta = 1.971$. The dashed line in the lower panel represents a power law with the clean exponent $-\Theta_{\rm DP}/\delta_{\rm DP} = -1.96712$.

D. Results for $k = 3$

We now turn to the case of $k = 3$ for which the aperiodic inhomogeneities are relevant according to the Harris-Luck criterion. Moreover, the renormalization group theory predicts activated dynamical scaling and log-periodic or double-log periodic oscillations in various observables.

Figure 5 shows an example of a density decay run starting from a fully active lattice for an inhomogeneity strength of $\lambda_A/\lambda_B = 0.04$.The figure clearly illustrates the

structure of the time evolution as the system forms a hierarchy of clusters of active sites that are modulated according to the underlying $k = 3$ generalized Fibonacci sequence. The corresponding time evolution of the density ρ of active sites progresses in steps; in contrast to the $k = 2$ case the steps become sharper and more pronounced with increasing time t.

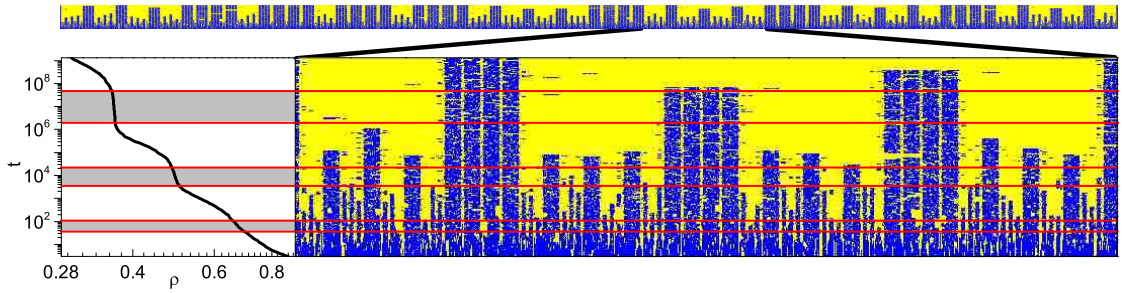

Fig. 5. Example of a density decay run, starting from a fully active lattice of 15 generations of the $k = 3$ chain (173383 sites). The inhomogeneity strength is $\lambda_A/\lambda_B = 0.04$. In the main panel, dark blue dots denote active sites while light yellow marks inactive sites. The left panel shows the corresponding density ρ of active sites. The horizontal lines are located at times that correspond to the inverse transition rates at different renormalization group steps, $t = \lambda_B^{-1},\ \mu^{-1}$.

To analyze the case $k = 3$ quantitatively, we performed extensive spreading runs. Figure 6 shows the time evolution of N_s and P_s for an inhomogeneity strength $\lambda_A/\lambda_B = 0.04$. Both observables show well-defined steps and plateaus as predicted in Sec. III E. They can also be seen in the upper panel of Fig. 7 which shows N_s vs. P_s. In contrast to the $k = 2$ case, the steps become more pronounced with increasing time. Moreover, they can be directly associated with the discrete values of the healing and infection rates appearing in the renormalization group.

From the upper panel of Fig. 7, the critical infection rate can be easily found. The critical data feature well-defined steps and plateaus while the subcritical and supercritical data curve away from the critical line as predicted. We performed analogous simulations for inhomogeneity strengths $\lambda_A/\lambda_B = 0.001$, 0.004, 0.01, 0.1 and 1. The resulting phase

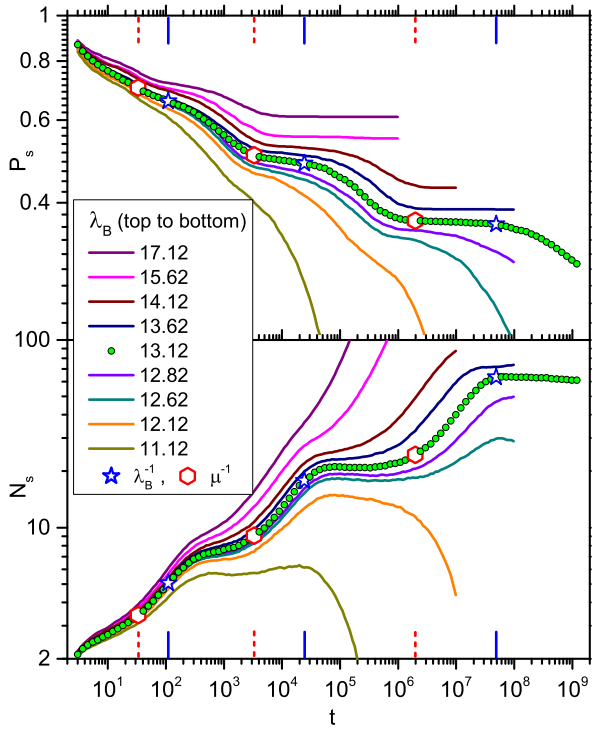

Fig. 6. Survival probability P_s and size N_s of the active cloud vs. time t for the case $k = 3$ and $\lambda_A/\lambda_B = 0.04$ (5000 trials). The steps and plateaus in the critical curve, $\lambda_B = 13.12$, become more pronounced with increasing time. They can be associated with the discrete values of λ and μ appearing in the renormalization group (marked by large stars and hexagons).

diagram is shown in Fig. 8. The Monte-Carlo data are in excellent agreement with the renormalization group prediction (23) for all $\lambda_A/\lambda_B \leq 0.1$ (even though the analytical result does not contain any adjustable parameters). Surprisingly, the analytical result is still a good approximation in the uniform case $\lambda_A/\lambda_B = 1$ where the renormalization group cannot be expected to work.

The effect of the inhomogeneity strength on the critical behavior is demonstrated in the lower panel of Fig. 7 which shows N_s vs. P_s for several values of λ_A/λ_B. If the (bare) inhomogeneities are very strong (small value of λ_A/λ_B), the steps in the critical N_s vs P_s curve are sharp and pronounced from the outset because the renormalization group is always in its asymptotic regime $\lambda_A \ll \mu \ll \lambda_B$. For weaker inhomogeneities, the

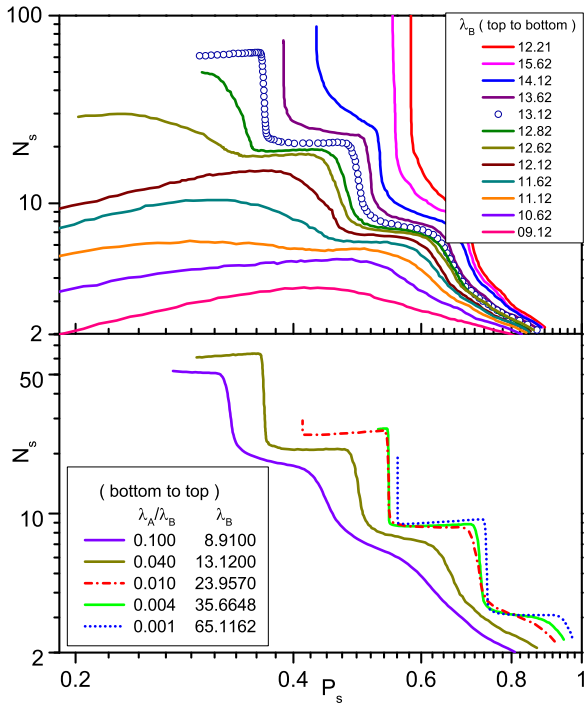

Fig. 7. Upper panel: N_s versus P_s for the case $k = 3$ and $\lambda_A/\lambda_B = 0.04$ (5000 trials). The maximum time is $t_{\max} = 1.4 \times 10^9$ at criticality. The critical curve, $\lambda_B = 13.12$, shows pronounced steps as predicted in Sec. III E. Lower panel: Critical curves for several inhomogeneity strengths λ_A/λ_B (5000 to 100000 trials).

oscillations of the N_s vs P_s curves are initially not very pronounced. With increasing time the steps become sharper because the renormalization group flows towards the asymptotic regime.

To compare the Monte-Carlo data and the renormalization group predictions quantitatively, we now investigate the critical N_s vs. P_s curve for $\lambda_A/\lambda_B = 0.04$ in detail. The exponent $\bar{\Theta}/\bar{\delta}$ can be found by fitting the envelope of the N_s vs. P_s curve. This means fitting equivalent discrete points, each representing one renormalization group step. This analysis, shown in Fig. 9 yields $\bar{\Theta}/\bar{\delta} = 3.79$. This value is in good agreement with the prediction of 3.91, in particular in view of the fact that we only have 3 steps to perform the fit. Figure 9 also allows us to determine the steps $\Delta \ln(P_s)$ and $\Delta \ln(N_s)$ between consecutive renormalization group steps. Using the data of the third step which is the last complete step

in our data, we find $\Delta \ln(P_s) = 0.284$ and $\Delta \ln(N_s) = 1.092$, again in good agreement with the renormalization group predictions of Sec. III E, 0.2819 and 1.104, respectively.

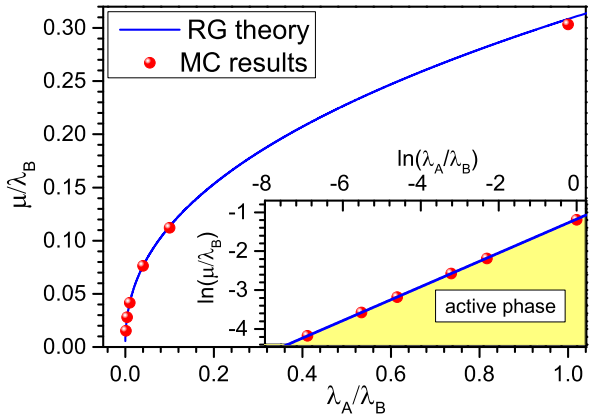

Fig. 8. Phase diagram of the contact process for $k = 3$. The dots are the Monte-Carlo results for $\lambda_A/\lambda_B = 0.001$, 0.004, 0.01, 0.04, 0.1, and 1. The solid line represents the renormalization group result (23).

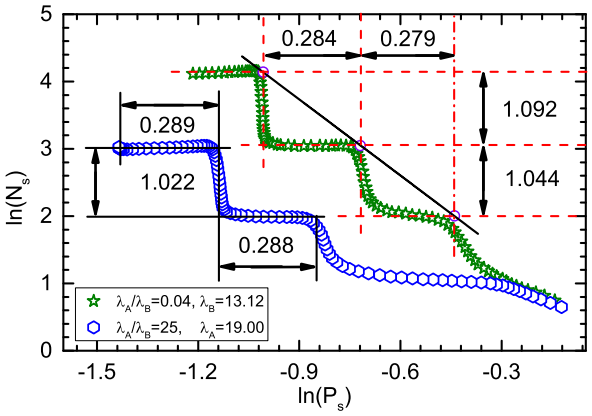

Fig. 9. Quantitative analysis of the critical N_s versus P_s curve for $k = 3$ and $\lambda_A/\lambda_B = 0.04$ (maximum time $t_{\max} = 1.4 \times 10^9$) and $\lambda_A/\lambda_B = 25$ (maximum time $t_{\max} = 2 \times 10^8$). The solid line is a fit of the envelop of the curve to the power law $N_s \sim P_s^{-\bar{\Theta}/\bar{\delta}}$ yielding $\bar{\Theta}/\bar{\delta} = 3.79$.

The renormalization group results of Sec. III were derived under the assumption $\lambda_A \ll \mu \ll \lambda_B$. It is important to investigate whether the resulting renormalization group fixed point attracts the flow from a larger part of parameter space. In other words, is the asymptotic critical behavior controlled by this fixed point even if the bare system violates the condition $\lambda_A \ll \mu \ll \lambda_B$. In the lower panel of Fig. 7, we have seen that the fixed point attracts the flow from regions where λ_A/λ_B is only moderately small. We now look at an extreme case in which the bare system strongly violates the condition. The second curve in Fig. 9 shows the critical N_s vs P_s data for $\lambda_A/\lambda_B = 25$. As expected, the two curves initially behave differently. However, the steps $\Delta \ln(P_s)$ and$\Delta \ln(N_s)$ forming at later times appear to be identical within the numerical errors. Moreover, we also performed density decay runs for $\lambda_A/\lambda_B = 25$. A figure (not shown) analogous to Fig. 5 clearly demonstrates that the same hierarchy of clusters forms at late times for $\lambda_A/\lambda_B = 0.04$ and $\lambda_A/\lambda_B = 25$. This strongly suggests that the renormalization group fixed point discovered in Sec. III also describes the critical behavior of the system with $\lambda_A/\lambda_B = 25$.

V. CONCLUSIONS

In summary, we have studied the one-dimensional contact process with aperiodically modulated transition rates by means of a real-space renormalization group and by Monte-Carlo simulations. We have focused on modulations according to three cases $k = 1, 2, 3$ of the generalized Fibonacci sequence defined by the inflation rules $A \to AB^k$ and $B \to A$. For $k = 1$ (the Fibonacci chain proper), the inhomogeneities are strongly irrelevant according to the Harris-Luck criterion at the clean DP critical point. Correspondingly, our numerical simulations yield critical behavior in the clean DP universality class even if the initial inhomogeneities are strong. This agrees with earlier results on the steady state density [36].

In the $k = 2$ case, the inhomogeneities are still irrelevant at the clean DP critical point, but just barely. This implies that their scale dimension is close to zero. The inhomogeneity strength therefore decreases only slowly with increasing length and time scales. Our Monte-Carlo simulations confirm this picture. If the (bare) inhomogeneities are weak, we again find critical behavior in the clean DP universality class. For strong inhomogeneities, the system shows unconventional behavior in an extended transient time regime that is controlled by the real-space renormalization group. The long-time evolution appears to approach the clean DP critical behavior. However, we could not reach the true asymptotic regime within our simulation time for strong inhomogeneities.

For $k \geq 3$, the aperiodic modulation of the transition rates is relevant at the clean DP critical point because the Harris-Luck criterion is violated. We have developed a renormalization group theory of the transition and identified a fixed point that describes unconventional criticality. At this infinite-modulation fixed point, the inhomogeneity strength diverges, and the method becomes asymptotically exact. The resulting critical behavior is characterized by activated dynamical scaling. Moreover, the time dependence of observables such as the density of active sites, the survival probability, and the size of the active cloud show striking plateaus and steps. They are a consequence of the discrete scale invariance of the generalized Fibonacci sequence and related to the log-periodic oscillations found in many aperiodic systems (see, e.g., [33]). Due to the activated dynamical scaling, the oscillations are actually *double-log* periodic in time. Analogous double-log oscillations should occur in other systems featuring activated scaling, for example in quantum spin chains [37].

We have numerically confirmed these renormalization group predictions for the case $k = 3$. The Monte-Carlo simulations also provide evidence for the critical behavior to be universal, i.e., it is valid for both weak and strong aperiodic modulations.

It is interesting to compare the phase transitions in the aperiodic contact process (for $k \geq 3$) and the disordered contact process. In both cases, the fluctuations of the

transition rates at criticality diverge with increasing length scale. In the disordered contact process, this leads to an infinite-randomness critical point [23, 38]; and for aperiodic rates, the critical point is of infinite-modulation type. Both these critical points feature unconventional activated dynamical scaling rather than the usual power-law scaling. In the disordered case, the critical point is accompanied by Griffiths singularities [24, 39, 40] which are missing in the aperiodic case because the generalized Fibonacci chains do not have rare regions. Conversely, the log-periodic oscillations of observables in the aperiodic chain do not exist in the disordered chain because the latter system has continuous rather than discrete scale invariance (in the statistical sense).

Our renormalization group method is similar to the approach used in Ref. [32] to study the aperiodic transverse-field Ising chain. In fact, the critical behavior of the contact process and the transverse-field Ising chain are identical in the cases in which the renormalization group correctly describes the critical point (i.e., $k \geq 3$). This mirrors the behavior of the corresponding random systems: The random transverse-field Ising chain [41] and the random contact process [23] feature the same critical exponents.

The main difference between the Ising chain and the contact process occurs for $k = 2$. For the Ising chain, $k = 2$ aperiodic modulations are exactly marginal according to the Harris-Luck criterion. This is reflected in the fact that the modulation strength stays constant under the renormalization group, leading to nonuniversal critical behavior [32]. In contrast, $k = 2$ aperiodic modulations of the contact process are weakly irrelevant. Correspondingly, the renormalization group works at best in a transient time regime while the asymptotic critical behavior appears to be in the clean DP universality class.

Recently, aperiodic sequences were used to construct complex networks with long-range connections; and the contact process on such networks was studied [42]. The nonequilibrium phase transition features power-law critical behavior with exponents that depend on the underlying network. Time-dependent quantities exhibit log-periodic oscillations due to the discrete scale invariance of the networks.

Let us finally comment on generalizations to higher dimensions. One could, for example, construct higher-dimensional aperiodic modulations of the transition rates by repeating identical one-dimensional sequences in the second (and third) direction. This would increase the relevance of the modulations in the Harris-Luck criterion because the clean correlation length exponent decreases with increasing dimension while the fluctuations of the distance to criticality are unchanged. In the random case, such correlated inhomogeneities lead to a smearing of the DP critical point [43] because rare regions undergo the transition independently. As the aperiodic systems do not have any rare regions, their behavior is likely different Alternatively, one could also look at more general tilings in two and three dimensions. Of particular interest are structures with unbounded fluctuations such as the tiling proposed in Ref. [44]. Studying the contact process on such lattices remains a task for future.

ACKNOWLEDGEMENTS

This work has been supported in part by the NSF under grants no. DMR-0906566, DMR-1205803, and PHYS-1066293.

APPENDIX: THE CASE $K = 2$

The general solution of the renormalization group developed in Sec. III C does not apply to the case $k = 2$ because the particular solution of the inhomogeneous recurrence (13) and (14) is not of the form $R_j = \bar{R} = \text{const}$ and $S_j = \bar{S} = \text{const}$. The reason is that the smaller eigenvalue of the coefficient matrix $\mathbf{T}_2$ takes the value $\zeta_-^2 = 1$.

In this appendix, we therefore directly solve the problem for $k = 2$. After introducing the variables $X_j = 2R_j + S_j$ and $Y_j = R_j - S_j$ into (13) and (14), the recurrence relations read

$$X_{j+1} = X_j + A\,, \tag{A1}$$

$$Y_{j+1} = 4Y_j + 2A\,. \tag{A2}$$

As the two equations are now decoupled, they can be easily solved,

$$X_j = X_0 + jA \tag{A3}$$

$$Y_j = -\frac{2}{3}A + 4^j\left(Y_0 + \frac{2}{3}A\right) \tag{A4}$$

where $X_0 = 2R_0 + S_0$ and $Y_0 = R_0 - S_0$. Transforming back to the variables R_j and S_j, we finally obtain

$$R_j = \frac{1}{3}\left[X_0 + jA - \frac{2}{3}A + 4^j\left(Y_0 + \frac{2}{3}A\right)\right]\,, \tag{A5}$$

$$S_j = \frac{1}{3}\left[X_0 + jA + \frac{4}{3}A - 2\times 4^j\left(Y_0 + \frac{2}{3}A\right)\right]\,. \tag{A6}$$

For $Y_0 + 2A/3 > 0$, the system is in the inactive phase because $R_j \to \infty$ and $S_j \to -\infty$ under the renormalization group. In contrast, the system is in the active phase for $Y_0 + 2A/3 < 0$. At criticality, $Y_0 + 2A/3 = 0$, both R_j and S_j increase linearly with j. The implies that the renormalization group method asymptotically fails because the transition rates eventually violate the condition $\lambda_A \ll \mu \ll \lambda_B$.

BIBLIOGRAPHY

[1] V. P. Zhdanov and B. Kasemo. Kinetic phase transitions in simple reactions on solid surfaces. *Surface Science Reports*, 20:113, 1994.

[2] B. Schmittmann and R. K. P. Zia. Statistical mechanics of driven diffusive systems. In C. Domb and J. L. Lebowitz, editors, *Phase Transitions and Critical Phenomena*, volume 17, page 1. Academic, New York, 1995.

[3] J. Marro and R. Dickman. *Nonequilibrium Phase Transitions in Lattice Models*. Cambridge University Press, Cambridge, 1999.

[4] H. Hinrichsen. Nonequilibrium critical phenomena and phase transitions into absorbing states. *Adv. Phys.*, 49:815, 2000.

[5] G. Odor. Universality classes in nonequilibrium lattice systems. *Rev. Mod. Phys.*, 76:663, 2004.

[6] S. Lübeck. Universal scaling behavior of nonequilibrium phase transitions. *Int. J. Mod. Phys. B*, 18:3977, 2004.

[7] U. C. Täuber, M. Howard, and B. P. Vollmayr-Lee. Applications of field-theoretic renormalization group methods to reaction-diffusion problems. *J. Phys. A*, 38:R79, 2005.

[8] M. Henkel, H. Hinrichsen, and S. Lübeck. *Non-equilibrium phase transitions. Vol 1: Absorbing phase transitions*. Springer, Dordrecht, 2008.

[9] P. Grassberger and A. de la Torre. *Ann. Phys. (NY)*, 122:373, 1979.

[10] H. K. Janssen. *Z. Phys. B*, 42:151, 1981.

[11] P. Grassberger. *Z. Phys. B*, 47:365, 1982.

[12] T. E. Harris. Contact interactions on a lattice. *Ann. Prob.*, 2:969, 1974.

[13] K. A. Takeuchi, M. Kuroda, H. Chate, and M. Sano. Directed percolation criticality in turbulent liquid crystals. *Phys. Rev. Lett.*, 99:234503, 2007.

[14] L. Corte, P. M. Chaikin, J. P. Gollub, and D. J. Pine. Random organization in periodically driven systems. *Nature Physics*, 4:420, 2008.

[15] Alexandre Franceschini, Emmanouela Filippidi, Elisabeth Guazzelli, and David J. Pine. Transverse alignment of fibers in a periodically sheared suspension: An absorbing phase transition with a slowly varying control parameter. *Phys. Rev. Lett.*, 107:250603, Dec 2011.

[16] S. Okuma, Y. Tsugawa, and A. Motohashi. Transition from reversible to irreversible flow: Absorbing and depinning transitions in a sheared-vortex system. *Phys. Rev. B*, 83:012503, Jan 2011.

[17] H. K. Janssen. Renormalized field theory of the Gribov process with quenched disorder. *Phys. Rev. E*, 55:6253, 1997.

[18] A. B. Harris. Effect of random defects on the critical behaviour of Ising models. *J. Phys. C*, 7:1671, 1974.

[19] M. Bramson, R. Durrett, and R. H. Schonmann. *Ann. Prob.*, 19:960, 1991.

[20] A. G. Moreira and R. Dickman. Critical dynamics of the contact process with quenched disorder. *Phys. Rev. E*, 54:R3090, 1996; R. Dickman and A. G. Moreira. Violation of scaling in the contact process with quenched disorder. *Phys. Rev. E*, 57:1263, 1998.

[21] I. Webman, D. Ben Avraham, A. Cohen, and S. Havlin. *Phil. Mag. B*, 77:1401, 1998.

[22] R. Cafiero, A. Gabrielli, and M. A. Munoz. *Phys. Rev. E*, 57:5060, 1998.

[23] J. Hooyberghs, F. Iglói, and C. Vanderzande. Strong-disorder fixed point in absorbing-state phase transitions. *Phys. Rev. Lett.*, 90:100601, 2003; Absorbing state phase transitions with quenched disorder. *Phys. Rev. E*, 69:066140, 2004.

[24] A. J. Noest. New universality for spatially disordered cellular automata and directed percolation. *Phys. Rev. Lett.*, 57:90, 1986; Power-law relaxation of spatially disordered stochastic automata and directed percolation. *Phys. Rev. B*, 38:2715, 1988.

[25] T. Vojta and M. Dickison. Critical behavior and Griffiths effects in the disordered contact process. *Phys. Rev. E*, 72:036126, 2005.

[26] M. M. de Oliveira and S. C. Ferreira. Universality of the contact process with random dilution. *J. Stat. Mech.*, 2008:P11001, 2008.

[27] T. Vojta, A. Farquhar, and J. Mast. Infinite-randomness critical point in the two-dimensional disordered contact process. *Phys. Rev. E*, 79:011111, 2009; Thomas Vojta. Monte carlo simulations of the clean and disordered contact process in three dimensions. *Phys. Rev. E*, 86:051137, Nov 2012.

[28] T. Vojta and M. Y. Lee. Nonequilibrium phase transition on a randomly diluted lattice. *Phys. Rev. Lett.*, 96:035701, 2006; M. Y. Lee and T. Vojta. Absorbing-state phase transitions on percolating lattices. *Phys. Rev. E*, 79:041112, 2009.

[29] J. M. Luck. A classification of critical phenomena on quasi-crystals and other aperiodic structures. *EPL (Europhysics Letters)*, 24(5):359, 1993.

[30] R.V. Moody, editor. *The Mathematics of Long-range Aperiodic Order*. Kluwer, Dordrecht, 1997.

[31] This is not a real restriction as the renormalization group steps of Sec. III alternate between modulated infection and healing rates.

[32] Fleury J Oliveira Filho, Maicon S Faria, and André P Vieira. Strong-disorder renormalization group study of aperiodic quantum ising chains. *J. Stat. Mech.*, 2012(03):P03007, 2012.

[33] Didier Sornette. Discrete-scale invariance and complex dimensions. *Physics Reports*, 297(5):239 – 270, 1998.

[34] R. Dickman. Reweighting in nonequilibrium simulations. *Phys. Rev. E*, 60:R2441, 1999.

[35] I. Jensen. Low-density series expansions for directed percolation: I. a new efficient algorithm with applications to the square lattice. *J. Phys. A*, 32:5233, 1999.

[36] M S Faria, D J Ribeiro, and S R Salinas. Critical behavior of a contact process with aperiodic transition rates. *J. Stat. Mech.*, 2008(01):P01022, 2008.

[37] André P. Vieira. Low-energy properties of aperiodic quantum spin chains. *Phys. Rev. Lett.*, 94:077201, Feb 2005.

[38] F. Igloi and C. Monthus. Strong disorder renormalization group approach of random systems. *Phys. Rep.*, 412:277, 2005.

[39] R. B. Griffiths. Nonanalytic behavior above the critical point in a random Ising ferromagnet. *Phys. Rev. Lett.*, 23:17, 1969.

[40] T. Vojta. Rare region effects at classical, quantum, and non-equilibrium phase transitions. *J. Phys. A*, 39:R143, 2006.

[41] D. S. Fisher. Critical behavior of random transverse-field Ising spin chains. *Phys. Rev. B*, 51:6411, 1995.

[42] Róbert Juhász and Géza Ódor. Scaling behavior of the contact process in networks with long-range connections. *Phys. Rev. E*, 80:041123, Oct 2009.

[43] T. Vojta. Broadening of a nonequilibrium phase transition by extended structural defects. *Phys. Rev. E*, 70:026108, 2004; M. Dickison and T. Vojta. Monte-Carlo simulations of the smeared phase transition in a contact process with extended defects. *J. Phys. A*, 38:1199, 2005.

[44] C. Godrèche and F. Lançon. A simple example of a non-pisot tiling with five-fold symmetry. *J. Phys. I France*, 2:207, 1992.

VI. INFINITE-RANDOMNESS CRITICALITY IN A RANDOMLY LAYERED HEISENBERG MAGNET

Fawaz Hrahsheh, Hatem Barghathi, and Thomas Vojta

Department of Physics, Missouri University of Science and Technology, Rolla, MO 65409, USA

ABSTRACT[*]

We study the ferromagnetic phase transition in a randomly layered Heisenberg magnet using large-scale Monte-Carlo simulations. Our results provide numerical evidence for the infinite-randomness scenario recently predicted within a strong-disorder renormalization group approach. Specifically, we investigate the finite-size scaling behavior of the magnetic susceptibility which is characterized by a non-universal power-law divergence in the Griffiths phase. We also study the perpendicular and parallel spin-wave stiffnesses in the Griffiths phase. In agreement with the theoretical predictions, the parallel stiffness is nonzero for all temperatures $T < T_c$. In contrast, the perpendicular stiffness remains zero in part of the ordered phase, giving rise to anomalous elasticity. In addition, we calculate the in-plane correlation length which diverges already inside the disordered phase at a temperature significantly higher than T_c. The time autocorrelation function within model *A* dynamics displays an ultraslow logarithmic decay at criticality and a nonuniversal power-law in the Griffiths phase.

[*]Published in Physical Review B **84**, 184202 (2011).

I. INTRODUCTION

When weak quenched disorder is added to a system undergoing a *classical* continuous phase transition, generically the critical behavior will either remain unchanged or it will be replaced by another critical point with different exponent values. Which scenario is realized depends on whether or not the clean critical point fulfills the Harris criterion [1]. In contrast, zero-temperature quantum phase transitions generically display much stronger disorder phenomena including power-law quantum Griffiths singularities [2, 3, 4], infinite-randomness critical points featuring exponential instead of power-law scaling [5, 6], and smeared phase transitions [7, 8]. A recent review of these phenomena can be found in Ref. [9], while Ref. [10] focuses on metalic systems and also discusses experiments.

The reason for the disorder effects being stronger at quantum phase transitions than at classical transitions is that quenched disorder is perfectly correlated in the *imaginary time* direction. Imaginary time behaves as an additional dimension at a quantum phase transition and becomes infinitely extended at zero temperature. Therefore, the impurities and defects are effectively "infinitely large" in this extra dimension, which makes them much harder to average out than the usual finite-size defects and so increases their influence.

For this reason, one should also expect strong unconventional disorder phenomena at classical thermal phase transitions in systems in which the disorder is perfectly correlated in one or more *space* dimensions. Indeed, such behavior has been observed in the McCoy-Wu model, a disordered classical two-dimensional Ising model having perfect disorder correlations in one of the two dimensions. In a series of papers, McCoy and Wu [11, 12, 13, 14] showed that this model exhibits an unusual phase transition featuring a smooth specific heat while the susceptibility is infinite over an entire temperature range. Fisher [5, 6] achieved an essentially complete understanding of this phase transition with the help of a strong-disorder renormalization group approach (using the equivalence between the McCoy-Wu model and the random transverse-field Ising chain). He determined that

the critical point is of exotic infinite-randomness type and is accompanied by power-law Griffiths singularities. In a classical Ising model with perfect disorder correlations in *two* dimensions, the disorder effects are even stronger than in the McCoy-Wu model: the sharp critical point is destroyed, and the transition is smeared over a range of temperatures [15, 16].

Recently, another classical system with perfect disorder correlations in two dimensions was investigated by means of a strong-disorder renormalization group [17]. This theory predicts that the randomly layered Heisenberg magnet features a sharp critical point (in contrast to the Ising case discussed above). However, it is of exotic infinite-randomness type. Somewhat surprisingly, it is in the same universality class as the quantum critical point of the random transverse-field Ising chain.

In this paper, we present the results of Monte-Carlo simulations of the randomly layered Heisenberg model. They provide numerical evidence in support of the above renormalization group predictions. Our paper is organized as follows. In Sec. II, we define our model and discuss its phase diagram. We also briefly summarize the predictions of the strong disorder renormalization group theory [17]. In Sec. III, we describe our Monte-Carlo simulations, we present the results and compare them to the theory. We conclude in Sec. IV.

II. MODEL AND RENORMALIZATION GROUP PREDICTIONS

We consider a ferromagnet consisting of a random sequence of layers made up of two different ferromagnetic materials, see sketch in Fig. 1.

Its Hamiltonian, a classical Heisenberg model on a three-dimensional lattice of perpendicular size $L_\perp$ (in z direction) and in-plane size $L_\parallel$ (in the x and y directions) is given by

$$H = -\sum_{\mathbf{r}} J_z^{\parallel} \left(\mathbf{S}_{\mathbf{r}} \cdot \mathbf{S}_{\mathbf{r}+\hat{\mathbf{x}}} + \mathbf{S}_{\mathbf{r}} \cdot \mathbf{S}_{\mathbf{r}+\hat{\mathbf{y}}}\right) - \sum_{\mathbf{r}} J_z^{\perp} \mathbf{S}_{\mathbf{r}} \cdot \mathbf{S}_{\mathbf{r}+\hat{\mathbf{z}}}. \tag{1}$$

Here, $\mathbf{S}_{\mathbf{r}}$ is a three-component unit vector on lattice site $\mathbf{r}$, and $\hat{\mathbf{x}}$, $\hat{\mathbf{y}}$, and $\hat{\mathbf{z}}$ are the unit vectors

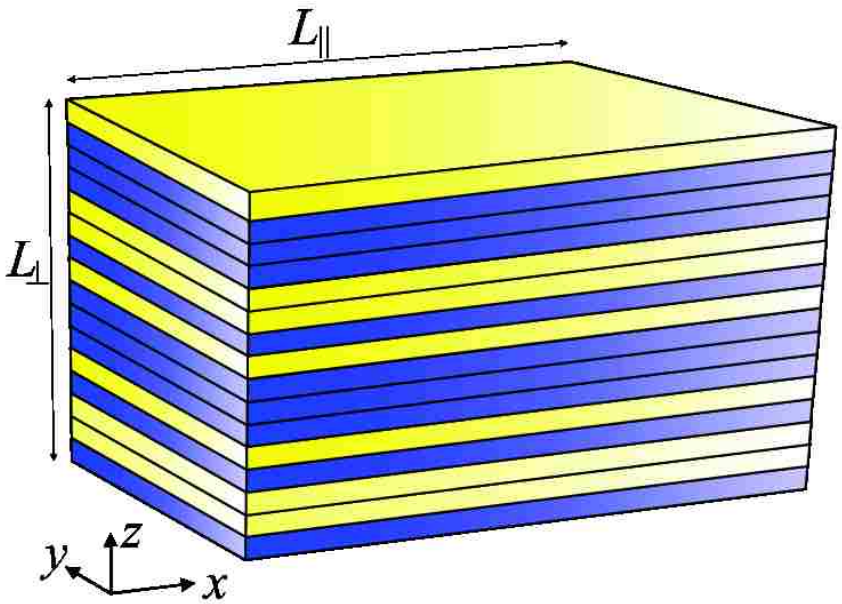

Fig. 1. Schematic of the layered Heisenberg magnet: It consistes of a random sequence of layers of two different ferromagnetic materials [17].

in the coordinate directions. The interactions within the layers, $J_z^{\parallel}$, and between the layers, $J_z^{\perp}$, are both positive and independent random functions of the perpendicular coordinate z.

In the following, we take all $J_z^{\perp}$ to be identical, $J_z^{\perp} \equiv J^{\perp}$, while the $J_z^{\parallel}$ are drawn from a binary probability distribution

$$P(J^{\parallel}) = (1-p)\,\delta(J^{\parallel} - J_u) + p\,\delta(J^{\parallel} - J_l) \tag{2}$$

with $J_u > J_l$. Here, p is the concentration of the "weak" layers while $1-p$ is the concentration of the "strong" layers.

The qualitative behavior of the model (1) is easily explained (see Fig. 2). At sufficiently high temperatures, the model is in a conventional paramagnetic (strongly disordered) phase. Below a temperature T_u (the transition temperature of a hypothetical system having $J_z^{\parallel} \equiv J_u$ for all z) but above the actual critical temperature T_c, rare thick slabs of strong layers develop local order while the bulk system is still nonmagnetic. This is the *para-*

magnetic (weakly disordered) Griffiths phase (or Griffiths region). In the *ferromagnetic* (weakly ordered) Griffiths phase, located between T_c and a temperature T_l (the transition temperature of a hypothetical system having $J_z^{\parallel} \equiv J_l$ for all z), bulk magnetism coexists with rare nonmagnetic slabs. Finally, below T_l, all slabs are locally ferromagnetic and the system is in a conventional ferromagnetic (strongly ordered) phase.

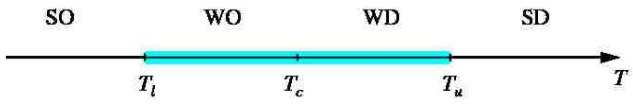

Fig. 2. Schematic phase diagram of the randomly layered Heisenberg magnet (1). SD and SO denote the conventional strongly disordered and strongly ordered phases, respectively. WD and WO are the weakly disordered and ordered Griffiths phases. T_c is the critical temperature while T_u and T_l mark the boundaries of the Griffiths phase .

In Ref. [17], the behavior in both Griffiths phases and at criticality has been derived within a strong-disorder renormalization group calculation. Here, we simply motivate and summarize the results. The probability of finding a slab of L_{RR} consecutive strong layers is given by simple combinatorics; it reads $w(L_{RR}) \sim (1-p)^{L_{RR}} = e^{-\tilde{p}L_{RR}}$ with $\tilde{p} = -\ln(1-p)$. Each such slab is equivalent to a two-dimensional Heisenberg model with an effective interaction $L_{RR}J_u$. Because the two-dimensional Heisenberg model is exactly at its lower critical dimension, the renormalized distance from criticality, ϵ, of such a slab decreases exponentially with its thickness, $\epsilon(L_{RR}) \sim e^{-bL_{RR}}$ [9, 18]. Combining the two exponentials gives a power-law probability density of locally ordered slabs,

$$\rho(\epsilon) \sim \epsilon^{\tilde{p}/b-1} = \epsilon^{1/z-1} \tag{3}$$

where the second equality defines the conventionally used dynamical exponent, z. It increases with decreasing temperature throughout the Griffiths phase and diverges as $z \sim 1/|T - T_c|$ at the actual critical point.

Many important observables follow from appropriate integrals of the density of states (3). The susceptibility can be estimated by $\chi \sim \int d\epsilon\, \rho(\epsilon)/\epsilon$. In an infinite system, the lower bound of the integral is 0; therefore, the susceptibility diverges in the entire temperature region where $z > 1$. A finite system size $L_\parallel$ in the in-plane directions introduces a nonzero lower bound $\epsilon_{\min} \sim L_\parallel^{-2}$. Thus, for $z > 1$, the susceptibility in the weakly disordered Griffiths phase diverges as

$$\chi(L_\parallel) \sim L_\parallel^{2-2/z} \tag{4}$$

and in the weakly ordered Griffiths phase, it diverges as

$$\chi(L_\parallel) \sim L_\parallel^{2+2/z}. \tag{5}$$

The strong-disorder renormalization group [17] confirms these simple estimates and gives $\chi \sim L_\parallel^2 [\ln (L_\parallel/a)]^{2\phi-1/\psi}$ at criticality where $\phi = (1+\sqrt{5})/2$ and $\psi = 1/2$ are critical exponents of the infinite randomness critical point.

The spin-wave stiffness ρ_s is defined by the work needed to twist the spins of two opposite boundaries by a relative angle θ. Specifically, in the limit of small θ and large system size, the free-energy density f depends on θ as

$$f(\theta) - f(0) = \frac{1}{2}\rho_s \left(\frac{\theta}{L}\right)^2. \tag{6}$$

Because the randomly layered Heisenberg model is anisotropic, we need to distinguish the parallel spin-wave stiffness $\rho_s^\parallel$ from the perpendicular spin-wave stiffness $\rho_s^\perp$. To calculate the parallel spin-wave stiffness, we apply boundary conditions at $x = 0$ and $x = L_\parallel$ and set $L = L_\parallel$ in Eq. (6) whereas the boundary conditions are applied at $z = 0$ and $z = L_\perp$ to calculate the perpendicular spin-wave stiffness with $L = L_\perp$ in Eq. (6).

Let us first discuss the parallel stiffness. In this case, the free energy difference $f(\theta) - f(0)$ is simply the sum over all layers participating in the long-range order (each having the same twisted boundary conditions). Thus, $\rho_s^{\parallel}$ is nonzero everywhere in the ordered phase. The strong-disorder renormalization group approach [17] predicts

$$\rho_s^{\parallel} \sim m \sim |T - T_c|^{\beta} \qquad (T < T_c) \tag{7}$$

where $\beta = (3 - \sqrt{5})/2$ is the order parameter exponent of the infinite randomness critical point. The parallel stiffness behaves like the total magnetization $m = |\sum_{\mathbf{r}} \langle \mathbf{S}_{\mathbf{r}} \rangle|/(L_{\perp} L_{\parallel}^2)$, because both renormalize additively under the strong-disorder renormalization-group theory [17].

If the twist θ is applied between the bottom ($z = 0$) and the top ($z = L_{\perp}$) layers, the local twists between consecutive layers will vary from layer to layer. Minimizing $f(\theta) - f(0)$ leads to $\rho_s^{\perp} \sim \langle 1/J_{eff}^{\perp} \rangle^{-1}$ where $J_{eff}^{\perp}$ are the effective couplings between the rare regions. Within the strong-disorder renormalization group approach, the distribution of the $J_{eff}^{\perp}$ follows a power law $p(J_{eff}^{\perp}) \sim (J_{eff}^{\perp})^{1/z-1}$. Thus, $\rho_s^{\perp} = 0$ in part of the ordered Griffiths phase. It only becomes nonzero once z falls below 1 at a temperature $T_s < T_c$. Between T_c and T_s, the system displays anomalous elasticity. Here, the free energy due to the twist scales with $f(\theta) - f(0) \sim L_{\perp}^{-1-z}$. Thus, the perpendicular stiffness formally vanishes as $\rho_s^{\perp} \sim L_{\perp}^{1-z}$ with increasing $L_{\perp}$.

To study the dynamical critical behavior, a phenomenological dynamics is added to the randomly layered Heisenberg model. The simplest case is a purely relaxational dynamics corresponding to model A in the classification of Hohenberg and Halperin [19].

The dynamic behavior can be characterized by the average time autocorrelation function

$$C(t) = \frac{1}{L_\perp L_\parallel^2} \int d^3r \langle \mathbf{S_r}(t) \mathbf{S_r}(0) \rangle, \tag{8}$$

where $\mathbf{S_r}(t)$ is the value of the spin at position $\mathbf{r}$ and time t.

The behavior of $C(t)$ in the weakly disordered Griffiths phase can be easily estimated. The correlation time of a single locally ordered slab is proportional to $1/\epsilon$ [17]. Summing over all slabs using the density of states (3) then gives

$$C(t) \sim \int d\epsilon \rho(\epsilon) e^{-\epsilon t} \sim t^{-1/z}. \tag{9}$$

The strong disorder renormalization group calculation [17] confirms this estimate. Moreover, at criticality, when $z \to \infty$, it gives an even slower logarithmic behavior

$$C(t) \sim [\ln(t/t_0)]^{\phi - 1/\psi}. \tag{10}$$

where t_0 is a microscopic length scale.

III. MONTE-CARLO SIMULATIONS

A. Overview

In this section we report results of Monte-Carlo simulations of the randomly layered Heisenberg magnet. Because the phase transition in this system is dominated by the rare regions, sufficiently large system sizes are required in order to get reliable results. We have simulated system sizes ranging from $L_\perp = 90$ to 800 and $L_\parallel = 10$ to 400. We have chosen $J_u = 1$ and $J_l = 0.25$ in Eq. (2). All the simulations have been performed for disorder concentrations $p = 0.8$. With these parameter choices, the Griffiths region ranges from $T_l \approx 0.63$ to $T_u \approx 1.443$. For optimal performance, we have used large numbers of disorder realizations, ranging from 100 to 7200, depending on the system size. While studying

the thermodynamics, we have used the efficient Wolff cluster algorithm [20] to eliminate critical slowing down. We have equilibrated every run by 100 Monte-Carlo sweeps, and we have used another 100 sweeps for measurements. To investigate the critical dynamics, we have equilibrated the system using the Wolff algorithm but then propagated the system in time by means of the Metropolis algorithm [21] which implements model A dynamics.

B. Thermodynamics

To test the finite-size behavior (4, 5) of the susceptibility, one needs to consider samples having sizes $L_\perp \gg L_\parallel$ such that $L_\perp$ is effectively infinite. We have used system sizes $L_\perp = 800$ and $L_\parallel = 10$ to 90. Figure 3 shows the susceptibility χ as a function of $L_\parallel$ for several temperatures in the Griffiths region between $T_l = 0.63$ and $T_u \approx 1.443$. In agreement with the theoretical predictions (4) and (5), χ follows a nonuniversal power law in $L_\parallel$ with a temperature-dependent exponent. Simulations for many more temperature values, in the range $T \approx 0.76 - 1.2$, yield analogous results.

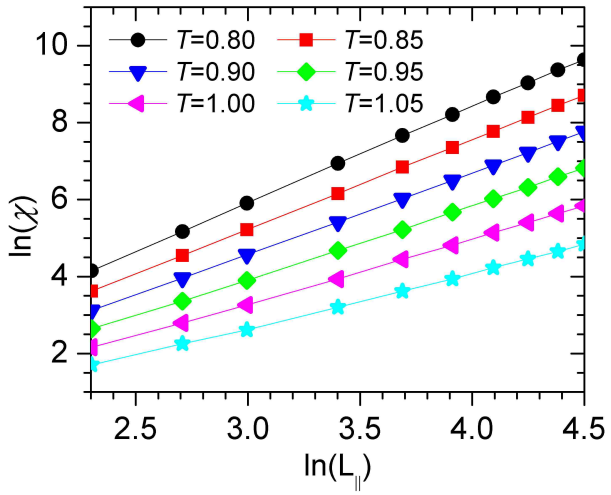

Fig. 3. Susceptibility χ as a function of in-plane system size $L_\parallel$ for several temperatures in the Griffiths region. The perpendicular size is $L_\perp = 800$; the data are averages over 300 disorder configurations. The solid lines are fits to the power laws (4, 5).

The values of the exponent z extracted from fits to (4, 5) are shown in Fig. 4 for the *paramagnetic* and *ferromagnetic* sides of the Griffiths region. z can be fitted to the predicted power law $z \sim 1/|T - T_c|$, as discussed after (3), giving the estimate $T_c \approx 0.933$.

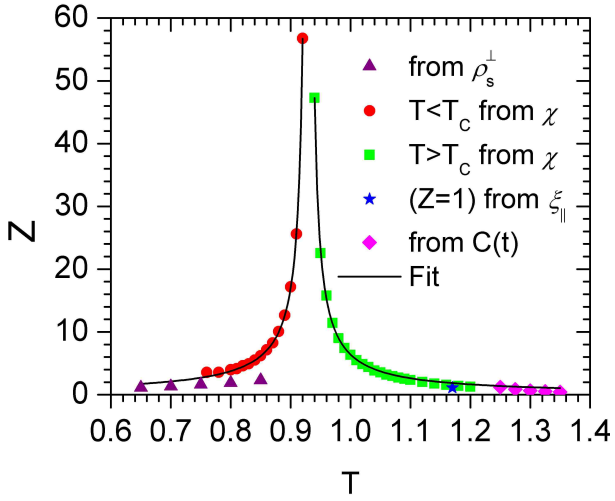

Fig. 4. Griffiths dynamical exponent z vs temperature. The data are extracted from the perpendicular stiffness data in Fig. 6(b), the susceptibility data in Fig. 3, the parallel correlation length data in Fig. 5 and the autocorrelation function data in Fig. 7. The solid lines are a power-law fit of z (extracted from Fig. 3) to (4) and (5).

For a deeper understanding of the thermodynamic critical phenomena of the layered Heisenberg model, we have also studied the behavior of the in-plane correlation lengths in Griffiths phase. Figure 5 shows the scaled correlation length $\xi_{\parallel}/L_{\parallel}$ as a function of temperature for different values of $L_{\parallel}$. Surprisingly, the curves cross at a temperature, $T \approx 1.17$, significantly higher than $T_c \approx 0.93$. This implies that the average in-plane correlation length diverges in part of the *disordered* phase.

To understand this behavior, we estimate the rare region contribution to the averaged in-plane correlation length. It can be calculated by integrating over the density of states (3) as

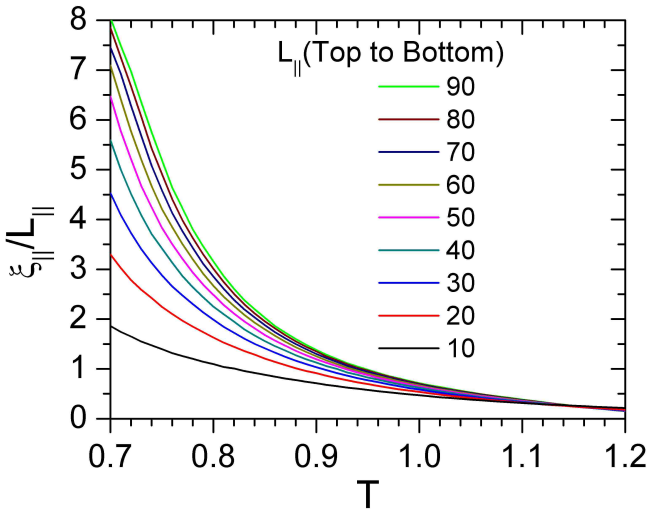

Fig. 5. Scaled in-plane correlation length $\xi_\parallel/L_\parallel$ as a function of temperature T for several in-plane system sizes $L_\parallel$ in the Griffiths region. The perpendicular size is $L_\perp = 800$; the data are averaged over 300 disorder configurations.

$$\xi_\parallel^2 \sim \int_0^{\epsilon_0} d\epsilon \rho(\epsilon) \xi_\parallel^2(\epsilon) \sim \int_0^{\epsilon_0} d\epsilon \epsilon^{1/z-1} \frac{1}{\epsilon} \tag{11}$$

where $\xi_\parallel^2(\epsilon) \sim 1/\epsilon$ is the dependence of the in-plane correlation length of a single region [17, 22] on the renormalized distance ϵ from criticality. Note that we average $\xi_\parallel^2$ instead of $\xi_\parallel$ because that is what numerically happens in the *second moment method* which defines $\xi_\parallel^2$ via

$$\xi_\parallel^2 = \frac{\sum_{\mathbf{r}} C(\mathbf{r}) \mathbf{r}^2}{\sum_{\mathbf{r}} C(\mathbf{r})} \tag{12}$$

with $C(\mathbf{r})$ being the spatial correlation function. The integral in (11) diverges for $z > 1$ and converges for $z < 1$. The in-plane correlation length therefore diverges already in the disordered Griffiths phase at the temperature at which the Griffiths dynamical exponent is $z = 1$. From Fig. 5 we estimate this temperature to be $T \approx 1.17$. As can be seen in Fig. 4, this value is in good agreement with the result extracted from the finite size behavior of χ.

We now turn to the spin-wave stiffness. Calculating the stiffness by actually carrying out simulations with twisted boundary conditions is not very efficient. However, the stiffness can be rewritten in terms of expectation values calculated in a conventional run with periodic boundary conditions. The resulting formula which is a generalization of that used by Caffarel *et al* [23] reads

$$\rho_s^{\perp} = \left\langle \sum_{\langle \mathbf{r},\mathbf{r}'\rangle} J_{\mathbf{r},\mathbf{r}'} \left[\mathbf{S}_{\mathbf{r}} \cdot \mathbf{S}_{\mathbf{r}'} - (\mathbf{S}_{\mathbf{r}} \cdot \hat{\mathbf{a}})(\mathbf{S}_{\mathbf{r}'} \cdot \hat{\mathbf{a}})\right] (z - z')^2 \right\rangle - \frac{1}{T} \left\langle \left(\sum_{\langle \mathbf{r},\mathbf{r}'\rangle} J_{\mathbf{r},\mathbf{r}'} \left[(\mathbf{S}_{\mathbf{r}} \times \mathbf{S}_{\mathbf{r}'}) \cdot \hat{\mathbf{a}}\right] (z - z') \right)^2 \right\rangle . \tag{13}$$

Here, $\hat{\mathbf{a}}$ can be any unit vector perpendicular to the total magnetization $\mathbf{m}$. For $\rho_s^{\parallel}$, $(z - z')$ has to be replaced by $(x - x')$. This formula is derived in appendix A.

Figure 6(a) shows the results for the perpendicular and parallel stiffnesses of our randomly layered Heisenberg model. We have used a system of size $L_{\perp} = 100$ and $L_{\parallel} = 400$. The figure shows that the two stiffness indeed behave very differently. The parallel stiffness $\rho_s^{\parallel}$ vanishes at $T \approx 0.9 - 0.95$ in good agreement with our earlier estimate of $T_c \approx 0.93$. In contrast, the perpendicular stiffness vanishes at a much lower temperature $T \approx 0.7$. Thus, in the range between $T \approx 0.7$ and T_c, the system displays anomalous elasticity, as predicted. (Note: The slight rounding of both $\rho_s^{\parallel}$ and $\rho_s^{\perp}$ can be attributed to finite-size effects.)

The results of the perpendicular spin-wave stiffness $\rho_s^{\perp}$ are analyzed in more detail in Fig. 6(b) for perpendicular sizes $L_{\perp} = 15 - 40$. We have used a parallel size $L_{\parallel} = 400$ and a temperature range $T = 0.65 - 0.85$ where the data are averaged over 1000 disorder configurations. The plot shows a non-universal power-law dependence of $\rho_s^{\perp}$ on $L_{\perp}$ which agrees with the prediction

$$\rho_s^{\perp} \sim L_{\perp}^{1-z}. \tag{14}$$

The dynamical exponents z extracted from fits of $\rho_s^\perp$ to (14) are also shown in Fig. 4. While they roughly agree with the values extracted from χ, the agreement is not very good. We believe this is due to the rather small $L_\perp$ values used.

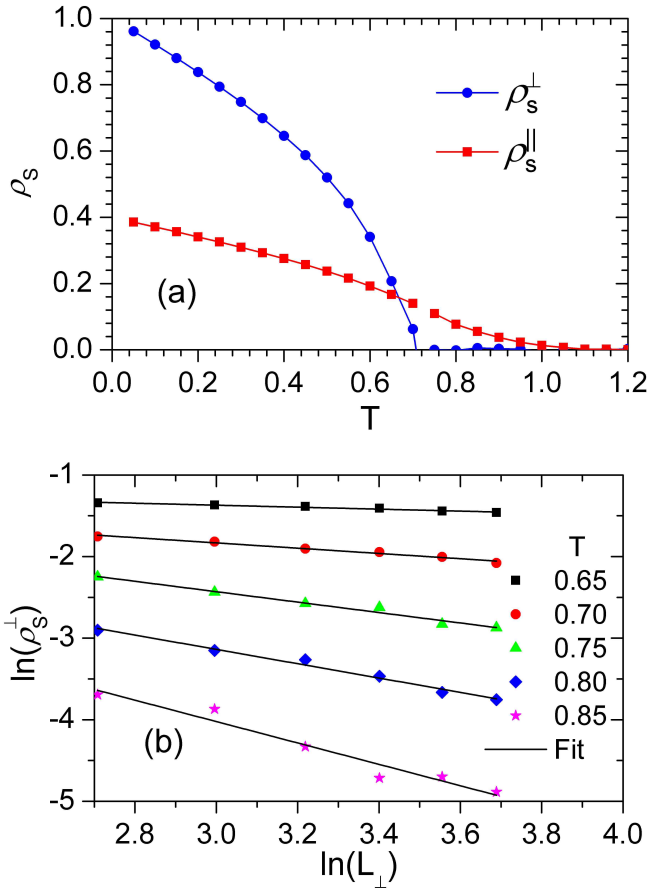

Fig. 6. (a) Perpendicular and parallel spin-wave stiffnesses ($\rho_s^\perp$ and $\rho_s^\parallel$, respectively) as functions of temperature T for system with sizes $L_\perp = 100$ and $L_\parallel = 400$. The data are averaged over 100 disorder configurations. (b) Perpendicular spin-wave stiffness as a function of $L_\perp$ for temperatures in the weakly ordered Griffiths phase and $L_\parallel = 400$. The data are averaged over 1000 disorder configurations. The solid lines are fits to (14).

C. Critical dynamics

To investigate the behavior of the autocorrelation function $C(t)$ in the weakly disordered Griffiths phase, we have used system sizes $L_\perp = 400$ and $L_\parallel = 100$ and temperatures

from $T = 1.25$ to 1.35. From figure 7, one can see that the long-time behavior of $C(t)$ in the Griffiths phase follows a non-universal power law which is in agreement with the prediction (9). Fits of the data to (9) can be used to obtain yet another estimate of the dynamical exponent z. The resulting values are shown in Fig. 4, they are in good agreement with those extracted from χ.

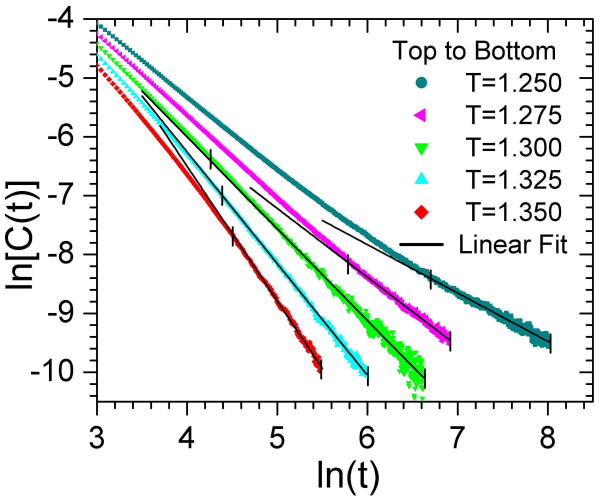

Fig. 7. Time autocorrelation function $C(t)$ for temperatures from $T = 1.25$ to 1.35 (within the Griffiths phase). The system sizes are $L_\perp = 400$ and $L_\parallel = 100$. The data are averaged over 1720 – 7200 disorder configurations. The solid lines are fits to the power-law prediction (9) (with the fit range marked).

Figure 8 shows the behavior of $C(t)$ near criticality plotted such that the expected logarithmic time-dependence (10) gives a straight line. We have used system sizes $L_\perp = 400$ and $L_\parallel = 230$ and temperatures from $T = 0.86$ to 0.91. We find that $C(t)$ indeed follows the prediction at an estimated $T_c \approx 0.895$. This estimate agrees reasonably well with that stemming from the finite-size behavior of χ. We attribute the remaining difference to the finite-size effects and (in case of $C(t)$) finite-time effects.

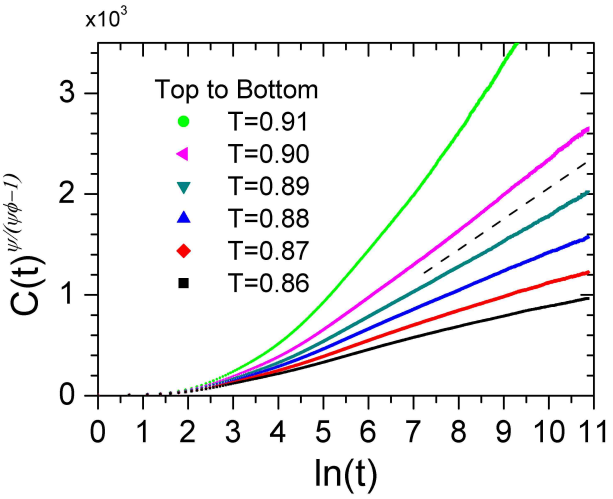

Fig. 8. Time autocorrelation function $C(t)$ for temperatures from $T = 0.86$ to 0.91 (near criticality). The system sizes are $L_\perp = 400$ and $L_\parallel = 230$. The data are averaged over 70 to 80 disorder configurations. The dashed line shows the logarithmic behavior (10) at the estimated critical temperature $T_c = 0.895$.

IV. CONCLUSIONS

To summarize, we have reported the results of large-scale Monte-Carlo simulations of the thermodynamics and dynamic behavior of a randomly layered Heisenberg model. Our results provide strong numerical evidence in support of the infinite-randomness scenario predicted within the strong-disorder renormalization group approach [17]. Morever, our data are compatible with the prediction that the randomly layered Heisenberg model is in the same universality class as the one-dimensional random transverse-field Ising model.

We would have liked to determine the complete set of critical exponents of the infinite-randomness critical point directly from the numerical data. To this end we have attempted to perform an anisotropic finite-size scaling analysis as in Refs. [24] or [25]. However, within the accessible range of system sizes of up to about 10^7 sites, the corrections to the leading scaling behavior were so strong that we could not complete the analysis. This task thus remains for the future.

An important question left unanswered by the strong-disorder renormalization group approach [17] is whether or not weakly or moderately disordered systems actually flow to the infinite-randomness critical point. The clean Heisenberg critical point is unstable against weak layered disorder because it violates the generalized Harris criterion $d_r \nu > 2$ where $d_r = 1$ is the number of random dimensions. Thus, weak layered randomness initially increases under renormalization. Our numerical parameter choices, $p = 0.8$ and $J_u/J_l = 4$ correspond to moderate disorder as the distribution is not particularly broad *on a logarithmic scale*. The fact that we do confirm infinte-randomness behavior for these parameters suggests that the infinite-randomness critical point may control the transition for any nonzero disorder strength. A numerical verification of this conjecture by simulating very weakly disordered systems would require even larger system sizes and is thus beyond our present computational capabilities.

Experimental verifications of infinite-randomness critical behavior and the accompanying power-law Griffiths singularities have been hard to come by, in particular in higher-dimensional systems. Only very recently, promising measurements have been reported [26, 27] of the quantum phase transitions in $CePd_{1-x}Rh_x$ and $Ni_{1-x}V_x$. The randomly layered Heisenberg magnet considered here provides an alternative realization of an infinite-randomness critical point. It may be more easily realizable in experiment because the critical point is classical, and samples can be produced by depositing random layers of two different ferromagnetic materials.

Magnetic multilayers with systematic variation of the critical temperature from layer to layer have already been produced [28], and our results would apply to random versions of these structures.

ACKNOWLEDGEMENTS

We acknowledge helpful discussions with S. Bharadwaj, P. Mohan, and R. Narayanan. This work was supported in part by the NSF under grant No. DMR-0906566.

APPENDIX: SPIN-WAVE STIFFNESS IN TERMS OF SPIN CORRELATION FUNCTIONS

Twisted boundary conditions, i.e., forcing the spins on one surface of the sample of size L to make an angle of θ with those on the opposite surface, lead to a change in the free energy density f. It can be parametrized by

$$f(\theta) - f(0) = \frac{1}{2}\rho_s \left(\frac{\theta}{L}\right)^2 . \tag{A1}$$

which defines the spin-wave stiffness ρ_s.

For definiteness, assume we apply a twist of θ around the perpendicular axis between the top and bottom surfaces of the sample. We parametrize the Heisenberg spin as

$$\mathbf{S}_\mathbf{r} = \begin{pmatrix} \sin(\vartheta_\mathbf{r})\cos(\phi_\mathbf{r}) \\ \sin(\vartheta_\mathbf{r})\sin(\phi_\mathbf{r}) \\ \cos(\vartheta_\mathbf{r}) \end{pmatrix}. \tag{A2}$$

The boundary conditions then read $\phi_\mathbf{r} = 0$ at the bottom ($z = 0$) surface and $\phi_\mathbf{r} = \theta$ at the top ($z = L_\perp$) surface. To eliminate the twisted boundary condition, we now perform the variable transformation

$$\psi_\mathbf{r} = \phi_\mathbf{r} - \theta \frac{z_\mathbf{r}}{L_\perp} \tag{A3}$$

which gives new boundary conditions of $\psi_\mathbf{r} = 0$ at both $z_\mathbf{r} = 0$ and $z_\mathbf{r} = L_\perp$.

Substituting the variable transformation in the Heisenberg Hamiltonian (1), we obtain

$$H = -\sum_{\langle \mathbf{r},\mathbf{r}'\rangle} J_{\mathbf{r},\mathbf{r}'}\Big\{ \sin(\vartheta_{\mathbf{r}})\ \sin(\vartheta_{\mathbf{r}'}) \\ \cos\left(\psi_{\mathbf{r}} - \psi_{\mathbf{r}'} + \frac{\theta}{L_\perp}(z-z')\right) + \cos(\vartheta_{\mathbf{r}})\ \cos(\vartheta_{\mathbf{r}'})\Big\} \tag{A4}$$

where the twist is "distributed" over the volume. Thus, the twist angle θ now appears as a parameter of the Hamiltonian. We can use standard methods to reformulate the second derivative of the free energy F as

$$\frac{\partial^2 F}{\partial \theta^2} = \frac{1}{T}\left\langle \frac{\partial H}{\partial \theta}\right\rangle^2 + \left\langle \frac{\partial^2 H}{\partial \theta^2}\right\rangle - \frac{1}{T}\left\langle \left(\frac{\partial H}{\partial \theta}\right)^2\right\rangle \tag{A5}$$

where the first term on the right hand side vanishes due to symmetry. Evaluating the derivatives of H for the Hamiltonian (A4) gives the spin-wave stiffness $\rho_s = L^2(\partial^2 f/\partial\theta^2)|_{\theta=0}$ as

$$\rho_s^\perp = \left\langle \sum_{\langle \mathbf{r},\mathbf{r}'\rangle} J_{\mathbf{r},\mathbf{r}'}\left[\mathbf{S}_{\mathbf{r}}\cdot\mathbf{S}_{\mathbf{r}'} - (\mathbf{S}_{\mathbf{r}}\cdot\hat{\mathbf{k}})(\mathbf{S}_{\mathbf{r}'}\cdot\hat{\mathbf{k}})\right](z-z')^2\right\rangle \\ -\frac{1}{T}\left\langle\left(\sum_{\langle \mathbf{r},\mathbf{r}'\rangle} J_{\mathbf{r},\mathbf{r}'}\left[(\mathbf{S}_{\mathbf{r}}\times\mathbf{S}_{\mathbf{r}'})\cdot\hat{\mathbf{k}}\right](z-z')\right)^2\right\rangle. \tag{A6}$$

Here, $\hat{\mathbf{k}}$ is the unit vector in the z-direction. The same equation was derived in Ref. [23] for the XY case. Equation A6 needs to be evaluated with fixed boundary conditions at the top and bottom layeres. Applying this formula to simulations with periodic boundary conditions leads to incorrect results in the Heisenberg case (even though it works in XY case). The reason is that Eq. (A6) is sensitive to twist in the XY plane only.

In the Heisenberg case this can be fixed by aligning the imaginary twist axis with a direction $\hat{\mathbf{a}}$ perpendicular to the total magnetization in each Monte-Carlo measurement. We use $\hat{\mathbf{a}} = (\mathbf{m}\times\hat{\mathbf{k}})/|\mathbf{m}\times\hat{\mathbf{k}}|$. The resulting formula for the spin-wave stiffness can be used

efficiently by Monte-Carlo simulations with periodic boundary conditions. It reads

$$\rho_s^{\perp} = \left\langle \sum_{\langle \mathbf{r},\mathbf{r}' \rangle} J_{\mathbf{r},\mathbf{r}'} \left[\mathbf{S}_{\mathbf{r}} \cdot \mathbf{S}_{\mathbf{r}'} - (\mathbf{S}_{\mathbf{r}} \cdot \hat{\mathbf{a}})(\mathbf{S}_{\mathbf{r}'} \cdot \hat{\mathbf{a}}) \right] (z - z')^2 \right\rangle - \frac{1}{T} \left\langle \left(\sum_{\langle \mathbf{r},\mathbf{r}' \rangle} J_{\mathbf{r},\mathbf{r}'} \left[(\mathbf{S}_{\mathbf{r}} \times \mathbf{S}_{\mathbf{r}'}) \cdot \hat{\mathbf{a}} \right] (z - z') \right)^2 \right\rangle . \tag{A7}$$

We have tested that this equation reproduces the results obtained directly from Eq. (A1).

BIBLIOGRAPHY

[1] A. B. Harris. Effect of random defects on the critical behaviour of Ising models. *J. Phys. C*, 7:1671, 1974.

[2] M. Thill and D. A. Huse. Equilibrium behaviour of quantum Ising spin glass. *Physica A*, 214:321, 1995.

[3] M. Guo, R. N. Bhatt, and D. A. Huse. Quantum griffiths singularities in the transverse-field ising spin glass. *Phys. Rev. B*, 54:3336, 1996.

[4] H. Rieger and A. P. Young. Griffiths singularities in the disordered phase of a quantum ising spin glass. *Phys. Rev. B*, 54:3328, 1996.

[5] D. S. Fisher. Random transverse field Ising spin chains. *Phys. Rev. Lett.*, 69:534, 1992.

[6] D. S. Fisher. Critical behavior of random transverse-field Ising spin chains. *Phys. Rev. B*, 51:6411, 1995.

[7] T. Vojta. Disorder-induced rounding of certain quantum phase transitions. *Phys. Rev. Lett.*, 90:107202, 2003.

[8] J. A. Hoyos and T. Vojta. Theory of smeared quantum phase transitions. *Phys. Rev. Lett.*, 100:240601, 2008.

[9] T. Vojta. Rare region effects at classical, quantum, and non-equilibrium phase transitions. *J. Phys. A*, 39:R143, 2006.

[10] T. Vojta. Quantum Griffiths effects and smeared phase transitions in metals: theory and experiment. *J. Low Temp. Phys.*, 161:299, 2010.

[11] B. M. McCoy and T. T. Wu. Random impurities as the cause of smooth specific heats near the critical temperature. *Phys. Rev. Lett.*, 21:549, 1968.

[12] B. M. McCoy and T. T. Wu. Theory of a two-dimensional Ising model with random impurities. i. thermodynamics. *Phys. Rev.*, 176:631, 1968.

[13] B. M. McCoy and T. T. Wu. Theory of a two-dimensional Ising model with random impurities. ii. spin correlation functions. *Phys. Rev.*, 188:982, 1969.

[14] B. M. McCoy. Incompleteness of the critical exponent description for ferromagnetic systems containing random impurities. *Phys. Rev. Lett.*, 23:383, 1969.

[15] T. Vojta. Smearing of the phase transition in Ising systems with planar defects. *J. Phys. A*, 36:10921, 2003.

[16] R. Sknepnek and T. Vojta. Smeared phase transition in a three-dimensional Ising model with planar defects: Monte-Carlo simulations. *Phys. Rev. B*, 69:174410, 2004.

[17] P. Mohan, R. Narayanan, and T. Vojta. Infinite randomness and quantum Griffiths effects in a classical system: the randomly layered Heisenberg magnet. *Phys. Rev. B*, 81:144407, 2010.

[18] T. Vojta and J. Schmalian. Quantum Griffiths effects in itinerant Heisenberg magnets. *Phys. Rev. B*, 72:045438, 2005.

[19] P. C. Hohenberg and B. I. Halperin. *Rev. Mod. Phys.*, 49:435, 1977.

[20] U. Wolff. Collective Monte-Carlo updating for spin systems. *Phys. Rev. Lett.*, 62:361, 1989.

[21] N. Metropolis, A. Rosenbluth, M. Rosenbluth, and A. Teller. Equation of state calculations by fast computing machines. *J. Chem. Phys.*, 21:1087, 1953.

[22] A. J. Bray. *Phys. Rev. Lett.*, 60:720, 1988.

[23] M. Caffarel, P. Azaria, B. Delamotte, and D. Mouhanna. Monte carlo calculation of the spin stiffness of the two-dimensional heisenberg model. *EPL (Europhysics Letters)*, 26(7):493, 1994.

[24] C. Pich, A. P. Young, H. Rieger, and N. Kawashima. Critical behavior and Griffiths-McCoy singularities in the two-dimensional random quantum Ising ferromagnet. *Phys. Rev. Lett.*, 81:5916, 1998.

[25] R. Sknepnek, T. Vojta, and M. Vojta. Exotic vs. conventional scaling and universality in a disordered bilayer quantum Heisenberg antiferromagnet. *Phys. Rev. Lett.*, 93:097201, 2004.

[26] T. Westerkamp, M. Deppe, R. Küchler, M. Brando, C. Geibel, P. Gegenwart, A. P. Pikul, and F. Steglich. Kondo-cluster-glass state near a ferromagnetic quantum phase transition. *Phys. Rev. Lett.*, 102:206404, 2009.

[27] S. Ubaid-Kassis, T. Vojta, and A. Schroeder. Quantum Griffiths phase in the weak itinerant ferromagnetic alloy $Ni_{1-x}V_x$. *Phys. Rev. Lett.*, 104:066402, 2010.

[28] Moreno Marcellini, Martin Pärnaste, Björgvin Hjörvarsson, and Maximilian Wolff. Influence of the distribution of the inherent ordering temperature on the ordering in layered magnets. *Phys. Rev. B*, 79(14):144426, Apr 2009.

VII. STRONG-RANDOMNESS PHENOMENA IN QUANTUM ASHKIN-TELLER MODEL

Hatem Barghathi[1], Fawaz Hrahsheh[1,2,5], José A. Hoyos[3], Rajesh Narayanan[4], and Thomas Vojta[5]

[1]*Department of Physics, Missouri University of Science and Technology, Rolla, MO 65409, USA*

[2]*Department of Physics, Jordan University of Science and Technology, Irbid 22110, Jordan*

[3]*Instituto de Física de São Carlos, Universidade de São Paulo, C.P. 369, São Carlos, São Paulo 13560-970, Brazil*

[4]*Department of Physics, Indian Institute of Technology Madras, Chennai 600036, India*

[5]*King Fahd University of Petroleum and Minerals, Dhahran 31261, Saudi Arabia*

Abstract[*]

The N-color quantum Ashkin-Teller spin chain is a prototypical model for the study of strong-randomness phenomena at first-order and continuous quantum phase transitions. In this paper, we first review the existing strong-disorder renormalization group approaches to the random quantum Ashkin-Teller chain in the weak-coupling as well as the strong-coupling regimes. We then introduce a novel general variable transformation that unifies the treatment of the strong-coupling regime. This allows us to determine the phase diagram for all color numbers N, and the critical behavior for all $N \neq 4$. In the case of two colors, $N = 2$, a partially ordered product phase separates the paramagnetic and ferromagnetic phases in the strong-coupling regime. This phase is absent for all $N > 2$, i.e., there is a direct phase boundary between the paramagnetic and ferromagnetic phases. In agreement with the quantum version of the Aizenman-Wehr theorem, all phase transitions are continuous,

[*]Published in Physica Scripta **T165**, 014040 (2015).

even if their clean counterparts are of first order. We also discuss the various critical and multicritical points. They are all of infinite-randomness type, but depending on the coupling strength, they belong to different universality classes.

1. INTRODUCTION

Simple models of statistical thermodynamics have played a central role in our understanding of phase transitions and critical phenomena. For example, Onsager's solution of the two-dimensional Ising model [1] paved the way for the use of statistical mechanics methods in the physics of thermal (classical) phase transitions. More recently, the transverse-field Ising chain has played a similar role for quantum phase transitions [2].

The investigation of systems with more complex phase diagrams requires richer models. For example, the quantum Ashkin-Teller spin chain [3, 4, 5] and its N-color generalization [6, 7, 8] feature partially ordered intermediate phases, various first-order and continuous quantum phase transitions, as well as lines of critical points with continuously varying critical exponents. Recently, the quantum Ashkin-Teller model has reattracted considerable attention because it can serve as a prototypical model for the study of various strong-randomness effects predicted to occur at quantum phase transitions in disordered systems [9, 10].

In the case of $N = 2$ colors, the correlation length exponent ν of the clean quantum Ashkin-Teller model varies continuously with the strength of the coupling between the colors. The disorder can therefore be tuned from being perturbatively irrelevant (if the Harris criterion [11] $d\nu > 2$ is fulfilled) to relevant (if the Harris criterion is violated). For more than two colors, the clean system features a first-order quantum phase transition. It is thus a prime example for exploring the effects of randomness on first-order quantum phase transitions and for testing the predictions of the (quantum) Aizenman-Wehr theorem [12, 13].

In this paper, we first review the physics of the random quantum Ashkin-Teller chain in both the weak-coupling and the strong-coupling regimes, as obtained by various implementations of the strong-disorder renormalization group. We then introduce a variable transformation scheme that permits a unified treatment of the strong-coupling regime for

all color numbers N. The paper is organized as follows: The Hamiltonian of the N-color quantum Ashkin-Teller chain is introduced in Sec. 2. Section 3 is devoted to disorder phenomena in the weak-coupling regime. To address the strong-coupling regime in Sec. 4, we first review the existing results and then introduce a general variable transformation. We also discuss the resulting phase diagrams and phase transitions. We conclude in Sec. 5.

2. N-COLOR QUANTUM ASHKIN-TELLER CHAIN

The one-dimensional N-color quantum Ashkin-Teller model [6, 7, 8] consists of N identical transverse-field Ising chains of length L (labeled by the "color" index $\alpha = 1 \ldots N$) that are coupled via their energy densities. It is given by the Hamiltonian

$$\begin{aligned} H = & - \sum_{\alpha=1}^{N} \sum_{i=1}^{L} \left(J_i S^z_{\alpha,i} S^z_{\alpha,i+1} + h_i S^x_{\alpha,i} \right) \\ & - \sum_{\alpha<\beta} \sum_{i=1}^{L} \left(K_i S^z_{\alpha,i} S^z_{\alpha,i+1} S^z_{\beta,i} S^z_{\beta,i+1} + g_i S^x_{\alpha,i} S^x_{\beta,i} \right) . \end{aligned} \tag{1}$$

$S^x_{\alpha,i}$ and $S^z_{\alpha,i}$ are Pauli matrices that describe the spin of color α at lattice site i. The strength of the inter-color coupling can be characterized by the ratios $\epsilon_{h,i} = g_i/h_i$ and $\epsilon_{J,i} = K_i/J_i$. In addition to its fundamental interest, the Ashkin-Teller model has been applied to absorbed atoms on surfaces [14], organic magnets, current loops in high-temperature superconductors [15, 16] as well as the elastic response of DNA molecules [17]. The quantum Ashkin-Teller chain (1) is invariant under the duality transformation $S^z_{\alpha,i} S^z_{\alpha,i+1} \to \tilde{S}^x_{\alpha,i}$, $S^x_{\alpha,i} \to \tilde{S}^z_{\alpha,i} \tilde{S}^z_{\alpha,i+1}$, $J_i \rightleftarrows h_i$, and $\epsilon_{J,i} \rightleftarrows \epsilon_{h,i}$, where $\tilde{S}^x_{\alpha,i}$ and $\tilde{S}^z_{\alpha,i}$ are the dual Pauli matrices [18]. This self-duality symmetry will prove very useful in fixing the positions of various phase boundaries of the model.

In the clean problem, the interaction energies and fields are uniform in space, $J_i \equiv J$, $K_i \equiv K$, $h_i \equiv h$, $g_i \equiv g$, and so are the coupling strengths $\epsilon_{h,i} \equiv \epsilon_h$ and $\epsilon_{J,i} \equiv \epsilon_J$. In the present paper, we will be interested in the effects of quenched disorder. We therefore take

the interactions J_i and transverse fields h_i as independent random variables with probability distributions $P_0(J)$ and $R_0(h)$. J_i and h_i can be restricted to positive values, as possible negative signs can be transformed away by a local transformation of the spin variables. Moreover, we focus on the case of nonnegative couplings, $\epsilon_{J,i}, \epsilon_{h,i} \geq 0$. In most of the paper we also assume that the coupling strengths in the bare Hamiltonian (1) are spatially uniform, $\epsilon_{J,i} = \epsilon_{h,i} = \epsilon_I$. Effects of random coupling strengths will be considered in the concluding section.

3. WEAK COUPLING REGIME

For weak coupling and weak disorder, one can map the Ashkin-Teller model onto a continuum field theory and study it via a perturbative renormalization group [19, 20, 21]. This renormalization group displays runaway-flow towards large disorder indicating a breakdown of the perturbative approach. Consequently, nonperturbative methods are required even for weak coupling.

Carlon et al. [22] therefore investigated the weak-coupling regime $|\epsilon_I| < 1$ of the two-color random quantum Ashkin-Teller chain using a generalization of Fisher's strong-disorder renormalization group [23, 24] of the random transverse-field Ising chain. Analogously, Goswami et al. [21] considered the N-color version for $0 \leq \epsilon_I < \epsilon_c(N)$ where ϵ_c is an N-dependent constant. In the following, we summarize their results to the extent necessary for our purposes, focusing on nonnegative ϵ_I.

The bulk phases of the random quantum Ashkin-Teller model (1) in the weak-coupling regime are easily understood. If the interactions J_i dominate over the fields h_i, the system is in the ordered (Baxter) phase in which each color orders ferromagnetically. In the opposite limit, the model is in the paramagnetic phase.

The idea of any strong-disorder renormalization group method consists in finding the largest local energy scale and integrating out the corresponding high-energy degrees

of freedom. In the weak-coupling random quantum Ashkin-Teller model, the largest local energy is either a transverse field h_i or an interaction J_i. We thus set the high-energy cutoff of the renormalization group to $\Omega = \max(h_i, J_i)$. If the largest energy is the transverse-field h_i, the local ground state $|\rightarrow\rightarrow \ldots \rightarrow\rangle$ has all spins at site i pointing in the positive x direction (each arrow represents one color). Site i thus does not contribute to the order parameter, the z-magnetization, and can be integrated out in a site decimation step. This leads to effective interactions between sites $i-1$ and $i+1$. Specifically, one obtains an effective Ising interaction

$$\tilde{J} = \frac{J_{i-1} J_i}{h_i + (N-1) g_i} \tag{2}$$

and an effective four-spin interaction

$$\tilde{K} = \frac{K_{i-1} K_i}{2[h_i + (N-2) g_i]} \,. \tag{3}$$

This implies that the coupling strength ϵ renormalizes as

$$\tilde{\epsilon}_J = \frac{\epsilon_{J,i-1} \epsilon_{J,i}}{2} \, \frac{1 + (N-1)\epsilon_{h,i}}{1 + (N-2)\epsilon_{h,i}} \,. \tag{4}$$

The recursion relations for the case of the largest local energy being the interaction J_i can be derived analogously or simply inferred from the self-duality of the Hamiltonian. In this case, the sites i and $i+1$ are merged into a single new site whose fields and coupling strength are given by

$$\tilde{h} = \frac{h_i h_{i+1}}{J_i + (N-1) K_i} \,, \tag{5}$$

$$\tilde{g} = \frac{g_i g_{i+1}}{2[J_i + (N-2) K_i]} \,, \tag{6}$$

$$\tilde{\epsilon}_h = \frac{\epsilon_{h,i} \epsilon_{h,i+1}}{2} \, \frac{1 + (N-1)\epsilon_{J,i}}{1 + (N-2)\epsilon_{J,i}} \,. \tag{7}$$

According to eqs. (4) and (7), the coupling strengths ϵ renormalize downward without limit under the strong-disorder renormalization group provided their initial values are sufficiently

small. Assuming a uniform initial ϵ_I, the coupling strength decreases if $\epsilon_I < \epsilon_c(N)$ with the critical value given by

$$\epsilon_c(N) = \frac{2N-5}{2N-2} + \sqrt{\left(\frac{2N-5}{2N-2}\right)^2 + \frac{2}{N-1}}\,. \tag{8}$$

It takes the value $\epsilon_c(2) = 1$ and increases monotonically with N towards the limit $\epsilon_c(\infty) = 2$.

If $\epsilon_I < \epsilon_c(N)$, the N random transverse-field Ising chains making up the random quantum Ashkin-Teller model asymptotically decouple. The low-energy physics of the random quantum Ashkin-Teller model is thus identical to that of the random transverse-field Ising chain. In particular, there is a direct quantum phase transition between the ferromagnetic and paramagnetic phases. In agreement with the self-duality of the Hamiltonian, it is located at $J_{\rm typ} = h_{\rm typ}$ where the typical values $J_{\rm typ}$ and $h_{\rm typ}$ are be defined as the geometric means of the distributions $P_0(J)$ and $R_0(h)$. The critical behavior of the transition is of infinite-randomness type and in the random transverse-field Ising universality class [24]. It is accompanied by power-law quantum Griffiths singularities.

4. STRONG COUPLING REGIME

4.1. Existing results

If $\epsilon_I > \epsilon_c(N)$, the coupling strengths increase under the renormalization group steps of Sec. 3. If they get sufficiently large, the energy spectrum of the local Hamiltonian changes, and the method breaks down. To overcome this problem, two recent papers have implemented versions of the strong-disorder renormalization group that work in the strong-coupling limit $\epsilon \to \infty$ [25, 26].

For large ϵ, the inter-color couplings in the second line of the Hamiltonian (1) dominate over the Ising terms in the first line. The low-energy spectrum of the local Hamiltonian therefore consists of a ground-state sector and a pseudo ground-state sector,

depending on whether or not a state satisfies the Ising terms [25]. For different numbers of colors N, this leads to different consequences.

For $N > 4$, the local binary degrees of freedom that distinguish the two sectors become asymptotically free in the low-energy limit. By incorporating them into the strong-disorder renormalization group approach, the authors of Ref. [25] found that the direct continuous quantum transition between the ferromagnetic and paramagnetic phases on the self-duality line $J_{\rm typ} = h_{\rm typ}$ persists in the strong-coupling regime $\epsilon_I > \epsilon_c(N)$. In agreement with the quantum Aizenman-Wehr theorem [13], the first order transition of the clean model is thus replaced by a continuous one. However, the critical behavior in the strong-coupling regime differs from the random transverse-field Ising universality class that governs the weak-coupling case. The critical point is still of infinite-randomness type, but the additional degrees of freedom lead to even stronger thermodynamic singularities. The method of Ref. [25] relies on the ground-state and pseudo ground-state sectors decoupling at low energies and thus holds for $N > 4$ colors only.

We now turn to $N = 2$. The strong-coupling regime of the two-color random quantum Ashkin-Teller model was recently attacked [26] by the variable transformation

$$\sigma_i^z = S_{1,i}^z S_{2,i}^z \,, \quad \eta_i^z = S_{1,i}^z \tag{9}$$

which introduces the product of the two colors as an independent variable. The corresponding transformations for the Pauli matrices $S_{1,i}^x$ and $S_{2,i}^x$ read

$$\sigma_i^x = S_{2,i}^x \,, \quad \eta_i^x = S_{1,i}^x S_{2,i}^x \,. \tag{10}$$

Inserting these transformations into the $N = 2$ version of the Hamiltonian (1) gives

$$\begin{aligned} H = & - \sum_i (K_i \sigma_i^z \sigma_{i+1}^z + h_i \sigma_i^x) - \sum_i (J_i \eta_i^z \eta_{i+1}^z + g_i \eta_i^x) \\ & - \sum_i (J_i \sigma_i^z \sigma_{i+1}^z \eta_i^z \eta_{i+1}^z + h_i \sigma_i^x \eta_i^x) \; . \end{aligned} \tag{11}$$

An intuitive physical picture of the strong-coupling regime $\epsilon \gg 1$ close to self duality, $h_{\rm typ} \approx J_{\rm typ}$, emerges directly from this Hamiltonian. The product variable σ is dominated by the four-spin interactions K_i while the behavior of the variable η_i which traces the original spins is dominated by the two-spin transverse fields g_i. All other terms vanish in the limit $\epsilon \to \infty$, i.e., the pair product variable and the spin variable asymptotically decouple. The system is therefore in a partially ordered phase in which the pair product variable σ^z develops long-range order while the spins remain disordered. A detailed strong-disorder renormalization group study [26] confirms this picture and also yields the complete phase diagram (see Fig. 1) as well as the critical behaviors of the various quantum phase transitions. For example, the transitions between the product phase and the paramagnetic and ferromagnetic phases (transitions 2 and 3 in Fig. 1) are both of infinite-randomness type and in the random transverse-field Ising universality class.

The strong-coupling behavior of the random quantum Ashkin-Teller chains with $N = 3$ and 4 colors could not be worked out with the above methods.

4.2. Variable transformation for N=3

In this and the following subsections, we present a method that allows us to study the strong-coupling regime of the random quantum Ashkin-Teller model for any number N of colors. It is based on a generalization of the variable transformation (9), (10) of the two-color problem. We start by discussing $N = 3$ colors which is particularly interesting because it is not covered by the existing work [25, 26]. Furthermore, it is the lowest number of colors for

which the clean system features a first-order transition. After $N = 3$, we consider general odd and even color numbers N which require slightly different implementations.

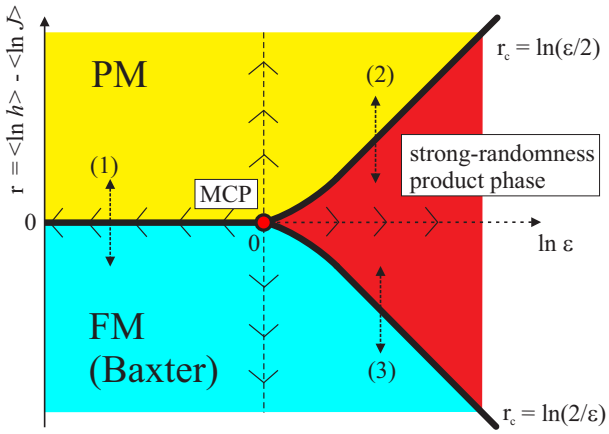

Figure 1. Schematic ground state phase diagram of the two-color random quantum Ashkin-Teller chain. For $\epsilon_I < \epsilon_c(1) = 1$, the paramagnetic and ferromagnetic phases are connected by a direct continuous quantum phase transition. For $\epsilon_I > 1$, they are separated by a partially ordered "product" phase characterized by strong randomness and renormalization group flow towards infinite coupling. The two regimes are separated by a multicritical point (MCP) at $\epsilon = 1$. (after [26]).

In the three-color case, the transformation is defined by introducing two pair variables and one product of all three original colors,

$$\sigma_i^z = S_{1,i}^z S_{3,i}^z, \quad \tau_i^z = S_{2,i}^z S_{3,i}^z, \quad \eta_i^z = S_{1,i}^z S_{2,i}^z S_{3,i}^z \, . \tag{12}$$

The corresponding transformation of the Pauli matrices $S_{\alpha,i}^x$ is given by

$$S_{1,i}^x = \sigma_i^x \eta_i^x, \quad S_{2,i}^x = \tau_i^x \eta_i^x, \quad S_{3,i}^x = \sigma_i^x \tau_i^x \eta_i^x \, . \tag{13}$$

Inserting these transformations into the Hamiltonian (1) yields

$$\begin{aligned} H = \quad & -\sum_i g_i \left(\sigma_i^x + \tau_i^x + \sigma_i^x \tau_i^x\right) \\ & -\sum_i K_i \left(\sigma_i^z \sigma_{i+1}^z + \tau_i^z \tau_{i+1}^z + \sigma_i^z \sigma_{i+1}^z \tau_i^z \tau_{i+1}^z\right) \\ & -\sum_i h_i \left(\sigma_i^x + \tau_i^x + \sigma_i^x \tau_i^x\right) \eta_i^x \\ & -\sum_i J_i \left(\sigma_i^z \sigma_{i+1}^z + \tau_i^z \tau_{i+1}^z + \sigma_i^z \sigma_{i+1}^z \tau_i^z \tau_{i+1}^z\right) \times \eta_i^z \eta_{i+1}^z . \end{aligned} \tag{14}$$

We see that the triple product η_i does not show up in the terms containing g_i and K_i. In the strong-coupling limit, $\epsilon \gg 1$, g_i and K_i are much larger than h_i and J_i. The behavior of the pair variables σ_i and τ_i is thus governed by the first two lines of (14) only and becomes independent of the triple products η_i. The η_i themselves are slaved to the behavior of the σ_i and τ_i via the large brackets in the third and fourth line of (14).

The qualitative features of the strong-coupling regime follow directly from these observations. The first two lines of (14) form a two-color random quantum Ashkin-Teller model for the variables σ_i and τ_i. As all terms in the brackets have the same prefactor, this two-color Ashkin-Teller model is right at its multicritical coupling strength ϵ_c (as demonstrated in Ref. [26] and shown in Fig. 1). The σ_i and τ_i thus undergo a direct phase transition between a paramagnetic phase for $g_{\text{typ}} > K_{\text{typ}}$ and a ferromagnetic phase for $g_{\text{typ}} < K_{\text{typ}}$. In agreement with the quantum Aizenman-Wehr theorem, the transition is continuous; it is in the infinite-randomness universality class of the random transverse-field Ising model. Moreover, in contrast to the $N = 2$ case, there is no additional partially ordered phase.

What about the triple product variables η_i? For large disorder, the brackets in the third and fourth line of (14) can be treated as classical variables. If the σ_i and τ_i order ferromagnetically, $\sigma_i^x + \tau_i^x + \sigma_i^x \tau_i^x$ vanishes (for all sites surviving the strong-disorder renormalization group at low energies) while in the paramagnetic phase, $\sigma_i^z \sigma_{i+1}^z +$

$\tau_i^z\tau_{i+1}^z + \sigma_i^z\sigma_{i+1}^z\tau_i^z\tau_{i+1}^z$ vanishes. Thus, each η_i becomes a classical variable that is slaved to the behavior of σ_i and τ_i. This means, the η_i align ferromagnetically if the σ_i and τ_i are ferromagnetic while they form a spin-polarized paramagnet if σ_i and τ_i are in the paramagnetic phase.

All these qualitative results are confirmed by a strong-disorder renormalization group calculation which we now develop for the case of general odd N.

4.3. Variable transformation and strong-disorder renormalization group for general odd N

For general odd $N > 2$, we define $N-1$ pair variables and one product of all colors

$$\sigma_{\alpha,i}^z = S_{\alpha,i}^z\, S_{N,i}^z \quad (\alpha = 1 \ldots N-1), \quad \eta_i^z = \prod_{\alpha=1}^{N} S_{\alpha,i}^z\,. \tag{15}$$

The corresponding transformation of the Pauli matrices $S_{\alpha,i}^x$ is given by

$$S_{\alpha,i}^x = \sigma_{\alpha,i}^x\,\eta_i^x \quad (\alpha = 1 \ldots N-1), \quad S_{N,i}^x = \prod_{\alpha=1}^{N-1} \sigma_{\alpha,i}^x\,\eta_i^x\,. \tag{16}$$

In terms of these variables, the Hamiltonian (1) reads

$$\begin{aligned} H = \quad & -\sum_i g_i \left[\sum_{\alpha<\beta}^{N-1} \sigma_{\alpha,i}^x\sigma_{\beta,i}^x + \sum_{\alpha=1}^{N-1}\prod_{k\neq\alpha}^{N-1} \sigma_{k,i}^x\right] \\ & -\sum_i K_i \left[\sum_{\alpha<\beta}^{N-1} \sigma_{\alpha,i}^z\sigma_{\alpha,i+1}^z\sigma_{\beta,i}^z\sigma_{\beta,i+1}^z + \sum_{\alpha=1}^{N-1} \sigma_{\alpha,i}^z\sigma_{\alpha,i+1}^z\right] \\ & -\sum_i h_i \left[\sum_{\alpha=1}^{N-1} \sigma_{\alpha,i}^x + \prod_{k=1}^{N-1} \sigma_{k,i}^x\right]\eta_i^x \\ & -\sum_i J_i \left[\sum_{\alpha=1}^{N-1}\prod_{k\neq\alpha}^{N-1} \sigma_{k,i}^z\sigma_{k,i+1}^z + \prod_{k=1}^{N-1} \sigma_{k,i}^z\sigma_{k,i+1}^z\right] \times \eta_i^z\eta_{i+1}^z. \end{aligned} \tag{17}$$

As in the three-color case, the N-product variable η_i does not appear in the terms containing the large energies g_i and K_i.

We now implement a strong-disorder renormalization group for the Hamiltonian (17). This can be conveniently done using the projection method described, e.g., by Auerbach [27] and applied to the random quantum Ashkin-Teller model in Ref. [26]. Within this technique, the (local) Hilbert space is divided into low-energy and high-energy subspaces. Any state ψ can be decomposed as $\psi = \psi_1 + \psi_2$ with ψ_1 in the low-energy subspace and ψ_2 in the high-energy subspace. The Schroedinger equation can then be written in matrix form

$$\begin{pmatrix} H_{11} & H_{12} \\ H_{21} & H_{22} \end{pmatrix} \begin{pmatrix} \psi_1 \\ \psi_2 \end{pmatrix} = E \begin{pmatrix} \psi_1 \\ \psi_2 \end{pmatrix} \tag{18}$$

with $H_{ij} = P_i H P_j$. Here, P_1 and P_2 project on the low-energy and high-energy subspaces, respectively. Eliminating ψ_2 from these two coupled equations gives $H_{11}\psi_1 + H_{12}(E - H_{22})^{-1} H_{21}\psi_1 = E\psi_1$. Thus, the effective Hamiltonian in the low-energy Hilbert space is

$$H_{\rm eff} = H_{11} + H_{12}(E - H_{22})^{-1} H_{21} \ . \tag{19}$$

The second term can now be expanded in inverse powers of the large local energy scale g_i or K_i.

In the strong-coupling regime, $\epsilon \gg 1$, the strong-disorder renormalization group is controlled by the first two lines of (17). It does not depend on the N-products η_i which are slaved to the σ_i and τ_i via the large brackets in the third and forth lines of (17).

If the largest local energy scale is the "Ashkin-Teller field" g_i, site i does not contribute to the order parameter and is integrated out via a site decimation. The recursions resulting from (19) take the same form as in the weak-coupling regime, i.e., the effective interactions and coupling strength are given by eqs. (2) to (4) [*].

[*]Strictly, (2) to (4) hold in the ground-state sector, $\tilde{\zeta} = 1$ while in the pseudo ground state, $\tilde{\zeta} = -1$, the transverse field h_i shows up with the opposite sign. This difference is irrelevant close to the fixed point

What about the product variable η_i? The bracket in the third line of the Hamiltonian (17) takes the value N while the bracket in the fourth line vanishes. However, because $h_i \ll g_i$, the value of η_i^x is *not* fixed by the renormalization group step. Thus $\tilde{\zeta}_i \equiv \eta_i^x$ becomes a classical Ising degree of freedom with energy $-Nh_i\tilde{\zeta}_i$ that is independent of the terms in the renormalized Hamiltonian. This means, it is "left behind" in the renormalization group step. Consequently, η_i^x plays the role of the additional "internal degree of freedom" first identified in Ref. [25].

The bond decimation step performed if the largest local energy is the four-spin interaction K_i can be derived analogously. The recursion relations are again identical to the weak-coupling regime, i.e., the resulting effective field and coupling are given by eqs. (5) to (7). In this step, the bracket in the fourth line of the Hamiltonian (17) takes the value N while the bracket in the third line vanishes. Thus, the renormalization group step leaves behind the classical Ising degree of freedom $\tilde{\zeta}_i \equiv \eta_i^z\eta_{i+1}^z$ with energy $-NJ_i\tilde{\zeta}_i$. In the bond decimation step, the additional "internal degree of freedom" of Ref. [25] is thus given by $\tilde{\zeta}_i \equiv \eta_i^z\eta_{i+1}^z$.

All of these renormalization group recursions agree with those of Ref. [25] where the renormalization group was implemented in the original variables for $N > 4$ colors.

4.4. *Variable transformation and strong-disorder renormalization group for general even N*

For general even $N \geq 4$, the variable transformation is slightly more complicated than in the odd N case. We define $N-2$ pair variables, a product of $N-1$ colors and a product of

because ϵ diverges (see Sec. 4.5). Analogous statements also holds for bond decimations and for even N.

all N colors,

$$\begin{aligned} \sigma^z_{\alpha,i} &= S^z_{\alpha,i}\, S^z_{N-1,i} \quad (\alpha = 1 \ldots N-2), \\ \eta^z_i &= \prod_{\alpha=1}^{N-1} S^z_{\alpha,i}\,, \quad \tau^z_i = \prod_{\alpha=1}^{N} S^z_{\alpha,i}. \end{aligned} \tag{20}$$

The Pauli matrices $S^x_{\alpha,i}$ then transform via

$$\begin{aligned} S^x_{\alpha,i} &= \sigma^x_{\alpha,i}\, \eta^x_i\, \tau^x_i \quad (\alpha = 1 \ldots N-2), \\ S^x_{N-1,i} &= \prod_{\alpha=1}^{N-2} \sigma^x_{\alpha,i}\, \eta^x_i \tau^x_i\,, \quad S^x_{N,i} = \tau^x_i\,. \end{aligned} \tag{21}$$

After applying these transformations to the Hamiltonian (1), we obtain

$$\begin{aligned} H &= -\sum_{i=1}^{\infty} g_i \left[\sum_{\alpha<\beta}^{N-2} \sigma^x_{\alpha,i}\sigma^x_{\beta,i} + \sum_{\alpha=1}^{N-2} \prod_{\beta\neq\alpha}^{N-2} \sigma^x_{\beta,i} + \right. \\ &\quad \left. + \left(\sum_{\alpha=1}^{N-2} \sigma^x_{\alpha,i} + \prod_{\beta=1}^{N-2} \sigma^x_{\beta,i} \right) \eta^x_i \right] \\ &\quad - \sum_{i=1}^{\infty} K_i \left[\sum_{\alpha<\beta}^{N-2} \sigma^z_{\alpha,i}\sigma^z_{\alpha,i+1}\sigma^z_{\beta,i}\sigma^z_{\beta,i+1} + \sum_{\alpha=1}^{N-2} \sigma^z_{\alpha,i}\sigma^z_{\alpha,i+1} + \right. \\ &\quad \left. + \left(\sum_{\alpha=1}^{N-2} \prod_{\beta\neq\alpha}^{N-2} \sigma^z_{\beta,i}\sigma^z_{\beta,i+1} + \prod_{\beta=1}^{N-2} \sigma^z_{\beta,i}\sigma^z_{\beta,i+1} \right) \tau^z_i\tau^z_{i+1} \right] \\ &\quad - \sum_{i=1}^{\infty} h_i \left[\left(\sum_{\alpha=1}^{N-2} \sigma^x_{\alpha,i}\eta^x_i + \prod_{\beta=1}^{N-2} \sigma^x_{\beta,i}\eta^x_i \right) + 1 \right] \tau^x_i \\ &\quad - \sum_{i=1}^{\infty} J_i \left[\sum_{\alpha=1}^{N-2} \prod_{\beta\neq\alpha}^{N-2} \sigma^z_{\beta,i}\sigma^z_{\beta,i+1} + \prod_{\beta=1}^{N-2} \sigma^z_{\beta,i}\sigma^z_{\beta,i+1} + \right. \\ &\quad \left. + \tau^z_i\tau^z_{i+1} \right] \eta^z_i\eta^z_{i+1}. \end{aligned} \tag{22}$$

In contrast to the odd N case, the decoupling between the pair variables $\sigma_{\alpha,i}$ and the $(N-1)$ and N-products η_i and τ_i is not complete. Each of the products is contained in one but

not both of the terms that dominate for strong coupling $\epsilon \gg 1$ (first two lines of (22)). As a result, the phase diagram in the strong-coupling regime is controlled by a competition between the $\sigma^z_{\alpha,i}$ and $\sigma^x_{\alpha,i}$ via the first two lines of (22) while the η_i and τ_i variables are slaved to them. It features a direct transition between the ferromagnetic and paramagnetic phases at $g_{\rm typ} = K_{\rm typ}$, in agreement with the self-duality of the original Hamiltonian.

To substantiate these qualitative arguments, we have implemented the strong-disorder renormalization group for the Hamiltonian (22), using the projection method as in the last subsection. In the case of a site decimation, i.e., if the largest local energy is the "Ashkin-Teller field" g_i, we again obtain the recursion relations (2) to (4). The variable τ_i^x is not fixed by the renormalization group. Thus $\tilde{\zeta}_i \equiv \tau_i^x$ represents the extra classical Ising degree of freedom that is left behind in the renormalization group step. Its energy is $-Nh_i\tilde{\zeta}_i$. If the largest local energy is the four-spin interaction K_i, we perform a bond decimation. The resulting recursions relations agree with the weak-coupling recursions (5) to (7). In this case, the product $\eta_i^z\eta_{i+1}^z$ is not fixed by the decimation step. Therefore, the left-behind Ising degree of freedom in this decimation step is $\tilde{\zeta}_i \equiv \eta_i^z\eta_{i+1}^z$ with energy $-NJ_i\tilde{\zeta}_i$.

The above strong-disorder renormalization group works for all even color numbers $N > 4$. For $N = 4$, an extra complication arises because the left-behind internal degrees of freedom $\tilde{\zeta}_i$ do not decouple from the rest of the Hamiltonian. For example, when decimating site i (because g_i is the largest local energy), the τ^z term in the fourth line of (22) mixes the two states of the left-behind τ_i^x degree of freedom in second order perturbation theory. An analogous problem arises in a bond decimation step. Thus, for $N = 4$ colors, the internal $\tilde{\zeta}_i$ degrees of freedom need to be kept, and the renormalization group breaks down. In contrast, for $N > 4$, the coupling between the internal $\tilde{\zeta}_i$ degrees of freedom and the rest of the Hamiltonian only appears in higher order of perturbation theory and is thus renormalization-group irrelevant.

4.5. Renormalization group flow, phase diagram, and observables

For color numbers $N = 3$ and all $N > 4$, the strong-disorder renormalization group implementations of the last two subsections all lead to the recursion relations (2) to (7). The behavior of these recursions has been studied in detail in Ref. [25]. In the following, we therefore summarize the resulting renormalization group flow, phase diagram, and key observables.

According to (4) and (7), the coupling strengths ϵ flow to infinity if their initial value $\epsilon_I > \epsilon_c(N)$. Moreover, the competition between interactions K_i and "fields" g_i is governed by the recursion relations (3) and (6) which simplify to

$$\tilde{K} = \frac{K_{i-1}K_i}{2(N-2)g_i}\,, \quad \tilde{g} = \frac{g_i g_{i+1}}{2(N-2)K_i} \tag{23}$$

in the large-ϵ limit. They take the same form as Fisher's recursions of the random transverse-field Ising model [24]. (The extra constant prefactor $2(N-2)$ is renormalization-group irrelevant). The renormalization group therefore leads to a direct continuous phase transition between the ferromagnetic and spin-polarized paramagnetic phases on the self-duality line $g_{\rm typ} = K_{\rm typ}$ (or, equivalently, $h_{\rm typ} = J_{\rm typ}$) . The renormalization group flow on this line is sketched in Fig. 2. In the weak-coupling regime, $\epsilon_I < \epsilon_c(N)$, the flow is towards the random-transverse field Ising quantum critical point located at infinite disorder and $\epsilon = 0$, as explained in Sec. 3. In the strong-coupling regime, $\epsilon_I > \epsilon_c(N)$, the N-color random quantum Ashkin-Teller model ($N = 3$ and $N > 4$) features a distinct infinite-randomness critical fixed point at infinite disorder and infinite coupling strength. It is accompanied by two lines of fixed points for $r = \ln(g_{\rm typ}/K_{\rm typ}) > 0$ ($r < 0$) that represent the paramagnetic (ferromagnetic) quantum Griffiths phases.

The behavior of thermodynamic observables in the strong-coupling regime at criticality and in the Griffiths phases can be worked out by incorporating the left-behind internal

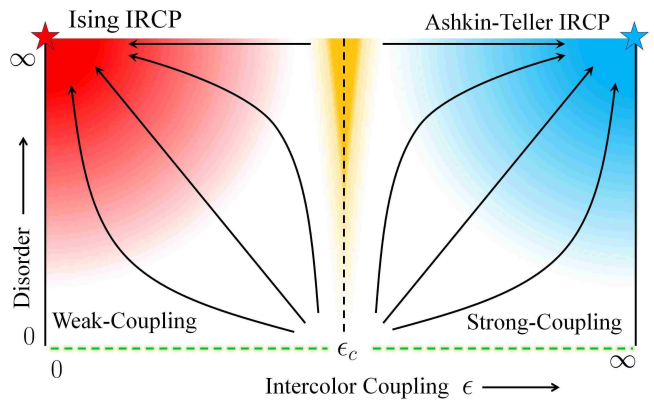

Figure 2. Schematic of the renormalization-group flow diagram on the self-duality line of the random quantum Ashkin-Teller model with $N = 3$ or $N > 4$ colors in the disorder–coupling strength parameter space. For $\epsilon < \epsilon_c(N)$ (left arrows), the critical flow approaches the usual Ising infinite-randomness critical point of [24]. For $\epsilon > \epsilon_c$ (right arrows), we find a distinct infinite-randomness critical point with even stronger thermodynamic singularities (after [25]).

degrees of freedom ζ in the renormalization-group calculation. This divides the renormalization group flow into two stages and leads to two distinct contributions to the observables [25]. For example, the temperature dependence of the entropy at criticality takes the form

$$S = C_1 \left[\ln\left(\frac{\Omega_I}{T}\right)\right]^{-\frac{1}{\psi\phi}} \ln 2 + C_2 \left[\ln\left(\frac{\Omega_I}{T}\right)\right]^{-\frac{1}{\psi}} N \ln 2, \tag{24}$$

where $\psi = 1/2$ is the tunneling exponent, $\phi = \frac{1}{2}(1 + \sqrt{5})$, C_1 and C_2 are nonuniversal constants, and Ω_I is the bare energy cutoff. The second term is the usual contribution of clusters surviving under the strong-disorder renormalization group to energy scale $\Omega = T$. The first term represents all internal degrees of freedom ζ left behind until the renormalization group reaches this scale. As $\phi > 1$, the low-T entropy becomes dominated by the extra degrees of freedom $S \to S_{\text{extra}} \sim [\ln(\Omega_I/T)]^{-1/(\phi\psi)}$. Analogously, in the Griffiths phases, the contribution of the internal degrees of freedom gives

$$S_{\text{extra}} \sim |r|^{\nu} (T/\Omega_I)^{1/(z+Az^{\phi})} \ln 2, \tag{25}$$

which dominates over the regular chain contribution proportional to $T^{1/z} N \ln 2$. Here, $\nu = 2$ is the correlation length critical exponent, and $z = 1/(2|r|)$ is the non-universal Griffiths dynamical exponent. Other observables can be calculated along the same lines [25].

The weak and strong coupling regimes are separated by a multicritical point located at $r = 0$ and $\epsilon_I = \epsilon_c(N)$. At this point, the renormalization group flow has two unstable directions, $r = \ln(g_{\rm typ}/K_{\rm typ})$ and $\epsilon_I - \epsilon_c(N)$. The flow in r direction can be understood by inserting $\epsilon_c(N)$ into the recursion relations (2) and (5) yielding

$$\tilde{J} = \frac{J_{i-1} J_i}{(1 + (N-1)\epsilon_c) h_i}, \quad \tilde{h} = \frac{h_i h_{i+1}}{(1 + (N-1)\epsilon_c) J_i}. \tag{26}$$

These recursions are again of Fisher's random transverse-field Ising type (as the prefactor $(1 + (N-1)\epsilon_c)$ is renormalization-roup irrelevant). Thus, the renormalization group flow at the multicritical point agrees with that of the weak-coupling regime. Note, however, that the N transverse-field Ising chains making up the Ashkin-Teller model do not decouple at the multicritical point. Thus, the fixed-point Hamiltonians of the weak-coupling fixed point and the multicritical point do not agree.

The flow in the ϵ direction can be worked out by expanding the recursions (4) and (7) about the fixed point value $\epsilon_c(N)$ by introducing $\delta_{J,i} = \epsilon_{J,i} - \epsilon_c$ and $\delta_{h,i} = \epsilon_{h,i} - \epsilon_c$. This leads to the recursions

$$\tilde{\delta}_J = \delta_{J,i} + \delta_{J,i+1} + Y \delta_{h_i}, \quad \tilde{\delta}_h = \delta_{h,i} + \delta_{h,i+1} + Y \delta_{J,i} \tag{27}$$

with $Y = \epsilon_c/[(1 + (N-1)\epsilon_c)(1 + (N-2)\epsilon_c)]$. Recursions of this type have been studied in detail by Fisher in the context of antiferromagnetic Heisenberg chains [28] and the random transverse-field Ising chain [24]. Using these results, we therefore find that δ scales as

$$\delta_{\rm typ}(\Gamma) \approx \Gamma^{\phi_Y} \delta_I, \qquad \phi_Y = \frac{1}{2}(1 + \sqrt{5 + 4Y}) \tag{28}$$

with the renormalization group energy scale $\Gamma = \ln(\Omega_I/\Omega)$. The crossover from the multicritical scaling to either the weak-coupling or the strong-coupling fixed point occurs when $|\delta_{\rm typ}|$ reaches a constant δ_x of order unity. It thus occurs at an energy scale $\Gamma_x = |\delta_x/\delta_I|^{1/\phi_Y}$.

5. CONCLUSIONS

To summarize, we have investigated the ground state phase diagram and quantum phase transitions of the N-color random quantum Ashkin-Teller chain which is one of the prototypical models for the study of various strong-disorder effects at quantum phase transitions. After reviewing existing strong-disorder renormalization group approaches, we have introduced a general variable transformation that allows us to treat the strong-coupling regime for $N > 2$ in a unified fashion.

For all color numbers $N > 2$, we find a direct transition between the ferromagnetic and paramagnetic phases for all (bare) coupling strengths $\epsilon_I \geq 0$. Thus, an equivalent of the partially ordered product phase in the two-color model does not exist for three or more colors. In agreement with the quantum version of the Aizenman-Wehr theorem [13], this transition is continuous even if the corresponding transition in the clean problem is of first order. Moreover, the transition is of infinite-randomness type, as predicted by the classification of rare regions effects put forward in Refs. [9, 29] and recently refined in Refs. [30, 31]. Its critical behavior depends on the coupling strength. In the weak-coupling regime $\epsilon < \epsilon_c(N)$, the critical point is in the random transverse-field Ising universality class because the N Ising chains that make up the Ashkin-Teller model decouple in the low-energy limit. In the strong-coupling regime, $\epsilon > \epsilon_c(N)$, we find a distinct infinite-randomness critical point that features even stronger thermodynamic singularities stemming from the "left-behind" internal degrees of freedom.

The novel variable transformation also allowed us to study the multicritical point separating the weak-coupling and strong-coupling regimes. Its renormalization-group flow has two unstable directions. The flow for $r = \ln(g_{\text{typ}}/K_{\text{typ}}) \neq 0$ and $\epsilon_I - \epsilon_c(N) = 0$ is identical to the flow in the weak-coupling regime implying identical critical exponents. The flow at $r = 0$ in the ϵ direction is controlled by different recursions for $\delta = \epsilon - \epsilon_c(N)$ which we have solved for general N.

So far, we have focused on systems whose (bare) coupling strengths are uniform $\epsilon_{J,i} = \epsilon_{h,i} = \epsilon_I$. What about random coupling strengths? If *all* $\epsilon_{J,i}$ and $\epsilon_{h,i}$ are smaller than the multicritical value $\epsilon_c(N)$, the renormalized $\tilde{\epsilon}$ decrease under the renormalization group just as in the case of uniform bare ϵ. If, on the other hand, *all* $\epsilon_{J,i}$ and $\epsilon_{h,i}$ are above $\epsilon_c(N)$, the renormalized values $\tilde{\epsilon}$ increase under renormalization as in the case of uniform bare ϵ. Therefore, our qualitative results do not change; in particular, the bulk phases are stable against weak randomness in ϵ. The same holds for the transitions between the ferromagnetic and paramagnetic phases sufficiently far away from the multicritical point. Note that this also explains why the randomness in ϵ produced in the course of the strong-disorder renormalization group is irrelevant if the initial (bare) ϵ are uniform: All renormalized ϵ values are on the same side of the multicritical point and thus flow either to zero or to infinity.

In contrast, the uniform-ϵ multicritical point itself is unstable against randomness in ϵ. The properties of the resulting random-ϵ multicritical point can be studied numerically in analogy to the two-color case [26]. This remains a task for the future.

ACKNOWLEDGEMENTS

We are grateful for the support from NSF under Grant Nos. DMR-1205803 and PHYS-1066293, from Simons Foundation, from FAPESP under Grant No. 2013/09850-7, and from CNPq under Grant Nos. 590093/2011-8 and 305261/2012-6. J.H. and T.V. acknowledge the hospitality of the Aspen Center for Physics.

References

[1] Lars Onsager. Crystal statistics. i. a two-dimensional model with an order-disorder transition. *Phys. Rev.*, 65:117–149, Feb 1944.

[2] S. Sachdev. *Quantum phase transitions*. Cambridge University Press, Cambridge, 1999.

[3] J. Ashkin and E. Teller. Statistics of two-dimensional lattices with four components. *Phys. Rev.*, 64:178–184, Sep 1943.

[4] Mahito Kohmoto, Marcel den Nijs, and Leo P. Kadanoff. Hamiltonian studies of the $d = 2$ ashkin-teller model. *Phys. Rev. B*, 24(9):5229–5241, Nov 1981.

[5] F Igloi and J Solyom. Phase diagram and critical properties of the (1+1)-dimensional ashkin-teller model. *J. Phys. A*, 17(7):1531, 1984.

[6] Gary S. Grest and Michael Widom. N-color Ashkin-Teller model. *Phys. Rev. B*, 24(11):6508–6515, Dec 1981.

[7] Eduardo Fradkin. N-color Ashkin-Teller model in two dimensions: Solution in the large-N limit. *Phys. Rev. Lett.*, 53(21):1967–1970, Nov 1984.

[8] R. Shankar. Ashkin-Teller and Gross-Neveu models: New relations and results. *Phys. Rev. Lett.*, 55(5):453–456, Jul 1985.

[9] T. Vojta. Rare region effects at classical, quantum, and non-equilibrium phase transitions. *J. Phys. A*, 39:R143, 2006.

[10] T. Vojta. Quantum Griffiths effects and smeared phase transitions in metals: theory and experiment. *J. Low Temp. Phys.*, 161:299, 2010.

[11] A. B. Harris. Effect of random defects on the critical behaviour of Ising models. *J. Phys. C*, 7:1671, 1974.

[12] Michael Aizenman and Jan Wehr. Rounding of first-order phase transitions in systems with quenched disorder. *Phys. Rev. Lett.*, 62:2503–2506, May 1989.

[13] Rafael L. Greenblatt, Michael Aizenman, and Joel L. Lebowitz. Rounding of first order transitions in low-dimensional quantum systems with quenched disorder. *Phys. Rev. Lett.*, 103:197201, Nov 2009.

[14] Per Bak, P. Kleban, W. N. Unertl, J. Ochab, G. Akinci, N. C. Bartelt, and T. L. Einstein. Phase diagram of selenium adsorbed on the ni(100) surface: A physical realization of the ashkin-teller model. *Phys. Rev. Lett.*, 54:1539–1542, Apr 1985.

[15] Vivek Aji and C. M. Varma. Theory of the quantum critical fluctuations in cuprate superconductors. *Phys. Rev. Lett.*, 99:067003, Aug 2007.

[16] Vivek Aji and C. M. Varma. Quantum criticality in dissipative quantum two-dimensional xy and ashkin-teller models: Application to the cuprates. *Phys. Rev. B*, 79:184501, May 2009.

[17] Zhe Chang, Ping Wang, and Ying-Hong Zheng. Ashkin Teller Formalism for Elastic Response of DNA Molecule to External Force and Torque. *Commun. Theor. Phys.*, 49:525–528, 2008.

[18] R.J. Baxter. *Exactly Solved Models in Statistical Mechanics*. Academic Press, New York, 1982.

[19] V. S. Dotsenko. Universality of the critical behaviour of the weakly disordered baxter model. *J. Phys. A*, 18(5):L241, 1985.

[20] T. Giamarchi and H. J. Schulz. Anderson localization and interactions in one-dimensional metals. *Phys. Rev. B*, 37:325–340, Jan 1988.

[21] P. Goswami, D. Schwab, and S. Chakravarty. Rounding by disorder of first-order quantum phase transitions: Emergence of quantum critical points. *Phys. Rev. Lett.*, 100:015703, 2008.

[22] Enrico Carlon, Péter Lajkó, and Ferenc Iglói. Disorder induced cross-over effects at quantum critical points. *Phys. Rev. Lett.*, 87:277201, Dec 2001.

[23] D. S. Fisher. Random transverse field Ising spin chains. *Phys. Rev. Lett.*, 69:534, 1992.

[24] D. S. Fisher. Critical behavior of random transverse-field Ising spin chains. *Phys. Rev. B*, 51:6411, 1995.

[25] Fawaz Hrahsheh, José A. Hoyos, and Thomas Vojta. Rounding of a first-order quantum phase transition to a strong-coupling critical point. *Phys. Rev. B*, 86:214204, Dec 2012.

[26] Fawaz Hrahsheh, José A. Hoyos, Rajesh Narayanan, and Thomas Vojta. Strong-randomness infinite-coupling phase in a random quantum spin chain. *Phys. Rev. B*, 89:014401, Jan 2014.

[27] A. Auerbach. *Interacting Electrons and Quantum Magnetism*. Springer, New York, 1998.

[28] D. S. Fisher. Random antiferromagnetic quantum spin chains. *Phys. Rev. B*, 50:3799, 1994.

[29] T. Vojta and J. Schmalian. Quantum Griffiths effects in itinerant Heisenberg magnets. *Phys. Rev. B*, 72:045438, 2005.

[30] Thomas Vojta and José A. Hoyos. Criticality and quenched disorder: Harris criterion versus rare regions. *Phys. Rev. Lett.*, 112:075702, Feb 2014.

[31] Thomas Vojta, John Igo, and José A. Hoyos. Rare regions and griffiths singularities at a clean critical point: The five-dimensional disordered contact process. *Phys. Rev. E*, 90:012139, Jul 2014.

SECTION

2. CONCLUSIONS AND OUTLOOK

In this dissertation, we have studied the stability of various kinds of phase transitions (quantum, classical and nonequilibrium) under the influences of several types of disorder and quasiperiodic modulations as well as the behavior that emerges in the presence of such inhomogeneities. Modulations and disorders can modify the critical behavior of a continuous phase transition and therefore change its universality class or destroy it by smearing. Moreover, they can destroy a first-order transition by turning it to a continuous one.

We have started with an introductory section which briefly discusses some general aspects of phase transitions and disordered systems. The rest of the dissertation consists of reprints of seven papers that have been published in peer-reviewed journals. In Paper I, we have studied the connectivity fluctuations in topologically disordered lattices. We have identified a broad class of disordered and quasiperiodically modulated lattices in which connectivity fluctuations are suppressed by topological constraints that introduce strong disorder anticorrelations in the lattice connectivity. This explains the apparent violations of the Harris and Imry-Ma criteria that have been reported is several research papers. Accordingly, we have derived modified criteria for phase transitions on topologically disordered lattices.

In Papers II and III, we have studied the effects of random-field disorder on the nonequilibrium continuous phase transitions of the generalized contact process in low dimensions. We have found that this transition violates the famous Imry-Ma criterion which predicts the destruction of continuous phase transitions in the presence of random-field disorder in low dimensions. In contrast, our transition survives random-field disorder.

We also investigated the resulting critical point of the transition in one dimension using large scale Monte-Carlo simulations.

Paper IV deals with the effects of the long-range correlated spatial disorder on the absorbing state phase transition in the contact process. We have found that long-range correlations increases the probability of finding rare active regions which then enhance the Griffiths singularities resulting in non-power-law Griffiths behavior. We believe that our theory holds also for classical and quantum equilibrium systems such as the quantum phase transition in random transverse-field Ising model.

In Paper V, using a real-space renormalization group method and extensive Monte-Carlo simulations, we have studied the nonequilibrium continuous phase transition of the simple contact process with transition rates that are modulated according to the quasiperiodic generalized Fibonacci chains. We have developed a complete theory that describes the resulting unconventional infinite-modulation critical point.

Paper VI studies the effect of quenched uncorrelated disorder on a layered classical Heisenberg model using Monte-Carlo simulations. We have found the critical point of the transition to be of the infinite-randomness type, it is accompanied by strong power-law Griffiths singularities, supporting previous predictions made by means of the strong disorder renormalization-group theory.

In Paper VII, we have developed a strong disorder renormalization group theory by which we show that disorder changes the first-order quantum phase transition of the N-color quantum Ashkin-Teller model to a continuous one even in the strong intercolor coupling case.

In summary, we have illustrated how quenched disorder and quasiperiodic modulations change the behavior of phase transitions in equilibrium and nonequilibrium systems. This brings us closer to a better understanding of the relation between such inhomogeneities and phase transitions. Moreover, our study gave rise to a few interesting questions. For example, based on the results of the topological disorder project (Paper I), it will be inter-

esting to explore the behavior of a quantum phase transition for which our modified Harris criterion predicts topological disorder to be relevant. This should result in novel critical behavior, different than that of generic disordered systems. In addition, this will also result in a significant modification of the quantum Griffiths singularities. Another interesting question is whether or not quasiperiodic modulations destroy a quantum first-order phase transition, and how such modulations modify the Imry-Ma criterion.

BIBLIOGRAPHY

[1] N. Goldenfeld. *Lectures on phase transitions and the renormalization group*. Addison-Wesley, Reading, 1992.

[2] P. Weiss, J. Phys. Radium, 6, 667, 1907.

[3] J. D. van der Waals,PhD thesis, University of Leiden, 1873.

[4] L. D. Landau. *Phys. Z. Sowjetunion*, 11:26, 1937.

[5] L. D. Landau. *Zh. Eksp. Teor. Fiz.*, 7:19, 1937.

[6] L. D. Landau. *Phys. Z. Sowjetunion*, 11:545, 1937.

[7] L. D. Landau. *Zh. Eksp. Teor. Fiz.*, 7:627, 1937.

[8] B. Widom. Surface tension and molecular correlations near the critical point. *J. Chem. Phys.*, 43:3892, 1965.

[9] L. P. Kadanoff et. Static phenomena near critical points: Theory and experiment. *Rev. Mod. Phys.*, 39:395–431, Apr 1967.

[10] B D Josephson. Inequality for the specific heat: I. derivation. *Proceedings of the Physical Society*, 92(2):269, 1967.

[11] G. S. Rushbrooke. On the thermodynamics of the critical region for the ising problem. *The Journal of Chemical Physics*, 39(3), 1963.

[12] T. Vojta. Rare region effects at classical, quantum, and non-equilibrium phase transitions. *J. Phys. A*, 39:R143, 2006.

[13] G. Odor. Universality classes in nonequilibrium lattice systems. *Rev. Mod. Phys.*, 76:663, 2004.

[14] H. Hinrichsen. Nonequilibrium critical phenomena and phase transitions into absorbing states. *Adv. Phys.*, 49:815, 2000.

[15] T. M. Liggett. *Interacting particle systems*. Springer, Berlin, 1985.

[16] T. E. Harris. Contact interactions on a lattice. *Ann. Prob.*, 2:969, 1974.

[17] R. Dickman. In V. Privman, editor, *Nonequilibrium Statistical Mechanics in One Dimension*. Cambridge University Press, Cambridge, 1997.

[18] P. Grassberger and A. de la Torre. *Ann. Phys. (NY)*, 122:373, 1979.

[19] J. Marro and R. Dickman. *Nonequilibrium Phase Transitions in Lattice Models*. Cambridge University Press, Cambridge, 1999.

[20] P. Grassberger. *Z. Phys. B*, 47:365, 1982.

[21] H. K. Janssen. *Z. Phys. B*, 42:151, 1981.

[22] G. Grinstein. Phases and phase transitions of quneched disordered systems. In E. G. D. Cohen, editor, *Fundamental Problems in Statistical Mechanics VI*, page 147. Elsevier, New York, 1985.

[23] Thomas Vojta. Phases and phase transitions in disordered quantum systems. *AIP Conference Proceedings*, 1550(1), 2013.

[24] Yoseph Imry and Michael Wortis. Influence of quenched impurities on first-order phase transitions. *Phys. Rev. B*, 19:3580–3585, Apr 1979.

[25] Yoseph Imry and Shang-keng Ma. Random-field instability of the ordered state of continuous symmetry. *Phys. Rev. Lett.*, 35:1399–1401, Nov 1975.

[26] Michael Aizenman and Jan Wehr. Rounding of first-order phase transitions in systems with quenched disorder. *Phys. Rev. Lett.*, 62:2503–2506, May 1989.

[27] A. B. Harris. Effect of random defects on the critical behaviour of Ising models. *J. Phys. C*, 7:1671, 1974.

[28] Kenneth G. Wilson. Renormalization group and critical phenomena. i. renormalization group and the kadanoff scaling picture. *Phys. Rev. B*, 4:3174–3183, Nov 1971.

[29] Kenneth G. Wilson. Renormalization group and critical phenomena. ii. phase-space cell analysis of critical behavior. *Phys. Rev. B*, 4:3184–3205, Nov 1971.

[30] F. Igloi and C. Monthus. Strong disorder renormalization group approach of random systems. *Phys. Rep.*, 412:277, 2005.

[31] C. Dasgupta and S.-K. Ma. Low-temperature properties of the random Heisenberg antiferromagnetic chain. *Phys. Rev. B*, 22:1305, 1980.

[32] S. K. Ma, C. Dasgupta, and C. K. Hu. Random antiferomagnetic chain. *Phys. Rev. Lett.*, 43:1434, 1979.

[33] D. S. Fisher. Critical behavior of random transverse-field Ising spin chains. *Phys. Rev. B*, 51:6411, 1995.

[34] D. S. Fisher. Random transverse field Ising spin chains. *Phys. Rev. Lett.*, 69:534, 1992.

[35] P. Pfeuty. An exact result for the 1d random Ising model in a transverse field. *Phys. Lett. A*, 72:245, 1979.

VITA

Hatem Nuri Barghathi was born in Benghazi, Libya. In May 1999, he received his B.S. with Honors in Physics from the Faculty of Sciences at the University of Benghazi, Benghazi, Libya. After teaching for one semester in the High Institute of Electrical and Electronic Skills, Benghazi, Libya, and for one semester in Al-Fateh Centre of Brilliants, Benghazi, Libya, he worked for six years at the Center for Renewable Energy and Water Desalination in the Environmental Radiation Measurement Laboratory, Benghazi, Libya. He was promoted to Head of Radiation Measurement Unit in 2007. In August 2007, he received his M.S. in Experimental Nuclear Physics from the Faculty of Sciences at the University of Benghazi, Benghazi, Libya.

In 2010, he joined the group of Dr. Thomas Vojta at the Missouri University of Science and Technology. In May 2012, he received his M.S. in Physics from the Missouri University of Science and Technology, Rolla, Missouri, USA. In December 2016, he received his Ph.D. in Physics from the same University.

During his Ph.D. he published seven journal papers and one conference paper. Based on his research he received several awards and travel grants from the Missouri University of Science and Technology, from the Physics Department, and from the American Physical Society (APS). Since 2012, he has been a member of the American Physical Society.